

**POLITECNICO DI TORINO**

Master of Science in Mechanical Engineering

**Noise and Vibration Sources in Electric Motor Industrial  
Applications**



**Supervisor:**

Prof. Alessandro Fasana

**Candidate:**

Matteo Laterra



# Contents

---

1	Background and Objective .....	5
1.1	Sate of the Art .....	5
1.2	Application Noise Project .....	6
2	Noise and Vibration Sources in Electric Motors.....	9
2.1	Three Phase Motor Working Principles.....	9
2.2	Stator and Rotating Magnetic Field.....	10
2.2.1	Variable Frequency Drive .....	11
2.3	Rotors and Electric Motor types.....	14
2.3.1	Induction Rotor and Slip velocity .....	15
2.3.2	Slip-Torque Characteristic .....	17
2.4	Noise and vibration sources .....	19
3	Analysis and Diagnostic .....	21
3.1	Signals and Sampling Theorem .....	21
3.2	Frequency-domain Analysis .....	22
3.2.1	Fourier Transformation and Discrete Fourier Transformation .....	23
3.2.2	Convolution theorem .....	26
3.2.3	Dirac's delta and impulse transformation.....	27
3.2.4	Repetitive pulse.....	28
3.2.5	Modulation.....	29
3.2.6	Envelope .....	31
3.3	Time-Frequency Analysis.....	33
3.3.1	Short Time Fourier Transform and Spectrogram .....	33
4	Induction Electric Motor Failure Analysis.....	35
4.1	Vibration Analysis Process.....	35
4.1.1	Vibration Sensors .....	36

4.1.2	Analog to Digital Converter .....	39
4.2	Damage Detection in Asynchronous Three Phase Electric Motor .....	40
4.2.1	Baseline.....	40
4.2.2	Stator Issues.....	41
4.2.3	Rotor Issues .....	44
4.2.4	Mounting Problems.....	47
5	Roller Bearings Vibration.....	49
5.1	Bearing Kinematics .....	49
5.2	Perfect bearing vibration.....	50
5.3	Local surface defects .....	51
5.3.1	Surface defects Frequencies.....	52
6	Acoustic .....	55
6.1	Acoustic .....	55
6.1.1	Sound definition .....	55
6.1.2	Sound Pressure .....	56
6.1.3	Acoustic Fields .....	58
6.1.4	Sound Intensity and Sound Power .....	59
6.1.5	Sound Level and Decibel Scale .....	60
6.2	Psychoacoustics.....	61
6.2.1	Loudness.....	62
6.3	Noise Sources and Sound Emission .....	63
6.3.1	Effective Sound Radiation.....	64
6.3.2	Transfer Path .....	65
6.4	Acoustic Measurements Instrumentation.....	66
6.4.1	Sound Intensity and Particle Velocity Probe .....	67
7	Application in scope .....	69
7.1	Test Bench Presentation.....	69

7.1.1	Data Acquisition Instrumentation and Setup.....	70
7.2	Electromagnetic Tests Results.....	73
7.2.1	Electric Motor 6, Baseline .....	74
7.2.2	Electric Motor 2, Rotor Eccentricity .....	79
7.2.3	Electric Motor 1, Broken Rotor Bar .....	82
7.2.4	Electric Motor 8, Baseline and Increased Air Gap.....	85
7.2.5	Electric Motor A, Baseline .....	88
7.2.6	Electric Motor D, Electrical Issues .....	90
7.2.7	Electric Motor C, Static Eccentricity .....	91
8	Conclusions.....	93
8.1	SKF's Application Noise Project Current Progress.....	94
	Bibliography.....	97



# 1 Background and Objective

---

In the design of products with rotating parts, the noise and vibration characteristics are high-priority aspects. Unwanted or annoying sounds in home, transport and working places could result in discomfort, low work efficiency and even serious health problems. For this reason, authorities create regulation and standard for reducing sound and vibration level. Besides the regulation context, silent applications are associated to a widespread feeling of safety, quality and comfort.

The correlation between dynamics of rotating machinery and sound radiation could be difficult to analyse, involving many different disciplines such as structural dynamics, acoustics, signal processing and experimental analysis. This process is made even more complex by the highly subjective nature of human sound perception.

Rolling bearings are one of the most used and critical components in rotating machines, due to their relatively low energy dissipation. Since they are typically used to transfer high forces and heavy loads under dynamic conditions, they have a significant influence in the vibrational and acoustical behaviour of the machinery.

For these reasons, *SKF* as a leading company in bearings manufacturing and condition monitoring has launched the “*Application Noise Project*”.

This thesis is the result of an eight months experimental research at the *SKF Solution Factory Moncalieri (TO)* within the noise and vibration project.

## 1.1 State of the Art

According to an internal research [SKF Roller Bearing Product Line 2015-2016] among 147 complains in the fields of noise and vibration, only 5 have been recognized by *SKF* as bearings quality issues (see Figure 1.1-1). Even if noise emission cannot be directly addressable to bearing quality, the market and customers highlight the need of specialised support to identify reliable solutions and fix noise problems.

Components quality tests currently in use (*SKF's VKL and MVH*) are used to precisely analyse the structure-borne noise and vibration of most common bearing types focusing on bearing's components quality level. Because of the wide variety of different application and operating condition, such tests are not able to simulate real working condition or to predict the response of final system.

The lack of literature in field of noise emission troubleshooting and of a clearly defined operative procedure can easily lead to false problem identification. The project is defined to enable *SKF* to map noise issues from the application point of view, developing and deploying a standardized and structured analysis process for the *Application Engineers*.



**Figure 1.1-1** Actual scenario.

## 1.2 Application Noise Project

The *Application Noise Project*, headed by Eng. *Angelico Approsio* (Project Manager), aims to bridge the gap between the increasing market request for silent application and the lack of a standardized approach to noise issues and troubleshooting. The project is focused on *Induction Three Phase Electric Motor* being present in many industrial and civil application like *Conveyors*, *Elevator* and *Escalator*. Automotive and *Electric Vehicles* are not included in the first phase of the project.

The project is divided into four *Work Packages* according to the desired outcomes (see

Figure 1.2-1):

- **Work package 1:** clear identification of noise issue from bearing and non-bearing related sources.
- **Work package 2:** enable Application Engineers to provide technical solution.
- **Work Package 3:** collect useful data and measurements to be used as database for noise issues problems and as input for *Product Develop* to design next bearing generations.
- **Work Package4:** secure a global standardized approach to handling noise complains.

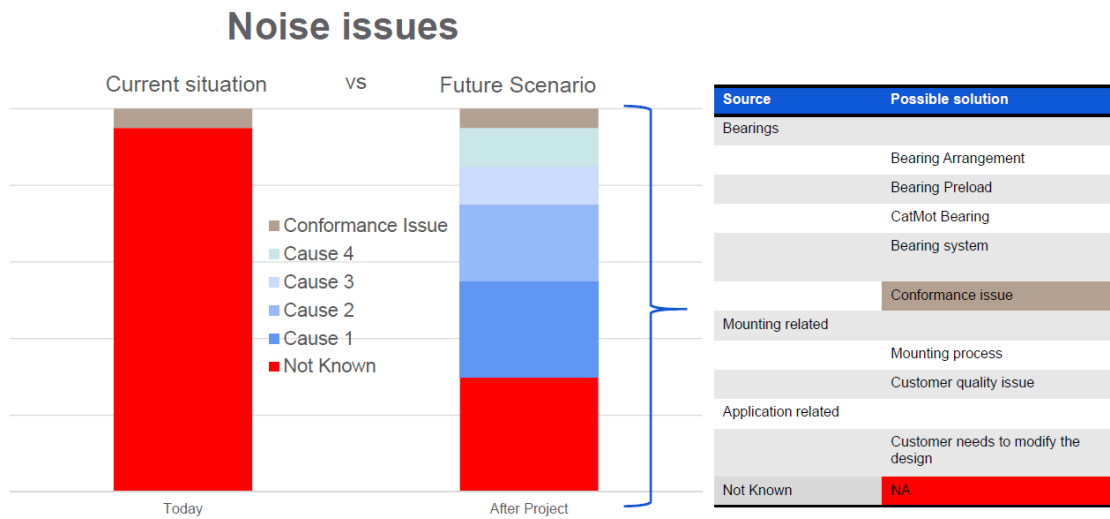


**Figure 1.2-1** Expected outcomes.

This thesis is centred on *Work Package 1*, analysing the Induction Three Phase Electric Motor sound emission, with particular attention to *Non-bearing related Noise Sources*.

The presentation will be developed in three main section:

- General introduction on electric motor noise sources, focused on induction three phase electric motor and its working principle.
- Theoretical presentation of the physical phenomena at stake, analysing vibration, sound emission and acquisition apparatus.
- Test campaign presentation and related results according to the project outcomes.

A limited part of the internship has been devoted to *Work Package 3*, assisting in the database design. Current progress and final outcomes will be presented in the conclusions.



## 2 Noise and Vibration Sources in Electric Motors

---

The AC motor segment accounted for a significant market share in 2018. AC motors are extensively used since their applications range from irrigation pumps to modern day robotics. The adoption of electric AC motors in the automotive industry has increased exponentially, owing to the advent of highly efficient and low-cost electronics, accompanied by improvements in permanent magnetic materials.

The growing demand for reliability, safety and comfort led to an increase in the research in both the vibration and the noise emission field.

Nowadays *Asynchronous Three Phase Electric Motors* make up the majority of all industrial motor segment, owing to their reliability and affordability.

According to this trend, this section will be devoted to a brief overview of the most common electric motor types available on the market with special reference to *Induction Three Phase Electric Motors* (used in the test campaign presented in Chapter 7).

### 2.1 Three Phase Motor Working Principles

In order to better understand the vibration sources in an asynchronous electric motor, a brief review of working principles and main quantities, needed for electric motor diagnosis, will be proposed.

The working principles of an electric motor, as a first approximation, can be summed up into three main principles, playing the lead in the interaction between components and in the power exchanges.

- Laplace's law: it is an equation describing the magnetic field generated by a electric current flowing in a conductor. It relates the magnetic field to the magnitude, direction, length of the conductor, and proximity of the electric current.
- Faraday's law of Induction: it is a law of electromagnetism based on the observation that the variation of the magnetic flux across a closed circuit generates an induced electromotive force in the circuit itself. It is the fundamental operating principle of transformers, inductors, and many type of electrical motors and generators.

- Lorentz Force: it is the force experienced by a conductor, carrying an electric current, when it is placed in a magnetic field.

For almost any kind of AC electrical motor the aim is to generate a rotating magnetic field at the stator level, while, according to the specific working principle, the main differentiation is due to the rotor interaction with the rotating magnetic field.

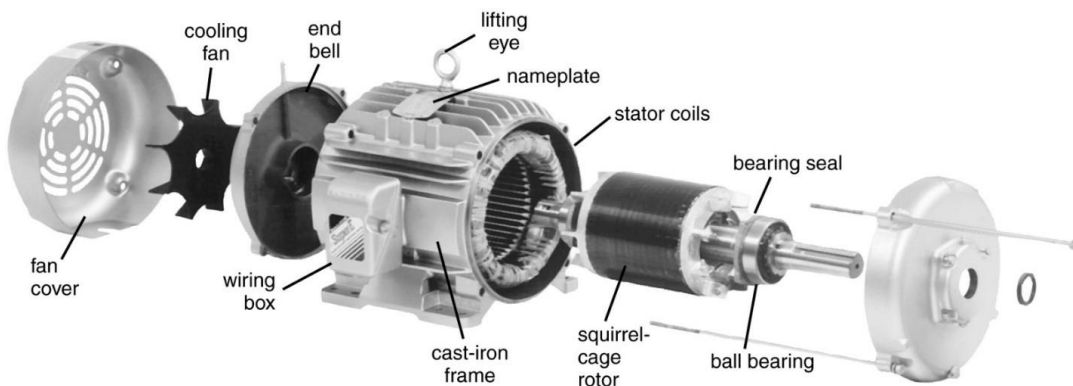


**Figure 2.1-1** Induction motor scheme of components.

In the following paragraph the components of a three phase electric motor will be presented highlighting the main characteristics and the physical principles at stake.

## 2.2 Stator and Rotating Magnetic Field

The stator is the stationary part of the electric motor and it is devoted to the generation of the rotating magnetic field. This objective can be reached by composing two different parts, the *stator core* and the *stator windings*. The stator core is made of a set of slotted silicon-steel sheets called laminations, allowing to direct the magnetic flux and limiting losses owing to eddy currents. The thickness of the lamination is inversely proportional to the magnitude of the generated magnetic field. Along the slots a set of insulated electrical coils are disposed, composing the stator windings responsible for the magnetic field generation.

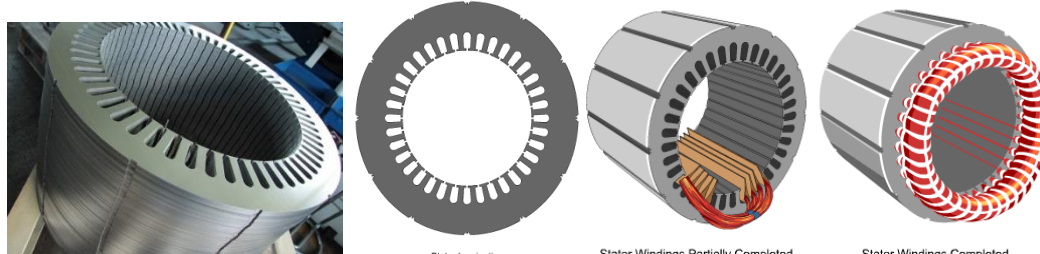


**Figure 2.2-1** Stator construction and windings.

In common industrial application, stator windings are fed by three phase AC currents which, along with the geometrical disposition of the polar pair, generate a rotating magnetic field according to the Laplace law.

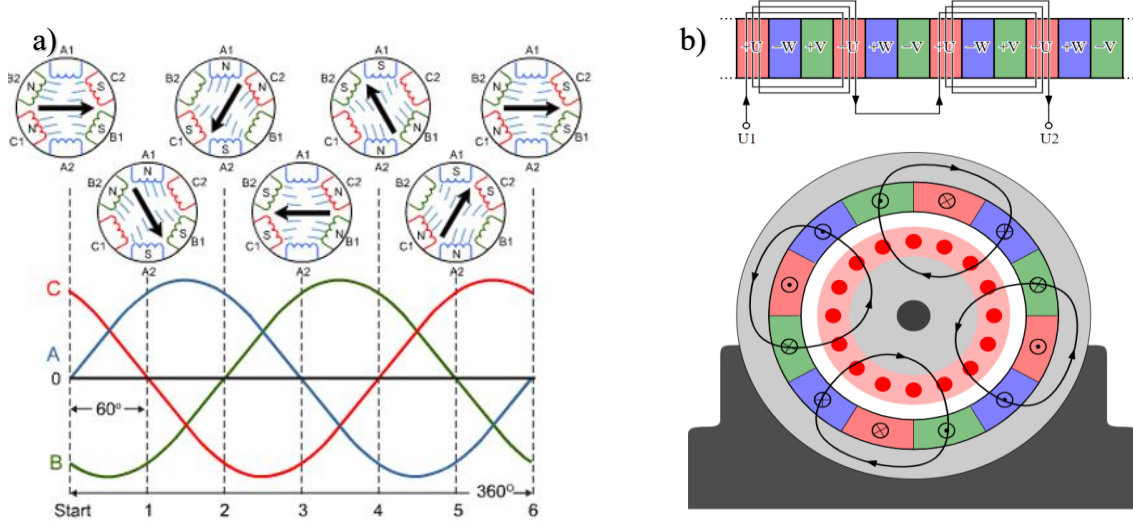


**Figure 2.2-2 a)** Rotating field generated by three phase feeding. **b)** Winding and flux schematization for a four poles motor.

The rotation speed of the generated magnetic field is defined as *synchronous speed*,  $N_s$  (in [rpm]), and it will be set by the feeding frequency according to the polar pair:

$$N_s = \frac{f_l \cdot 120}{p}$$

Being  $f_l$  the line frequency and  $p$  the number of poles.

Based on the above, it is clear that once settled the feeding frequency,  $f_l$ , and the numbers of poles, the rotation speed of the magnetic field is fixed and can be considered as characteristic of the electric machine.

Except for few applications, the impossibility to regulate the magnetic field speed, and consequently the rotor velocity, could be limiting, for this reason *adjustable-speed drives* are often used to control electro-mechanical systems.

Next paragraph will be devoted to a brief presentation of the variable frequency drive, analysing the working principles and the effects on the resulting magnetic field.

## 2.2.1 Variable Frequency Drive

A *Variable Frequency Drive* (VFD) is an electronic controller which allows to set AC motor speed, torque and spinning direction by acting on motor input frequency and voltage. The improvements in power electronics technologies along with the market requests for a more

adaptive product, have contributed to the VFD costs and size reduction, becoming nowadays widespread.

Among the main advantage of using VFD controllers there are:

- Energy costs reduction: in application that do not require the electric motor to run at full speed, VFD allows to match the rotation velocity with the load requirements.
- Tighter process control: allowing the motor to operate at the most efficient speed for its application.

Although the market offers different type of VFDs, according to the topologies and the applications, the most common in industrial practice is the *Voltage-source Inverter drive* (VSI) coupled to a three phase induction motor. In this thesis only VSI drive will be analysed being the type used in test campaign.

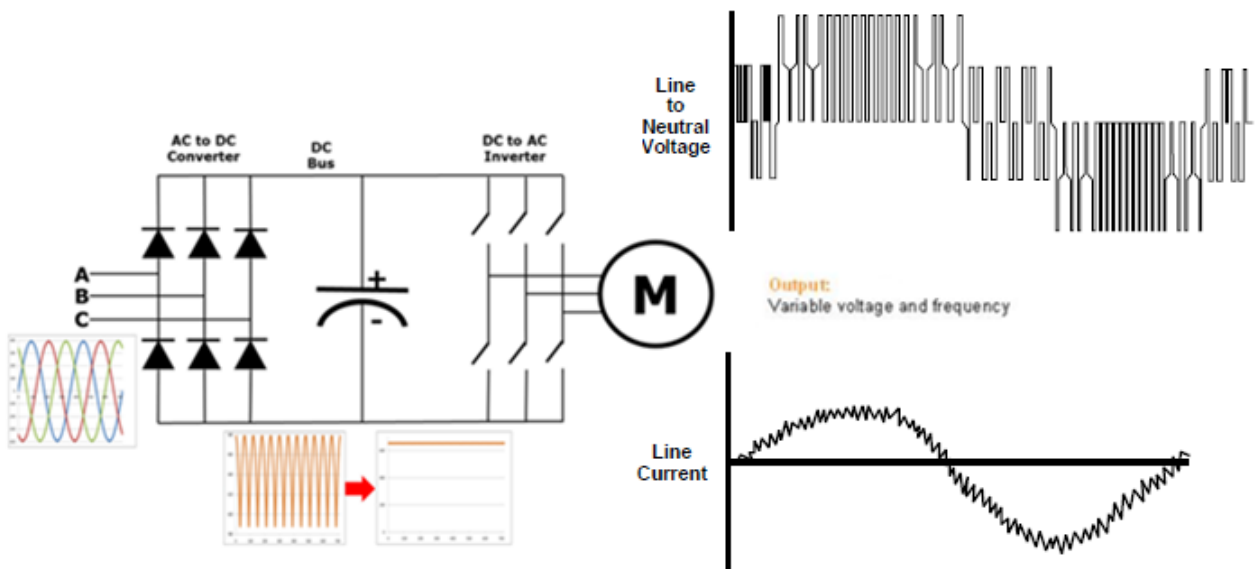


**Figure 2.2-3** VFD components schemes and expected output.

As per Figure 2.2-3, a VFD is composed by three main components. The input signal is rectified by mean of a diodes bridge, which produces a DC voltage influenced by the AC ripple. To get rid of this oscillation a capacitor (working as a filter) is added, delivering a smooth voltage to the *DC to AC inverter*. Acting on the switches, composing the DC to AC inverter, it is possible to control the voltage sign and the pulse width for each phase (see Figure 2.2-4).

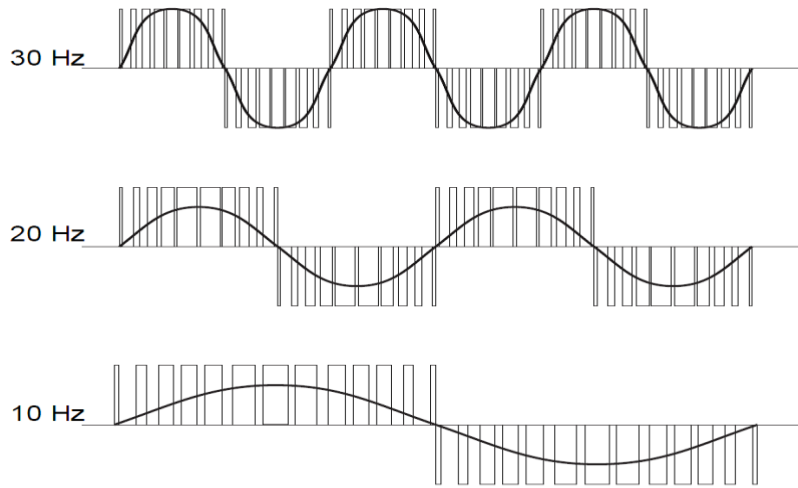


**Figure 2.2-4** VFD output voltage modulation for different frequencies.

The final voltage output waveform is known as *Pulse Width Modulation* (PWM) and it is generated by multiples pulses of the inverter switches at short intervals. The pulse modulation frequency is defined as *Carrier frequency*.

It is important to note (see Figure 2.2-5) that while the inlet voltage follows the PMW waveform, the current assumes a smoother sinusoid-like trend. This characteristic is due to the stator windings that behave like inductors.

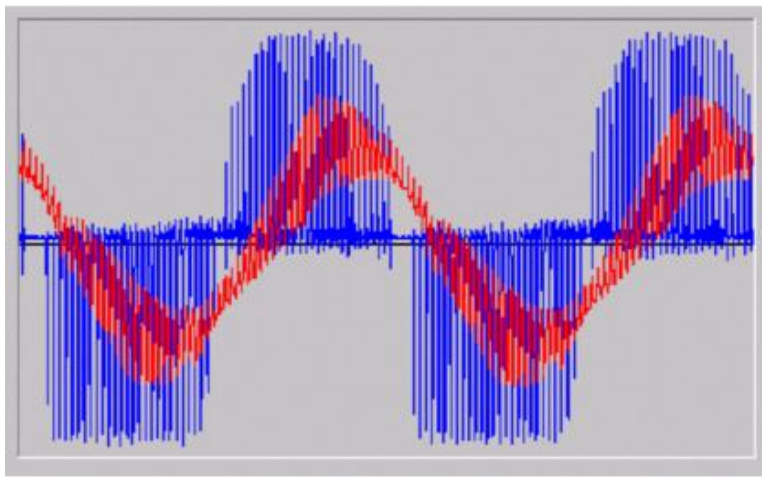


**Figure 2.2-5** Voltage PWM (blue line) and current (red line) measurements for a real induction motor VFD driven.

PWM waveform introduces some critical issues, since stator windings are subjected to high and repetitive voltage picks. When the voltage differential becomes large enough (from phase to phase or turn to turn) some energy could be released in form of sparks, damaging the insulation layer between stator conductors. Moreover, running a motor at a speed lower than the design condition could cause an insufficient ventilation, limiting the cooling effect and

generating damages due to overheating (which is one of the main causes for electric motor failure).

For these reasons *NEMA (National Electrical Manufacturer Association)* standard regulates *Inverter Duty Motor*. According to the standard, an Inverter Duty Motor should be able to mitigate potential failure modes of a motor powered by VFD by adopting insulations systems able to withstand voltages spikes and protects against overheating. Moreover, NEMA standard regulates grounding devices and bearings degree of insulation. More information can be found in *NEMA MG1 Part 31.4.4.2*.

## 2.3 Rotors and Electric Motor types

Once explained how a rotating magnetic field can be obtained at the stator level, we have to transform the input electrical power in mechanical power, that is the task of the *Rotor*.

The rotor is the rotating part of the electrical motor and, like the stator, is made of a set of slotted silicon steel lamination pressed together to form a cylindrical magnetic circuit.

Depending on the type of magnetic interaction between stator and rotor a first distinction can be done (see Figure 2.3-1):

- **Synchronous Motor:** in the most common types of synchronous motor, rotor generates its own magnetic field which aims to align with the stator magnetic field generating torque. This means that the rotor speed  $N_r$ , is equal to the stator rotating magnetic field speed  $N_s$ . The rotor magnetic field can be obtained by using *permanent magnets* or by adopting a *DC-excited rotor* in which the local magnetic field is generated by using DC-excited electromagnets.

Other types of synchronous motors (Reluctance Motor, Hysteresis Motor) are nowadays available on the market but they will not be treated in this thesis.

- **Asynchronous Motor:** the rotor magnetic field is induced by the variation of the flux of the stator magnetic field along the rotor electric circuits. Being the working principle of this type of motor based on the flux variation (according to Faraday's law of Induction), to obtain torque there must be a relative motion between the rotating magnetic field and the electric circuits composing the rotor, so the rotor speed  $N_r$  must be lower than the stator magnetic field speed  $N_s$ .

Asynchronous motor and its rotor will be further presented in next paragraph.

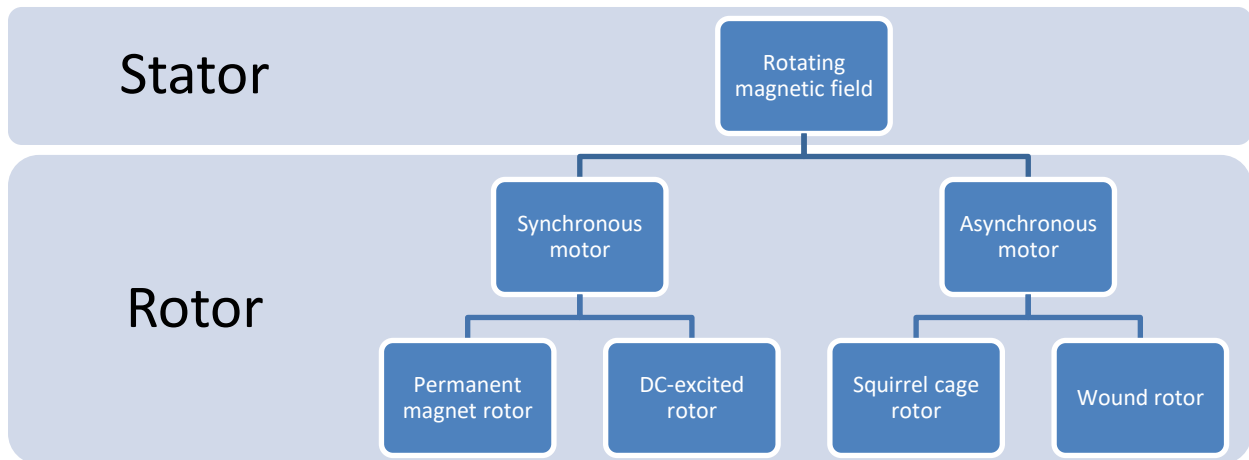


**Figure 2.3-1** Main rotor types and, an electric motor difference.

### 2.3.1 Induction Rotor and Slip velocity

For asynchronous induction motor, the most common type of rotor is the *squirrel cage* type, consisting of a set of copper or aluminium bars installed into the laminations slots. Rotor bars are then connected to an end-ring placed at each end of the rotor which is in charge to close the electric circuit (see Figure 2.3-2). Rotor bar shapes influence motor characteristics allowing to minimize starting currents or to maximize low-speed torque depending on the specific application. Thanks to their reliability and the low manufacturing costs, squirrel cage induction motors are widespread in industry ranging from low power application (less than 1 [KW]) up to 10[MW].

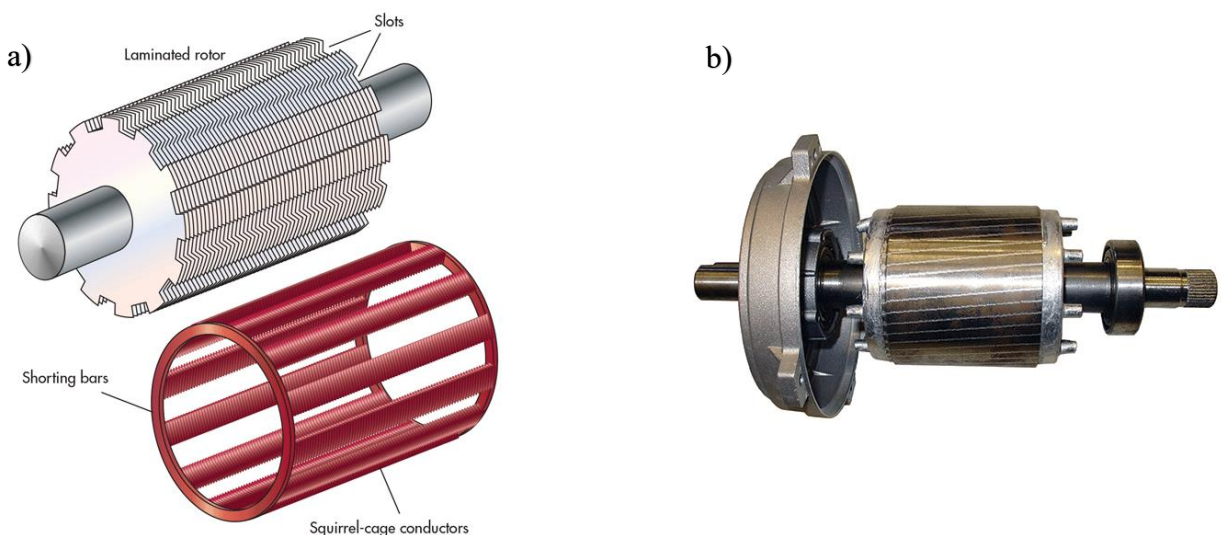


**Figure 2.3-2 a)** Squirrel cage rotor scheme **b)** Real squirrel cage rotor picture.

To better understand the working principles, let's focus on only one winding composing the rotor (see Figure 2.3-3).

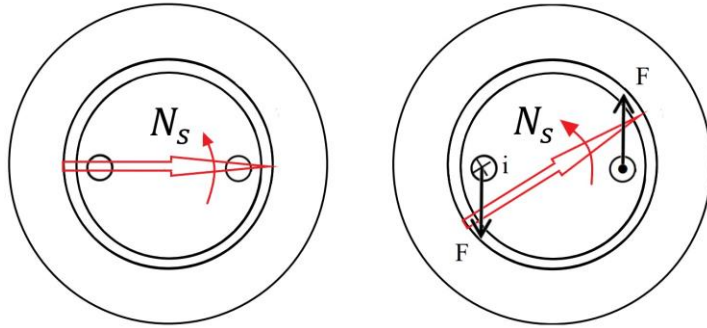


**Figure 2.3-3** Qualitative scheme of flux change across one rotor winding.

According to Faraday's law of induction, the flux changing (due to the rotation of the stator magnetic field) generates in the winding an induced *electromotive force* (EMF) proportional to the rate of change of the magnetic flux according to the law:

$$\varepsilon(t) = -\frac{d\Phi_B}{dt}$$

Being  $\varepsilon$  the EMF and  $\Phi_B$  the flux of the magnetic field  $B$  across the winding (*in [Wb]*).

The induced EMF generates, according to the *impedance* of the winding, a current in the winding itself that will interact with the stator magnetic field producing torque. The magnitude of the force on each branch of the winding will be coherent with Lorentz law, which for a conductor can be written in the form:

$$\vec{F} = I\vec{l} \times \vec{B}$$

Being  $\vec{F}$  is the force experienced by the conductor while “ $\times$ ” expresses the cross product between the current direction vector “ $I\vec{l}$ ” and the magnetic field.

It is interesting to note that the same phenomena could be explained by the interaction between the stator magnetic field and the rotor magnetic field generated in accordance with Laplace's Law.

It is clear that, to generate torque there must be a relative motion between the rotating magnetic field and the windings constituting the squirrel cage. The presence of the mechanical load will cause the rotor to be always slower than the stator rotating field. The difference between the rotating stator magnetic field and the rotor speed can be expressed by the *Slip* parameter, defined as:

$$s = \frac{N_s - N_r}{N_s}$$

Slip parameter gives information not only about the speed difference between the rotor and the stator magnetic field but also on the frequency of the currents induced in the rotor

windings. The flux variation across the rotor winding will generate an AC current in the windings themselves whose frequency  $F_s$  (in [Hz]) is correlate to slip by the relation:

$$F_s = \frac{sN_s}{60}$$

This behaviour is of prevailing importance to understand the *Slip-Torque* characteristic of an induction three phase motor treated in next paragraph.

### 2.3.2 Slip-Torque Characteristic

According to the previous paragraph, the torque delivered from an induction motor is strictly related to slip, being a parameter of the rapidity of flux changing across the rotor winding.

In Figure 2.3-4, Slip-Torque characteristic can be divided into two zones, an unstable region, identified by the starting torque  $T_{AVV}$  and the initial transient, and a stable region where, according to the external load, the working point can be placed. The stable region can further be divided into two parts in relation to its dependency on the slip. For low slip values (moving from right to left on the blue slip axis in Figure 2.3-4) a linear trend could be shown, while increasing the slip (approaching to the maximum torque value  $T_{MAX}$ ) a dramatic change in the curve slope determines a degradation of the torque behaviour.

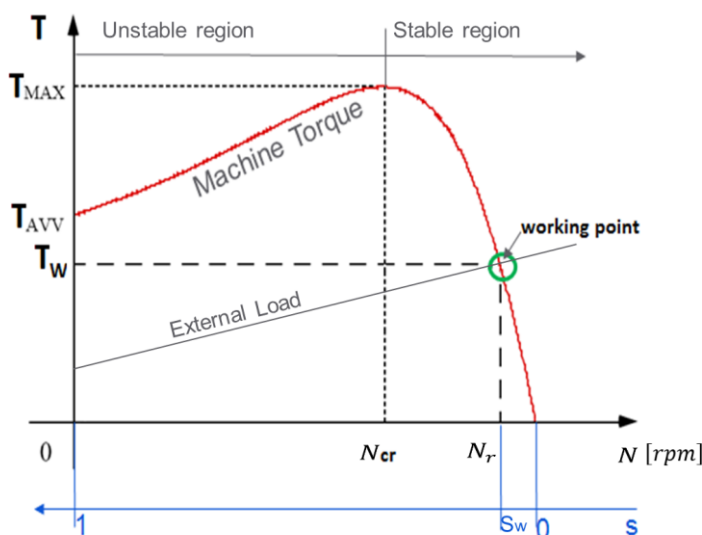


**Figure 2.3-4** Slip torque characteristic and working point for an induction three phase motor.

This phenomenon is strictly related to the slip frequency and to the characteristic of the currents in the rotor bars. According to the previous paragraph, because of the induced EMF, in the rotors conductive elements there will be an AC current oscillating at the slip frequency. From an electrical point of view, the closed circuit, constituting the rotor winding, can be

considered as an electrical impedance characterized by a resistance and an internal inductance which introduces a delay in the rotor bar currents with respect to the induced EMF. This phase displacement will be proportional to the slip frequency. Phase displacement will moreover have effects on the Lorentz forces acting on the conductor: a delay in currents generation will result in a weaker interaction with the rotating magnetic field.

From a practical point of view, we have to balance two contrasting principle, on the one hand increasing the slip results in a growth of the flux change rate on the rotor windings (according to Faraday's law of induction), on the other hand the phase lag results in the breakdown of the Lorentz force.

For low slip values, ranging from 1% in big motors up to 8% in smaller motors, the induced EMF varies at a very low frequency. In this condition, the inductive reactance of the rotor has a secondary effect promoting a direct proportionality between slip and torque (see Figure 2.3-5 a).

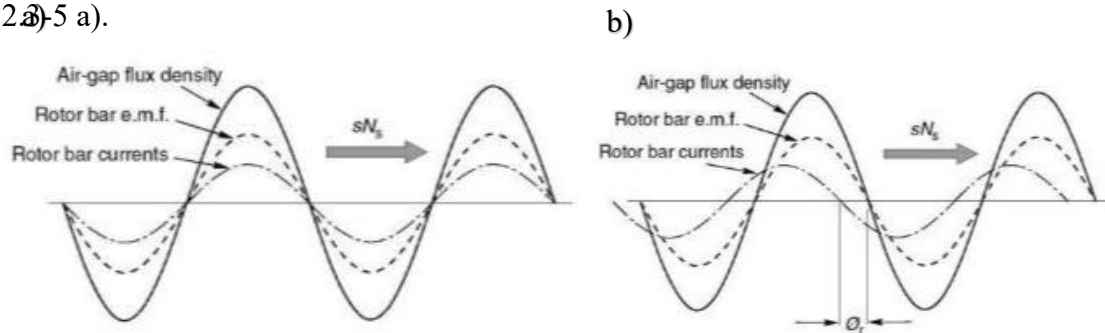


**Figure 2.3-5 a)** Rotor phase diagram for low slip values. **b)** Rotor phase diagram for high slip values.

For high slip values, the effect of the Lorentz force degradation, due to the phase displacement (see Figure 2.3-5 b), becomes predominant resulting in a decrease of the torque which strongly influences the starting torque  $T_{AVV}$ .

To overcome this characteristic several technical solutions have been developed. The *Wound Rotor* construction will be presented as example.

Instead of rotor bars, a wound rotor, presents three sets of windings with connections brought out to three slip-rings mounted on the shaft (see Figure 2.3-6). By connecting the rotor slip-rings to external resistances, it is possible to change the winding impedance characteristic decreasing the phase difference resulting in a higher starting torque.

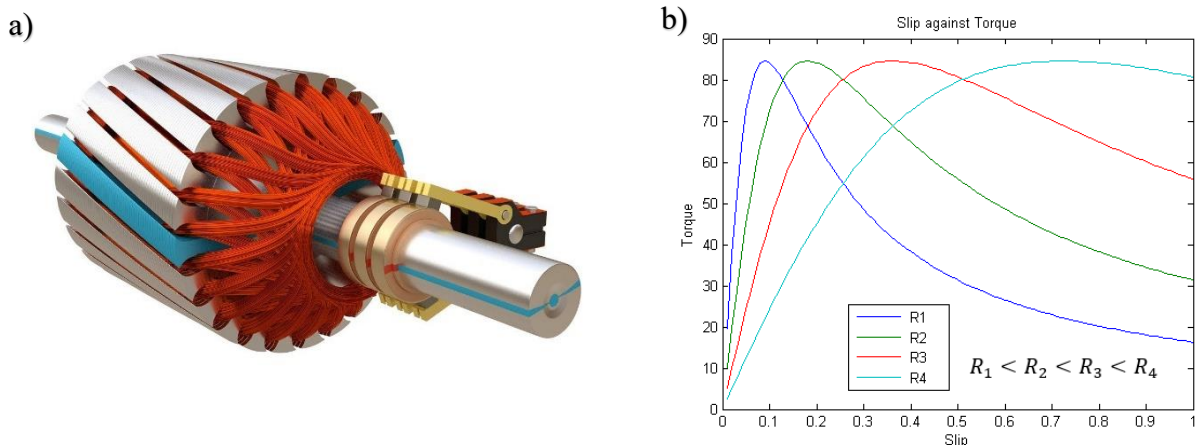


**Figure 2.3-6 a)** Wound Rotor construction. **b)** Slip torque characteristic for different value of external resistances.

Even if this kind of motors requires a more severe maintenance, they are used in application requiring high starting torques like elevators and hoists.

## 2.4 Noise and vibration sources

Electric motor itself is a mechanical system in which different parts interact exchanging forces, motion and power.

As suggested from conventional wisdom, emitted sound and vibration are strictly related phenomena, but the correlation between the vibration sources and the emitting surface is much less intuitive. To clarify this concept let's think to an acoustic guitar. By picking a chord we generate a vibration source, but the sound will be instead emitted by the *Soundboard*. Radiated sound will be therefore the result not only of the vibrating chord but also of the interaction between all the components of the instrument. This easy example introduces two fundamental concepts (that will be further presented in Chapter 6):

- *Transfer Path*: it is the path between the vibration source and the emitting surface.
- *Effectiveness of sound radiation*: it is the capability of a structure to emit sound.

Characterising the sound radiation emitted by an electric motor implies different steps: the identification of vibration sources and of the emitting surface, and the detection of the transfer path between them.

Vibration sources in electrical motor can be divided, to a first approximation, into two main categories: *mechanical* and *electromagnetic*.

By mechanical vibration sources are intended all the perturbation induced by the dynamic behaviour of the rotating system.

Most common mechanical vibration sources are:

- Imbalance: unavoidable residual rotor imbalance will generate system vibrations.
- Bearings: they are a critical component of rotating systems. Bearings can act as a passive element in the transfer path, transmitting vibrations from its source to the emitting surface, or, due to their dynamics, like an active element generating vibrations. Roller bearing vibrations will be further discuss in Chapter 5.
- Misalignment: shaft misalignment is generally introduced by the coupling of the electric machine with the application.
- Cooling system: ventilation needed for the electric motor cooling system is often provide by integrated fans. Fan introduces both, vibrational and acoustic perturbation. On the one hand it influences the dynamics of the rotor, on the other hand the blades motion in the air generates perturbation known as *airborne sound*.

By electromagnetic sources are intended all the vibrations derived by the magnetic interaction between stator and rotor or by the feeding systems. By way of example, VFD feeding will introduce in the system a high noise component characterised by a tonal sound at the same wavelength of the settled carrier frequency (see Paragraph 2.2.1).

All these aspects will be further detailed in the next chapters analysing the measurement procedures and their effects on the system.

## 3 Analysis and Diagnostic

---

In the field of noise and vibrations, understanding the basics of signal theory is essential to perform useful measurements and to correctly interpret measurement results. In this chapter different signal analysis methods will be presented highlighting advantages but also limits.

### 3.1 Signals and Sampling Theorem

Signals may describe any physical phenomenon that changes over time. Analog to digital converters are used to digitalise a signal, so to switch from a continuous behaviour, which characterizes the physical phenomenon, to a discrete sequence of numbers called *samples* (see Figure 3.1-1).

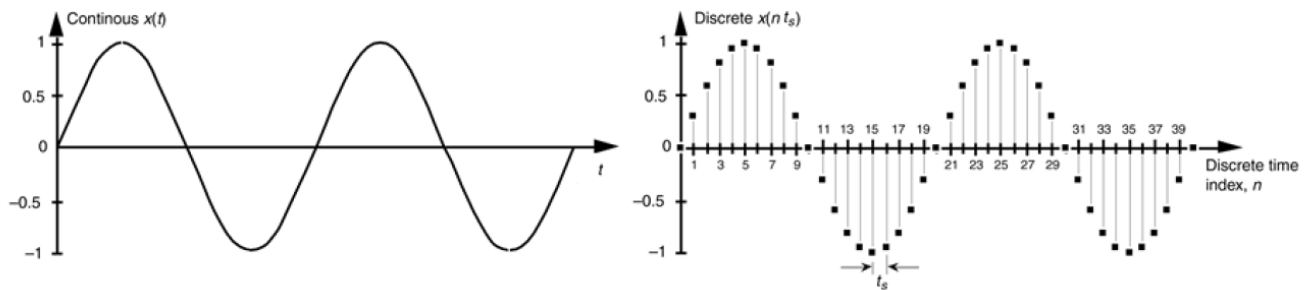


**Figure 3.1-1** Analogue to digital conversion.

The time interval between two consecutive measurements is called *sampling interval*  $t_s$  and its inverse is defined as *sampling frequency* ( $f_s = 1/t_s$ ).

Under the hypothesis of a continuous-time signal of finite bandwidth, *Nyquist-Shannon sampling theorem*, establishes a sufficient condition, for the sampling frequency, such that no actual information is lost in the digitalisation process. This theorem states that a signal should be sampled at least at twice the highest frequency that is present in the signal itself:

$$f_s = 2f_{max}$$

Although this theorem gives important prescription, in practical investigation is almost never possible to know in advance the frequency content of a signal and so to respect the hypothesis of finite bandwidth. To disregard this requirement implies not only the information loss but also, the high-frequency content will interfere with the low-frequency content generating a phenomenon called *aliasing* (see Figure 3.1-2).

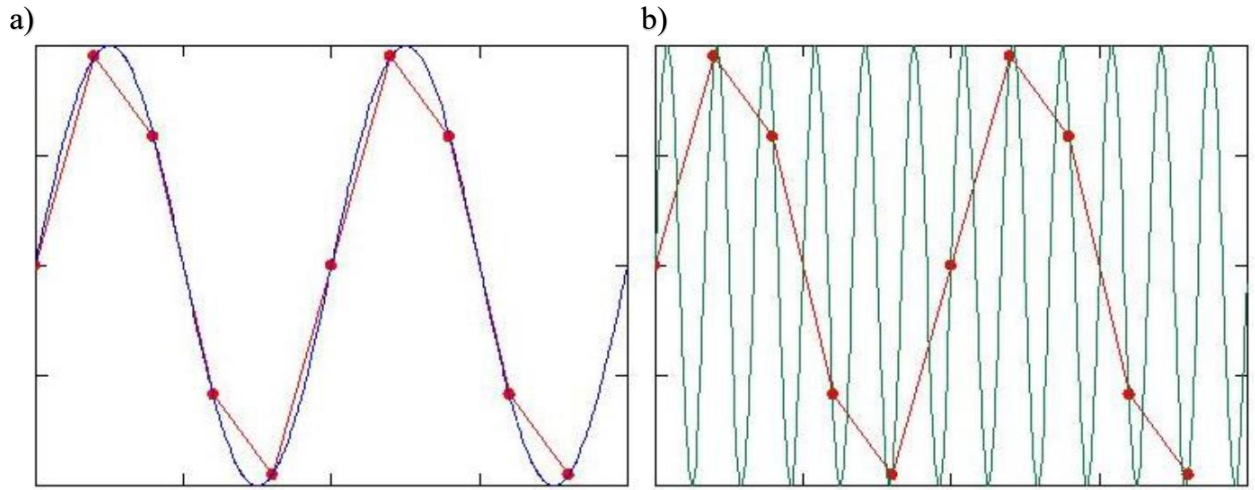


**Figure 3.1-2** **a)** Sampling frequency suitable to analyse the signal. **b)** Undersampled signal, causes the apparent frequency of the reconstructed signal to be much lower than the original signal.

Given a certain sampling frequency, any frequency in the signal higher than the Nyquist frequency ( $f_N = f_s/2$ ) will cause aliasing.

Measured signals usually contain a wide range of frequencies, therefore, to avoid aliasing, a pre-filter is needed to limit the signal's highest frequency before sampling.

With a chosen sampling frequency, a low-pass filter with the Nyquist frequency as the cut-off frequency should be used.

Being the filter non-ideal, to avoid any unexpected aliasing, laboratory practice prescribes to use a sampling frequency of at least 2,56 times the maximum frequency in the signal (stated by the cut-off frequency).

Thanks to its relatively simple approach, time-domain signal processing, is generally used to characterize the response of a system to an excitation. However, it is not possible to analyse the frequency content of the signal which on the other hand is strictly related to the excitation sources.

Specific frequency contents could be directly related to electric motor driven application characteristics or issues, becoming a fundamental instrument in fields of predictive maintenance and troubleshooting.

## 3.2 Frequency-domain Analysis

Joseph Fourier discovered that signals can not only be expressed in the time domain, but that they can equally well be represented in the so-called *frequency domain*. This means that a signal can be represented by a sum of sinusoids, each with its own phase and amplitude.

Frequency domain analysis shows clear advantages in rotating machinery applications and in bearing defects identification.

This paragraph will be devoted to the definition of the frequency domain, analysing the mathematical model and the method used to overcome its limits in real applications.

### 3.2.1 Fourier Transformation and Discrete Fourier Transformation

The Fourier transform is a mathematical tool to express a function in a series of trigonometric functions. In the field of dynamics and noise and vibration analysis it is generally used to transform signals between the time domain and the frequency domain.

The Fourier transform is an extension of the *Fourier series* that results when the period of the represented function is lengthened and allowed to approach infinity.

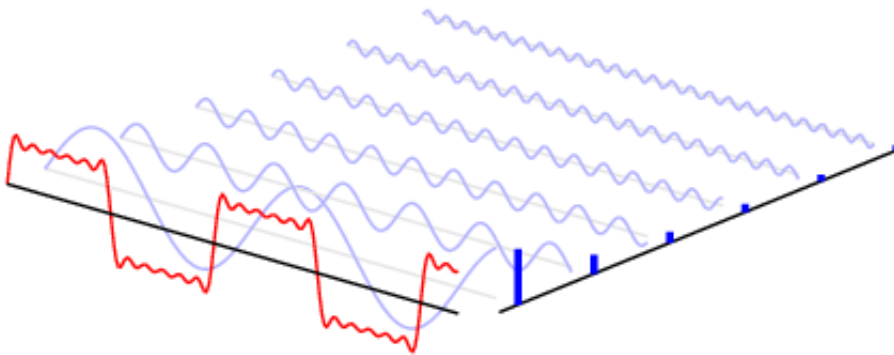


**Figure 3.2-1** A signal (red) decomposed in its harmonic components.

Consider a general signal “ $s(t)$ ” like the red one in Figure 3.2-1. According to the Fourier transformation, it can be defined as a series of harmonic contribution according to the law (*inverse Fourier transform*):

$$s(t) = \int_{-\infty}^{+\infty} \hat{s}(f) e^{i2\pi ft} df$$

being  $\hat{s}(f) = \mathcal{F}[s(t)]$  the Fourier transformation of the time signal  $s(t)$ , defined according to the following equation.

$$\hat{s}(f) = \mathcal{F}[s(t)] \stackrel{\text{def}}{=} \int_{-\infty}^{+\infty} s(t) e^{-i2\pi ft} dt$$

Joseph Fourier was the first mathematician to introduce the inverse theorem, allowing to transpose a signal from the time domain to the frequency domain.

Like any other mathematical instrument, Fourier transformation, to be reliable needs some conditions. In this case the time function  $s(t)$  should be integrable in the interval  $]-\infty, +\infty[$ . This request goes strongly against practical application, in which:

- Time function is almost never known a priori
- Recording time is limited.

Fourier transform applied to digital signals has to be adjusted and the result is called *discrete Fourier transform* (DFT).

As explained in paragraph 3.1, the results of sampling process consist of a sequence  $x[n]$  of  $N$  equally spaced records of a continuous time phenomenon  $x(t)$ , so that:

$$x[n] = x(nt_s), \quad n = 0, 1, 2, \dots, N - 1$$

being  $t_s$  the sampling interval of an overall time interval of  $T = Nt_s$ .

When using discrete signals, the Fourier transformation is computed by means of Fourier series:

$$\hat{x}[\omega_k] \stackrel{\text{def}}{=} \sum_{n=0}^{N-1} x[n] e^{-i\omega_k n T/N}$$

being  $\omega_k$  the discrete frequency in  $[rad/s]$ . The frequency resolution, which is the minimum change in frequency content detectable in the spectrum, is strictly related to the sampling frequency according to the law:

$$\Delta f = \frac{1}{T} = \frac{1}{Nt_s} = \frac{f_s}{N}$$

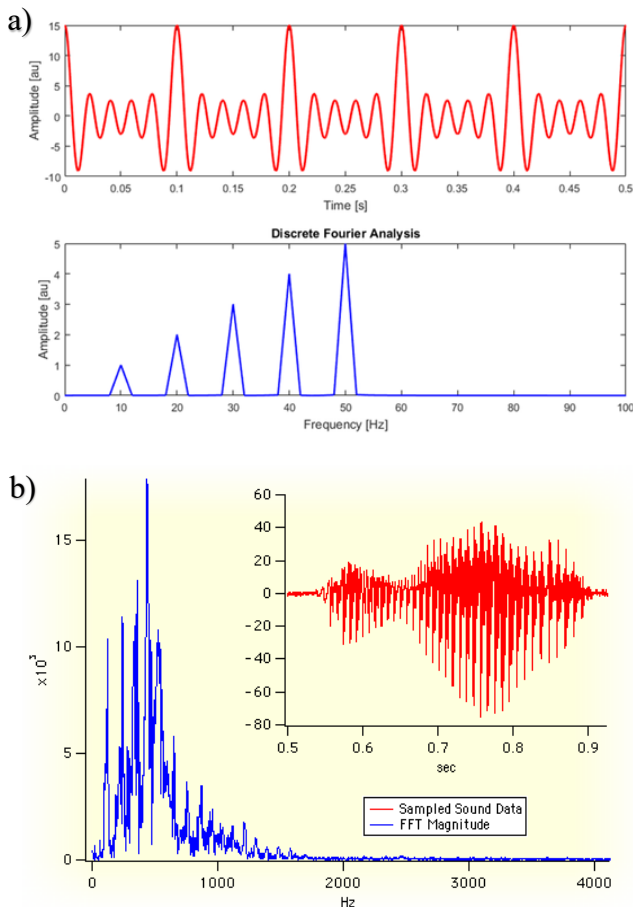


**Figure 3.2-2** a) DFT of a signal. b) Real spectra of an acoustic signal.

In practice a *fast Fourier transform* (FFT) algorithm is used to compute the discrete transformation.

The FFT can be applied to finite time signals, by replicating the signal itself to reach periodicity (see Figure 3.2-3).

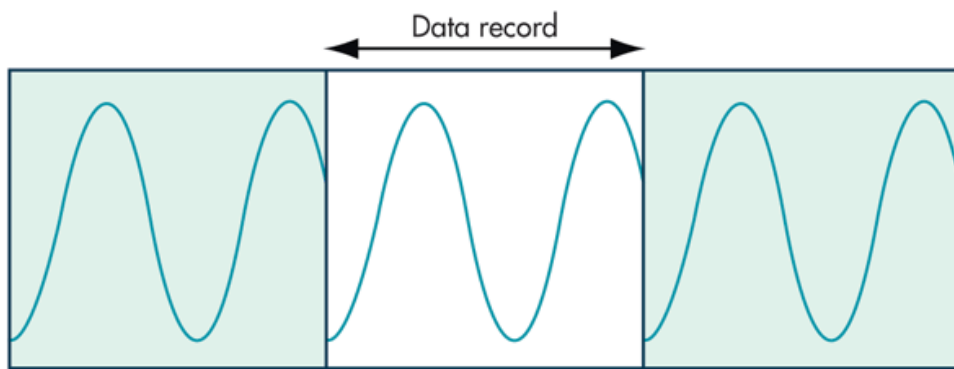


**Figure 3.2-3** Schematization of signal repetition.

Being the periodicity of the analysed signal almost never known in advance, and in some case even not existing, the signal replication generates discontinuities. This deviation from the

mathematical model causes in the Fourier spectrum a smearing of energy around the true frequencies of the signal. This phenomenon is called *leakage* and it can be reduced by multiplying the signal to a so-called *windowing* function.

As a general rule windowing functions cause the boundary of the signal to be suppressed while retaining the centre part of the signal. There are many different types of windowing function according to the needs of particular application, in this paragraph the *Hann* window will be presented by way of example.

The Hann (or cosine taper) window for a signal in the time interval between 0 and  $T$  is defined by:

$$\omega_H(t) = 0,5 - 0,5 * \cos\left(\frac{2\pi t}{T}\right)$$

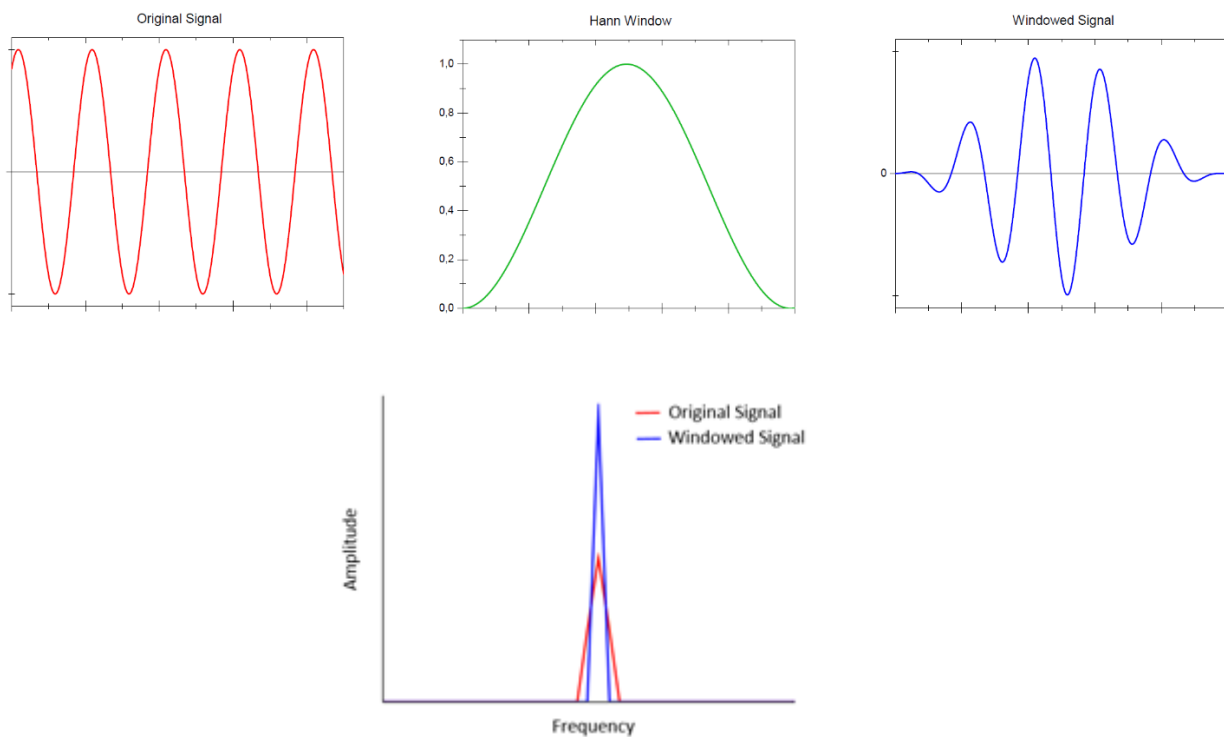


**Figure 3.2-4** Signal transformation by Hann windowing.

### 3.2.2 Convolution theorem

Convolution is an important technique used in signal analysis and image processing. Convolution theorem is particularly useful to understand spectra of two signals multiplied with each other.

From a mathematical point of view, convolution between two signals in time domain is defined as:

$$s(t) * q(t) = \int_{-\infty}^{+\infty} s(\tau)q(t - \tau)d\tau$$

Which formally indicates the multiplication of the function  $q(t)$  with the function  $s(t)$  when the former is shifted over the latter.

The main disadvantage of convolution is its computational complexity, and the interpretation of its results. However, it can be proved that the convolution in time domain can be turned in a simple multiplication in frequency domain and vice versa:

$$\begin{aligned} s(t) * q(t) &\xleftrightarrow{\mathcal{F}} \hat{s}(f)\hat{q}(f) \\ \hat{s}(f) * \hat{q}(f) &\xleftrightarrow{\mathcal{F}} s(t)q(t) \end{aligned}$$

being  $\hat{s}(f)$  and  $\hat{q}(f)$  the Fourier transform of  $s(t)$  and  $q(t)$ .

This behaviour makes the convolution easier to be performed in frequency domain and its results more intuitive.

### 3.2.3 Dirac's delta and impulse transformation

Impulse like excitations are quite common in rotating machinery analysis, as they can be generated by local defects in the bearing's components or by dirt particles.

In order to understand how to interpret the spectrum we need a mathematical model to be adapted to real cases.

Dirac's delta distribution is defined by the following property:

$$\delta(t) = \begin{cases} 0 & t \neq 0 \\ \infty & t = 0 \end{cases}$$

with,

$$\int_{-\infty}^{+\infty} \delta(t)dt = 1$$

It is "infinitely peaked" at  $t = 0$  with the total area of unity.

The important property of the delta distribution is that, given a time function  $s(t)$ , it is possible to state:

$$\int_{-\infty}^{+\infty} s(t)\delta(t)dt = s(0)$$

for any function  $s(t)$ .

It can be proved that the Fourier transform of Dirac's delta distribution is:

$$\mathcal{F}[\delta(t)] = \int_{-\infty}^{+\infty} \delta(t) e^{-i2\pi f t} dt = 1$$

Which is a unitary constant function in frequency domain.

Dirac's delta distribution is, in real application, never reachable, pulse like excitation are more similar to short rectangular function.

Given a rectangular function in time  $x(t)$ , with unit length and amplitude, its Fourier transform will be:

$$\mathcal{F}[x(t)] = \int_{-\infty}^{+\infty} x(t) e^{-i2\pi f t} dt = \frac{\sin(\pi f)}{\pi f}$$

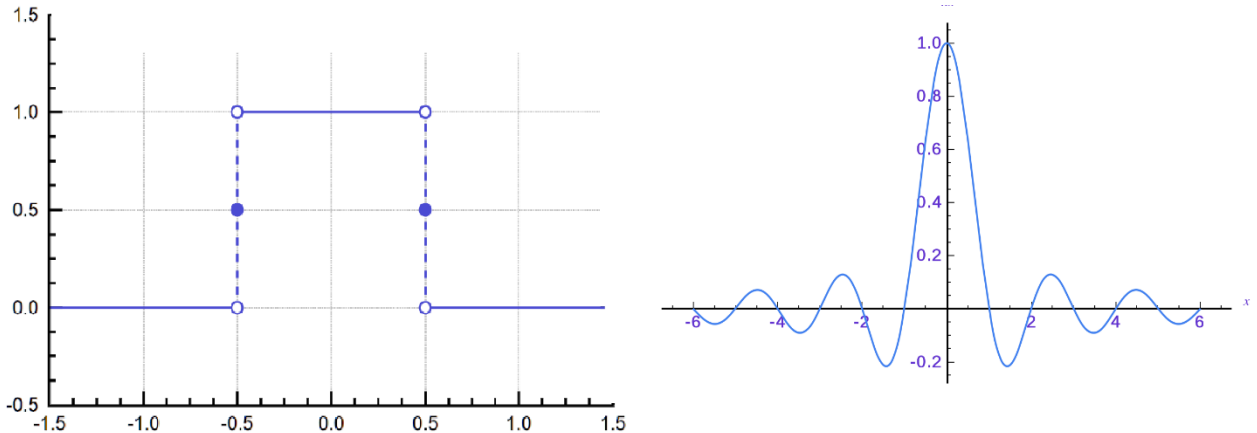


**Figure 3.2-5** Rectangular function and its Fourier transform.

### 3.2.4 Repetitive pulse

In real application is quite common to face repetitive pulses; this phenomenon could be caused by surface defects on rolling bearings. Each time a rolling element rolls over a defect, a pulse will be generated.

To understand what to expect, let's consider a rectangular function  $x(t)$  which repeats itself with a period  $T$  (see Figure 3.2-6).

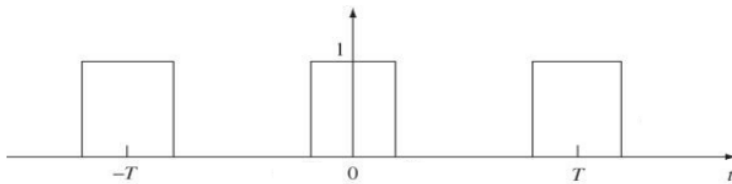


**Figure 3.2-6** Rectangular pulse train of period  $T$ .

Such a pulse train can be seen as the convolution of the time function  $x(t)$  with a series of Dirac's pulses  $p(t) = \sum_{n=-\infty}^{\infty} \delta(t - nT)$ , so that the final signal can be written as:

$$s(t) = p(t) * x(t) = \int_{-\infty}^{+\infty} \left[ \sum_{n=-\infty}^{\infty} \delta(\tau - nT) \right] x(t - \tau) d\tau$$

Transporting it in the frequency domain we get:

$$\hat{s}(f) = \hat{p}(f)\hat{x}(f)$$

It can be proved that the Fourier transform of a pulse train is again a pulse train, so  $\hat{s}(f)$  will be a pulse train whose amplitude follows  $\hat{x}(f)$  (see Figure 3.2-7).

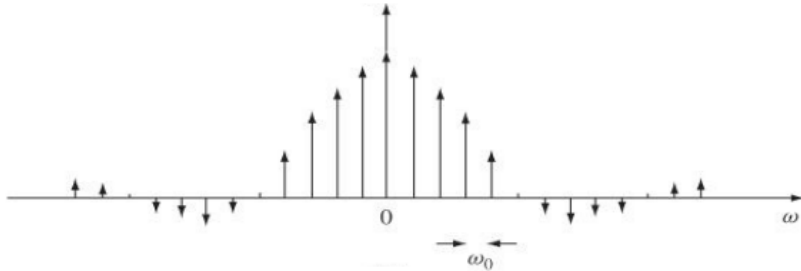


**Figure 3.2-7** Coefficient magnitude of the Fourier transform.

Pulses excite all the system frequencies generating broad spectra, this phenomenon added to the background noise of the machinery could make it difficult, in practical application, to recognize repetitive pulse excitations.

### 3.2.5 Modulation

Fluctuation of load or changing in the distance between the excitation and the sensing apparatus will result in a *modulation* of the signal. Modulation occurs when a signal behaviour is modified by another signal.

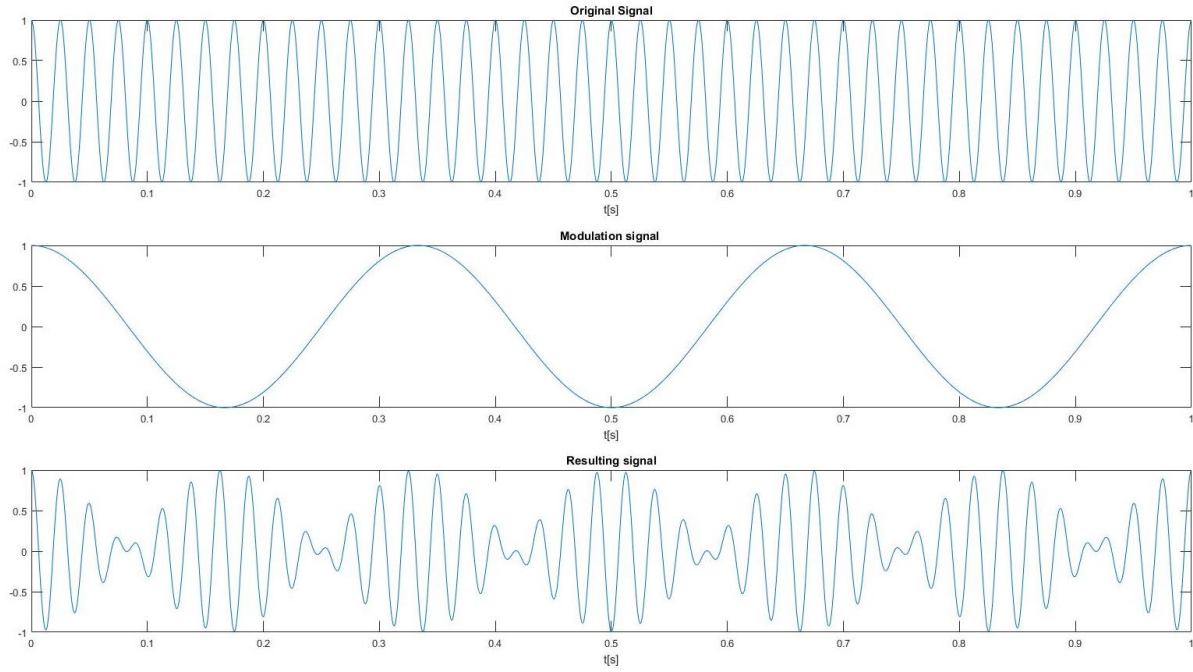


**Figure 3.2-8** Signal modulation.

By way of example let's suppose to have a 40 [Hz] (figure 3.2-7 a) cosine signal modulated by a 3 [Hz] cosine signal (figure 3.2-7 b), the resulting signal  $s(t)$  will be:

$$s(t) = \cos(3t) \cos(40t) = \frac{1}{2}(\cos((40 + 3)t) + \cos((40 - 3)t))$$

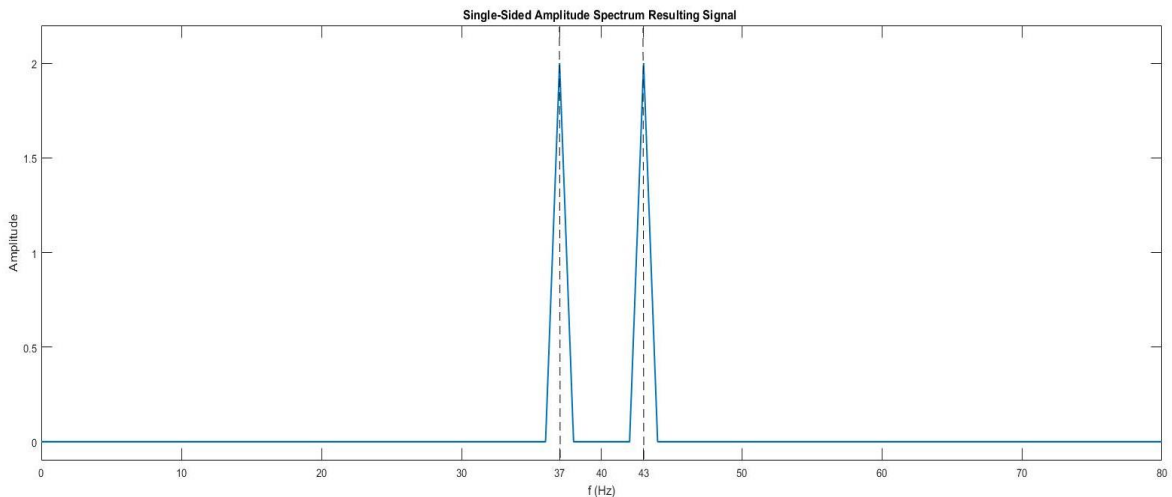


**Figure 3.2-9** Resulting spectra of a modulated signal.

As possible to see in Figure 3.2-9 the 40 [Hz] frequency disappear and is replaced by two side-bands at 37 [Hz] and 43 [Hz]. In this case, result can be easily obtained by using trigonometrical equation but it can be proved that the same results can be obtained by using convolution in frequency domain. Although it could seem a complication in the analysis, modulation can be used as a trademark of some specific types of damages.

### 3.2.6 Envelope

As said in the previous paragraph, energy spread along the spectrum due to pulses or pulses train could cause defects to be hidden when relatively simple time domain or frequency domain analysis are performed. Specialised analysis methods have been developed in order to better detect such a signal.

*Envelope* technique is of large use in bearing defects analysis. When a rolling element rolls over a surface defect or a dust particle, it generates pulses characterize by low amplitude at higher frequencies than the normal vibration of the application.

The envelope algorithm will be explained by following the example of Figure 3.2-11. A signal (sinusoidal) at 10 [Hz] is disturbed by a pulse-like excitation with a repetition frequency of 30 [Hz] and a centre pulse frequency of 250 [Hz] (see Figure 3.2-10).

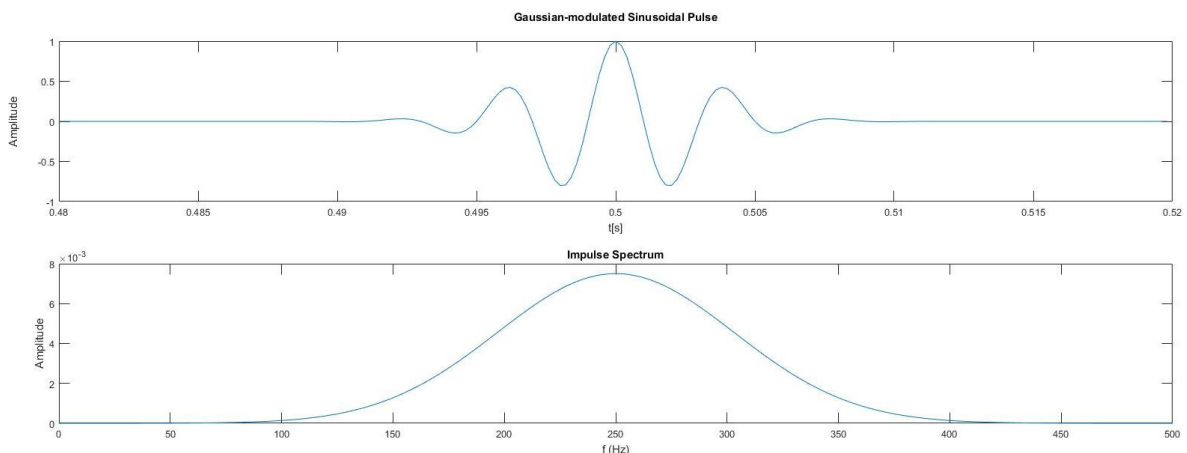


**Figure 3.2-10** Gaussian-modulated sinusoidal pulse with a centre pulse frequency of 250 [Hz] and its FFT.

Although the 30 [Hz] excitation is almost clear in time domain there is no trace in the spectrum (see Figure 3.2-11 a).

Envelope algorithm is made of different steps, in this section, they will be listed and explained:

- Band-pass filter: in the first step a frequency range of interests is settled. In this way it is possible to avoid the interference of other phenomena. This step is crucial because it

could be difficult to know in advance in which band the repetitive impulsive event is located. On field experience and a good knowledge of the application working point and components could help in setting the right band.

- Rectification: once the time signal has been filtered, it is rectified by a power function. As seen in Paragraph 3.2.4 when a pattern is repeated in time domain, its frequency content is “sampled” in frequency domain. The sampling frequency will be equal to the repetition frequency. In Figure 3.2-11 a it is possible to see two side bands at 30 [Hz] from the centre pulse frequency of 250 [Hz]. Using a power function of the time domain signal, implies convolution in frequency domain. This means that the 30 [Hz] spacing will result in a high response at 30 [Hz] (see Figure 3.2-11 c).
- Low-pass filter: in order to make the results clearer, a final low-pass filter is added. In this way the results are smoother and the interference with higher frequency phenomena is avoided.

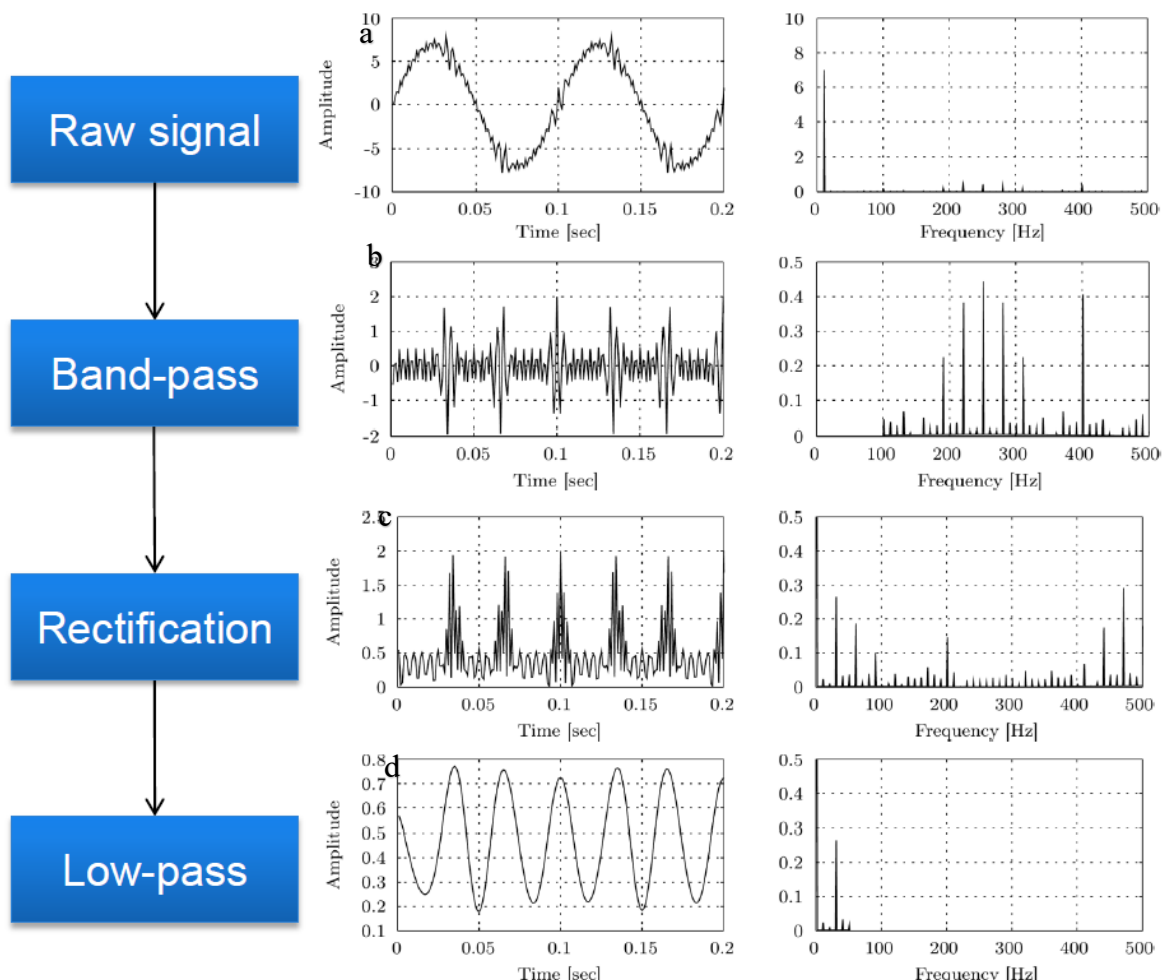


**Figure 3.2-11** Envelope algorithm schematization.

Although envelope technique is a powerful instrument in bearings defects analysis, it has some limits. As said before, its results strongly depend on the band-pass filter choice and moreover small irregularities in bearing rotation could cause oscillations of the repetition period.

Other, more advanced, methods have been developed, based on envelope, in order to overcome these limits, but they will not be analyzed in this thesis.

### 3.3 Time-Frequency Analysis

A time-frequency analysis visualizes the changes of a spectrum over time. These methods are generally used to analyze non-stationary phenomena, like transient, or to detect impulsive or temporary phenomena which are non-repetitive, like dirt particles or temperature gradients.

#### 3.3.1 Short Time Fourier Transform and Spectrogram

Spectrograms are used to trace the trend of the frequency content of a phenomenon changing in time. They are obtained by sliding a window  $w(t)$  over the acquired signal  $a(t)$ . The frequency spectrum, at each time position, will be defined by the Fourier transform of the signal lying under the window. This algorithm is called *Short Time Fourier Transform*.

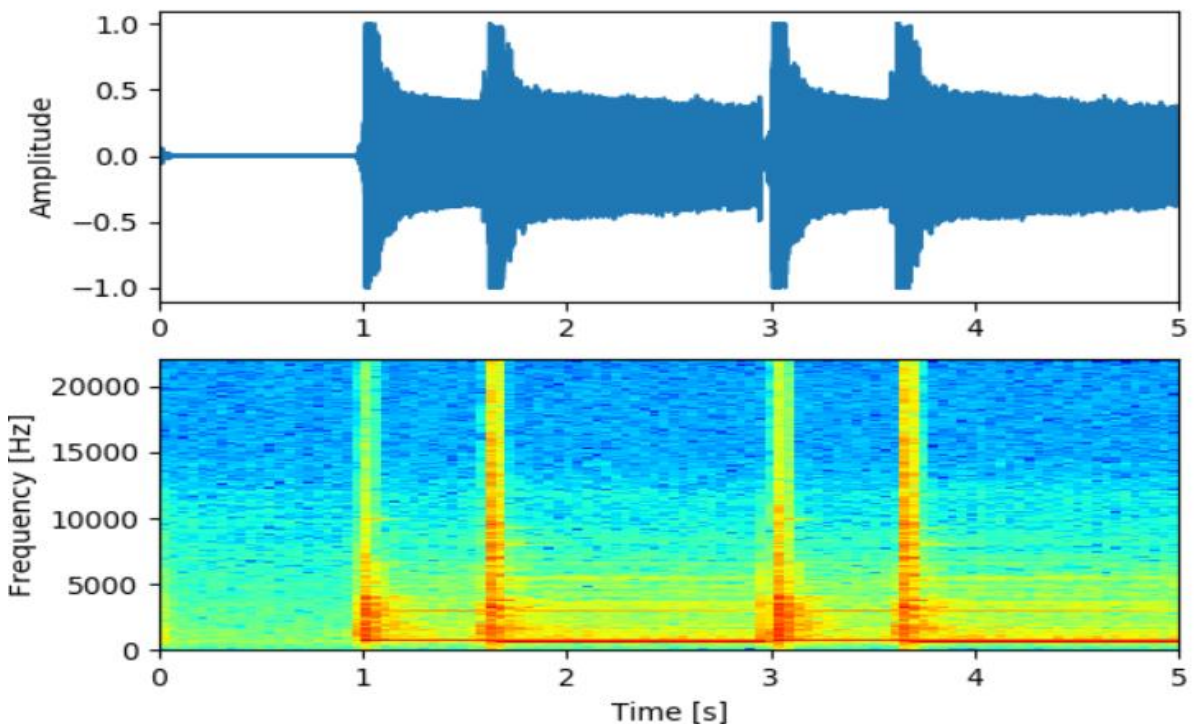


**Figure 3.3-1** Spectrogram example.

From an operative point of view, spectrogram requires a proper choice of the windows and a long acquisition time, but it is anyway a powerful instrument to detect impulsive phenomena or to obtain a preliminary overview of the application condition.

## 4 Induction Electric Motor Failure Analysis

---

This chapter will be devoted to the failure analysis of a *Three Phase Induction Electric Motor*, providing a bridge from the theoretical knowledge of the working principles and signal analysis, to actual monitoring and measuring practice.

The chapter will be divided into two parts, a general presentation of the instrumentation and the setting parameters, relevant for the measurements, and the analysis of the most common failure causes from both the physical and the vibrational point of view.

### 4.1 Vibration Analysis Process

Measuring and presenting a vibration signal requires a series of electronic devices, all fulfilling an essential task (see Figure 4.1-1).

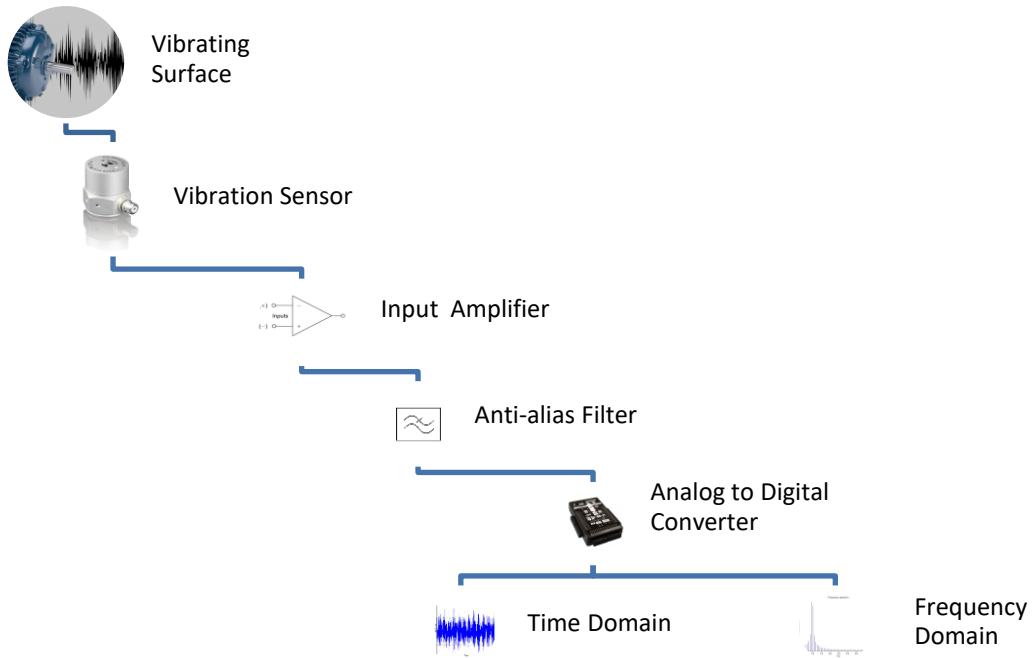


**Figure 4.1-1** Schematic view of a vibration measurement process.

The initial vibration is acquired by the sensor, which produces a very weak signal which has to be amplified. After being amplified, the signal is filtered to avoid aliasing and digitalized at a fixed sampling frequency. Obtained signal can be finally presented in time domain or can be used for further post-processing (like FFT or Envelope) on the basis of the items under investigation.

The resulting measurement is strictly influenced by the elements involved in the process, so it is important to understand components role and limits.

#### 4.1.1 Vibration Sensors

A vibration measured on the surface of a structure can be expressed in one of the three time-dependent variables in the equation of motion: displacement " $x$ ", velocity " $\dot{x}$ " and acceleration " $\ddot{x}$ ". This quantity can be measured directly (according to the sensor type) or derived one from the other. Once reported in the frequency domain, they can be converted using simple multiplication or division of the original signal amplitude (see Figure 4.1-2).

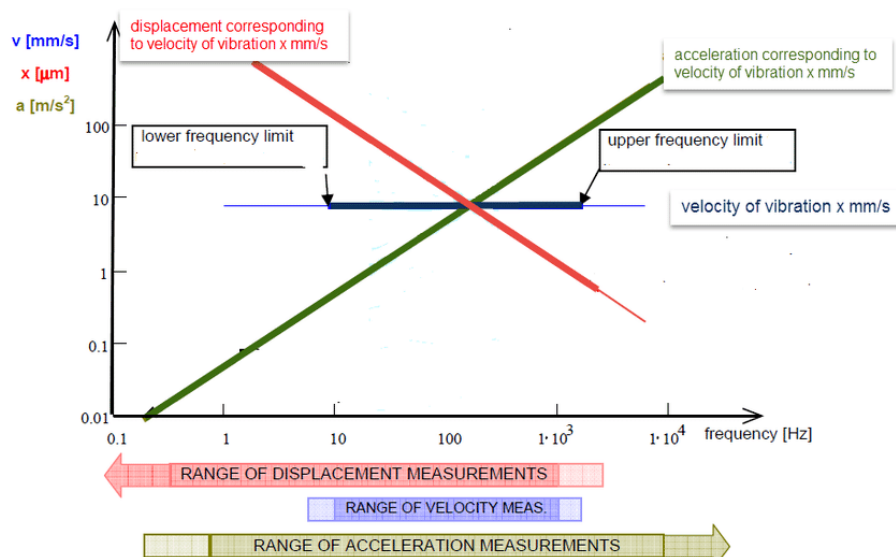


**Figure 4.1-2** Typical relation between displacement, velocity and acceleration for a sinusoidal single frequency vibration.

It is clear that, even if each quantity can be derived from any of the other, different types of sensors are more suitable, or in some case strictly requested, in different applications.

Accelerometers are the most used sensor in vibration measurements, because of their cost effectiveness, the good obtainable resolution and because their design can be easily adapted for a specific frequency range.

Market offers a wide range of accelerometers different by technology and application fields. In this thesis the *Piezoelectric Accelerometers* will be analysed, being the most common and the type used in the test campaign presented in Chapter 7.

Figure 4.1-3 shows the working scheme of a piezoelectric accelerometer mounted on a vibrating element. Indicating with the subscript " $b$ " the quantity related to the vibrating basement, the motion equation of the system can be written as:

$$m\ddot{x} + c\dot{x} + kx = c\dot{x}_b + kx_b$$

being  $m$  the seismic mass in [ $Kg$ ],  $c$  the damping in [ $Ns/m$ ] and  $k$  the stiffness in [ $N/m$ ].

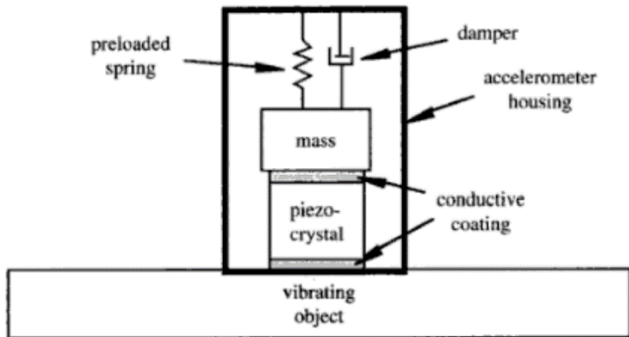


**Figure 4.1-3** Schematic drawing of a piezoelectric accelerometer.

Transfer function can be calculated between motion of the vibrating base and the motion of the seismic mass obtaining the *Frequency Response Function* (FRF):

$$H(\omega) = \frac{x(\omega)}{x_b(\omega)} = \frac{1 + 2i\xi(\omega/\omega_n)}{1 - (\omega/\omega_n)^2 + 2i\xi(\omega/\omega_n)}$$

with  $\omega_n = \sqrt{k/m}$ ,  $\xi = c/2\sqrt{mk}$  and  $i$  is the imaginary unit.

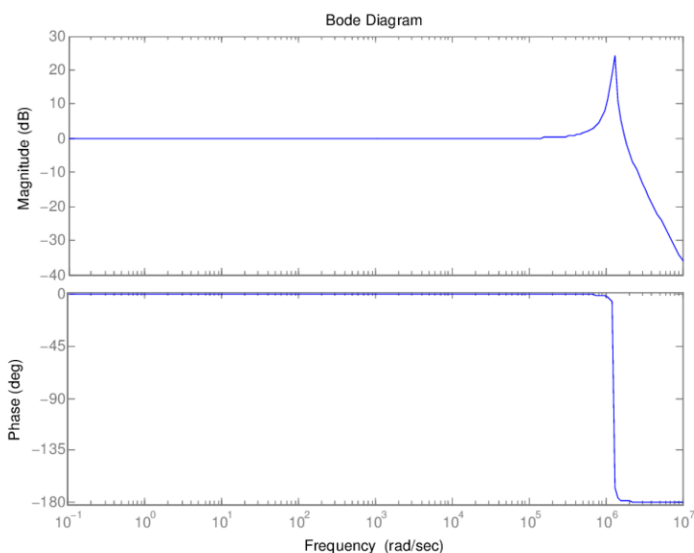


**Figure 4.1-4** Bode diagram of an accelerometer.

By tracing the *Bode diagram* of the accelerometer (see Figure 4.1-4) it is possible to understand that there is a linear zone in which the amplitude of the response signal is almost not influenced by the vibration frequency. This behaviour (obtained by correctly choosing the

accelerometer parameters  $m$ ,  $k$  and  $c$ ) influences one of the main parameters of the accelerometer, the *Bandwidth*.

Another important aspect in choosing an accelerometer is its *Sensitivity*, which refers to the conversion ratio between the physical quantity and the output voltage. Sensitivity is generally measured in Volts per unit of acceleration ( $[V/g]$ ). It could be improved by increasing the seismic mass, but this will also lower the resonance frequency implying a reduction of the bandwidth.

#### *Dynamic*

- Sensitivity: 100 mV/g
- Sensitivity precision:  $\pm 10\%$  at  $+25^\circ\text{C}$  ( $+77^\circ\text{F}$ )
- Acceleration range: 80 g peak
- Amplitude linearity: 1 %
- Frequency range:
  - $\pm 10\%$ ; 1.0 to 5 000 Hz
  - $\pm 3\text{ dB}$ ; 0.7 to 10 000 Hz
- Resonance frequency: Mounted, minimum 22 kHz
- Transverse sensitivity:  $\leq 5\%$  of axial



**Figure 4.1-5** Real accelerometer data sheet.

The proper response of the accelerometer also depends on its mounting (see Figure 4.1-6). In order to obtain reliable measurements, the connection must be always as rigid as possible (especially for high frequency content). For this reason, adhesion by mean of beeswax, cement glue or bolted connection are the most common sensor mounting methods.

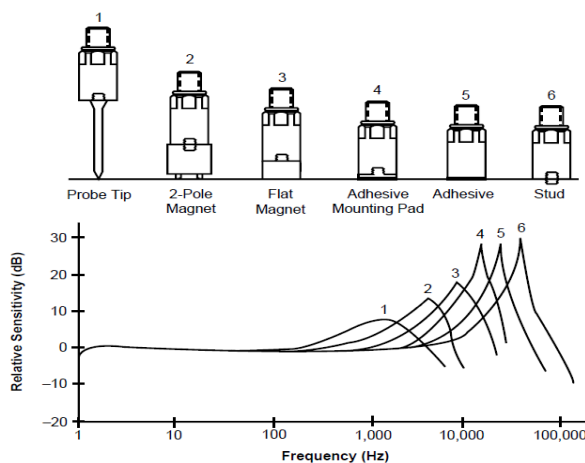


**Figure 4.1-6** Schematic relation between mounting and bandwidth.

#### 4.1.2 Analog to Digital Converter

Vibrating sensors provide continuous time signal which has to be discretized before being processed. As presented in previous chapter, this is the task of the *Analog to Digital Converters* (ADC).

Details of ADC's architecture and working principles are out of the scope of this thesis, so the presentation will be limited to the main ADC parameter influencing the measurement.

One of the main parameters of the ADC is its *Resolution*. Resolution,  $Q$ , indicates the discretization of the amplitude (vertical axes). This parameter is strictly related to the *Number of bits* " $n_{bits}$ " of the ADC according to the relation:

$$Q = \frac{E_{FSR}}{2^{n_{bits}} - 1}$$

where  $E_{FSR}$  is the *full-scale voltage range*, defined by overall voltage measurements range.

Resolution determines the minimum measurable variation and the magnitude of the quantization error. While the number of bits is imposed by the ADC, the full-scale range is, in many actual devices, regulable as function of the expected outcomes. Choosing the right interval allows to minimize the errors and obtain reliable measurements.

Another important parameter to keep in mind when setting the ADC is the *frequency resolution*, which as expressed in Chapter 5, is dependent on the sampling frequency and on the number of sampling (so to the acquisition time) by the relation:

$$\Delta f = \frac{1}{T} = \frac{1}{Nt_s} = \frac{f_s}{N}$$

A very short frequency resolution implies an elongation of the measurement and processing time, which in the actual monitoring practice is not advisable. Moreover, since a measurement is expected to be representative of a specific working condition of the application, a too long acquisition time increases the possibility of external disturbance.

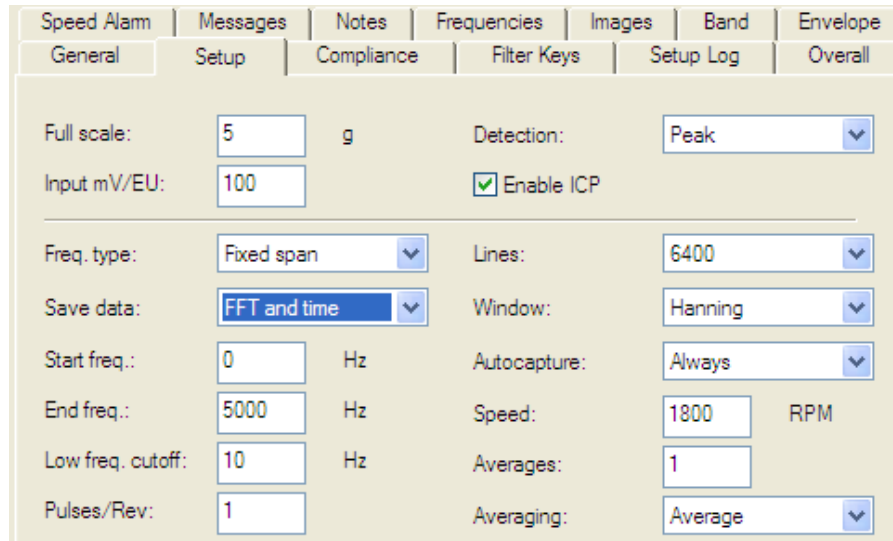


**Figure 4.1-7** User setting interface of a real portable vibration analyser.

Figure 4.1-7 shows the setting interface of a vibration analyser. The frequency resolution is, in this case, not directly expressed but it can be derived by the parameter “*lines*”, dividing the frequency range (from 0 to 5000 [Hz]) by the number of lines (6400), with respect to the example of Figure 4.1-7. It is interesting to note that in this case the acquisition time is not settable, but it will be defined by the system in relation to the required frequency resolution.

## 4.2 Damage Detection in Asynchronous Three Phase Electric Motor

In this part of the chapter the principal damages detectable in asynchronous three phase electric motor will be analysed from the vibrational point of view. The presentation will be divided into four parts: baseline (normal vibration for a well-functioning motor), stator damages, rotor damages and mounting problems.

### 4.2.1 Baseline

As presented in Chapter 2, very strong forces are exchanged between rotor and stator. The impossibility to operate with an ideal constant airgap and the dynamic property of the rotor

will anyway generate vibrations, also for a well-functioning motor.

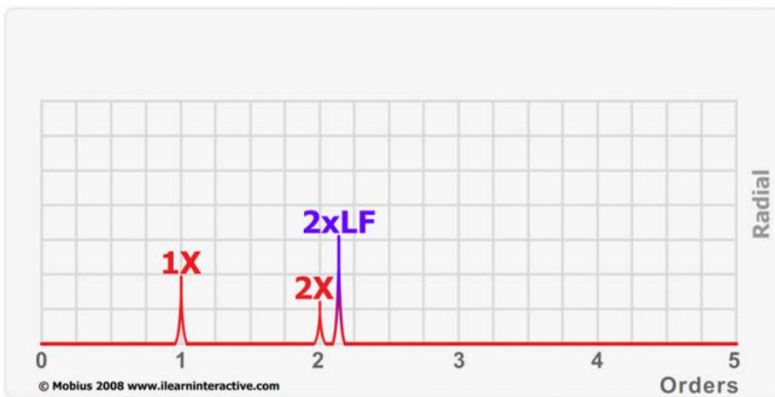


**Figure 4.2-1** Expected spectrum for a well-functioning motor.

Figure 4.2-1 shows the expected spectra for a new electric motor without evident damages.  $1X$  indicated the rotation speed of the rotor, consequently “ $#X$ ” will be its integer multiples. This notation is quite common in vibrational analysis when dealing with rotational machine and it will be used from now on.

The spectrum shows two main effects:

- Peaks at the rotational speed  $1X$ , and its harmonic at  $2X$ : they are generated by the rotor residual unbalance.
- A peak at twice the line frequency “ $2xLF$ ”: it is due to the magnetic interaction between the rotor and the stator which variates at twice the feeding frequency. This effect is known as *Magnetostriction* and it is always present in electric motor spectra.

It is interesting to note that the second harmonic of the rotational speed could be very similar to the peak at twice the line frequency but not equal (the case of asynchronous motor). A high level of frequency resolution could be requested to well distinguish them in a real spectrum.

## 4.2.2 Stator Issues

Stator damages could be of electrical or mechanical nature. Stator is the stationary part of the electric machine and it has to provide structural support and connection to the power grid.

### 4.2.2.1 Static Magnetic Field Unbalance

When the magnetic field is statically unbalanced the effect will result in a localized increase of the magnetostriction effect. This effect, as seen for the baseline, generates vibration at twice the line frequency.

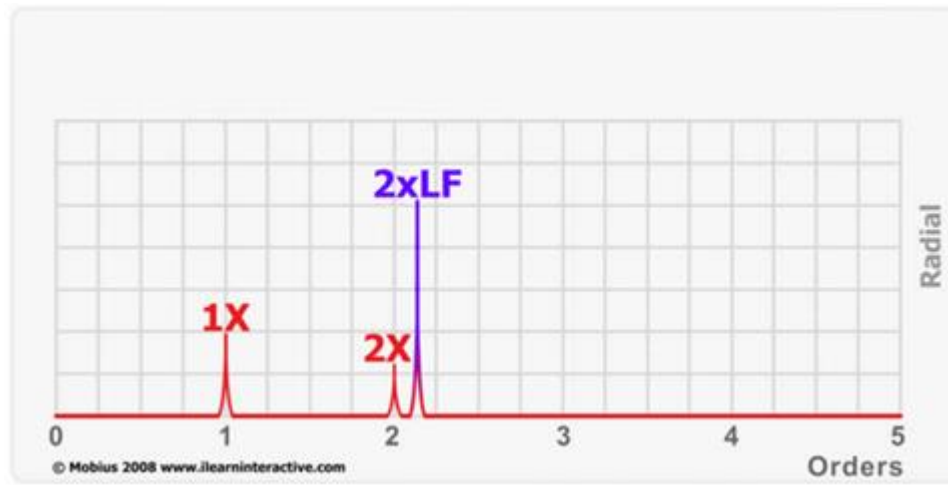


**Figure 4.2-2** Expected spectrum for magnetic field unbalance.

The issues which can generate a magnetic field unbalance, can be of different nature:

- Stator eccentricity: it is the case in which the rotor is not spinning in the centre of the stator.

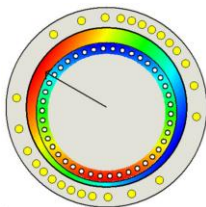


**Figure 4.2-3** Airgap discontinuity for a rotor static eccentricity.

- Loose iron and shorted laminations: it is the case in which the issues involve stator electrical problems. Loose iron and shorted laminations generate a localized loss of electric power which results in the variation of the stator magnetic field intensity. The resulting spectra is the same as in Figure 4.2-2.
- Soft foot and warped bases: these are problems related to the anchorage of the motor. If the motor base is not perfectly planar, the hold down bolts generate a distortion of the frame resulting in an uneven airgap. This problem can be easily solved by the use of shims or acting on the foundation.

#### 4.2.2.2 Loose Connection

Normal motor vibration could cause the electrical connections to become weak. In the limit case of one feeding phase missing the spectrum will result as in Figure 4.2-4.

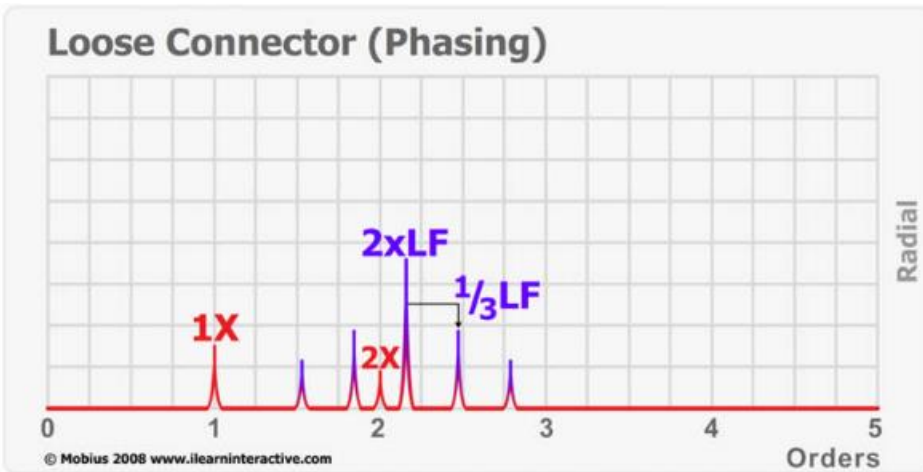


**Figure 4.2-4** Expected spectrum for loose connection issues.

Like other stator problems, the effects are to be searched in the proximity of twice the line frequency. The spectrum shows sidebands (of “ $2xLF$ ”) spaced of one third of the line frequency, which is a typical example of modulation (as presented in Chapter 5). The absence of one feeding phase will generate a discontinuity in the rotating field velocity. According with modulation theory the resulting signal can be seen as the composition two signals, the rotating magnetic field and a disturbance acting at one third of the rotating field frequency.

#### 4.2.2.3 VFD Powered Motor

When the motor is powered by VFD the line frequency will depend on the chosen settings, so the peak at twice the line frequency will be translated. Another important characteristic of VFD driven motor is the high frequency content generated by its working principle.

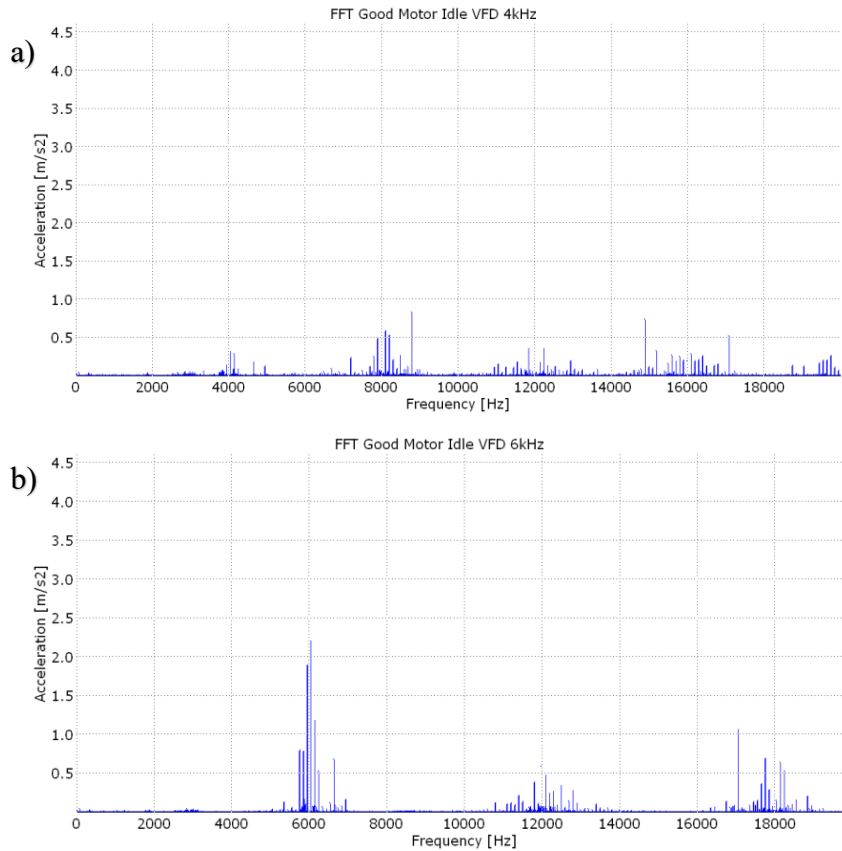


**Figure 4.2-5** VFD driven motor spectra for two different carrier frequency: a) 4 [KHz], b)6 [KHz].

Figure 4.2-5 shows how the VFD introduces high frequency content in relation to the imposed carrier frequency and its harmonics.

### 4.2.3 Rotor Issues

Rotor related problems could be of mechanical or electrical nature. Rotor is the rotating part of the machine, devoted to the mechanical power transmission. Rotor vibration could be generated by rotor issues themselves or can be induced by the coupled load. In this part we will analyse only the rotor damages without considering its connection to the external load. As a general rule, rotor problems induce unbalancing phenomena rotating in space. Relative position between sensors and unbalancing phenomena will therefore change in time inducing modulation phenomena.

#### 4.2.3.1 Eccentric Rotor

As in the case of eccentric stator, this phenomenon generates an uneven airgap, but in this case it rotates at the same speed of the rotor. The motion of the discontinuity sources compared to the sensor position generates modulation and sidebands.

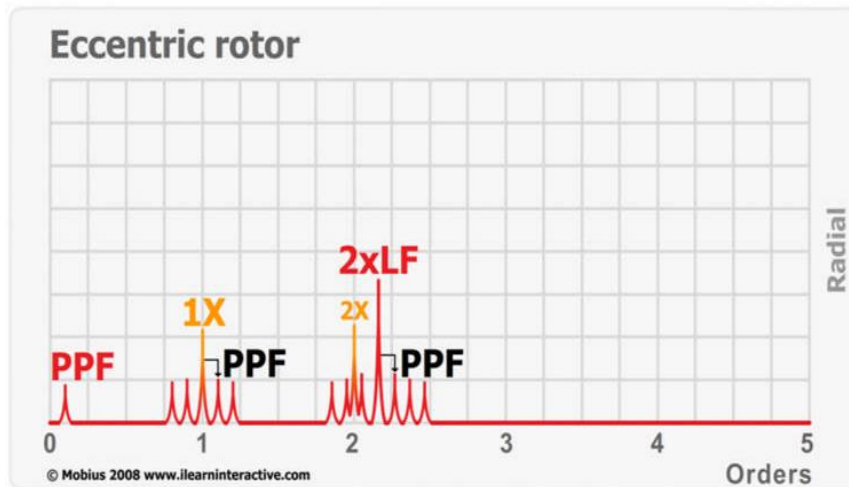


**Figure 4.2-6** Expected spectrum for loose connection issues.

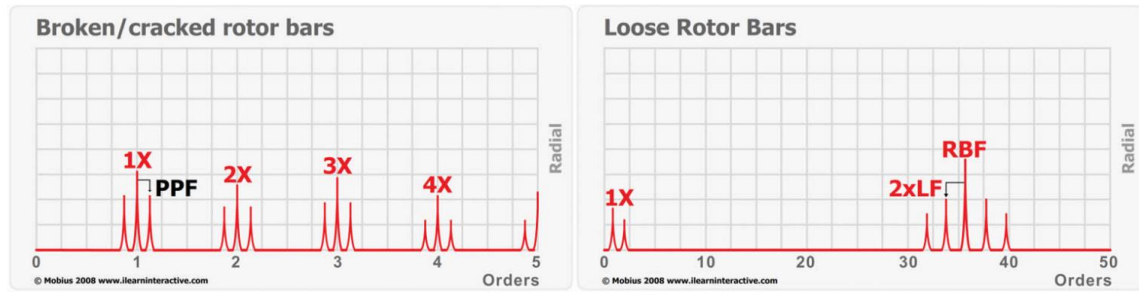
Figure 4.2-6 shows sidebands of both the rotor speed “1X” and twice the line frequency. Sidebands are spaced by the *Poles Pass Frequency* (PPF), which is defined as the slip frequency multiplied by the number of poles.

$$PPF = F_s p$$

The modulation is not related to the absolute velocity of the discontinuity sources, but to the relative motion between the rotor eccentricity and the stator rotating magnetic field. Slip values are generally very low (1% for big motors), so to well identify sidebands a high level of resolution should be set.

#### 4.2.3.2 Broken Rotor Bar

Rotor bar problems are quite common in motor working in frequent start/stop condition. During transient, currents in the rotor rise at much greater level than the steady working condition, generating overheating and rapid thermal expansion. This behaviour causes strains, which along with high level of torque could cause bar crack or looseness. Rotor bar issues induce an increase in other rotor bar currents, which try to compensate for the torque loss triggering a chain reaction.



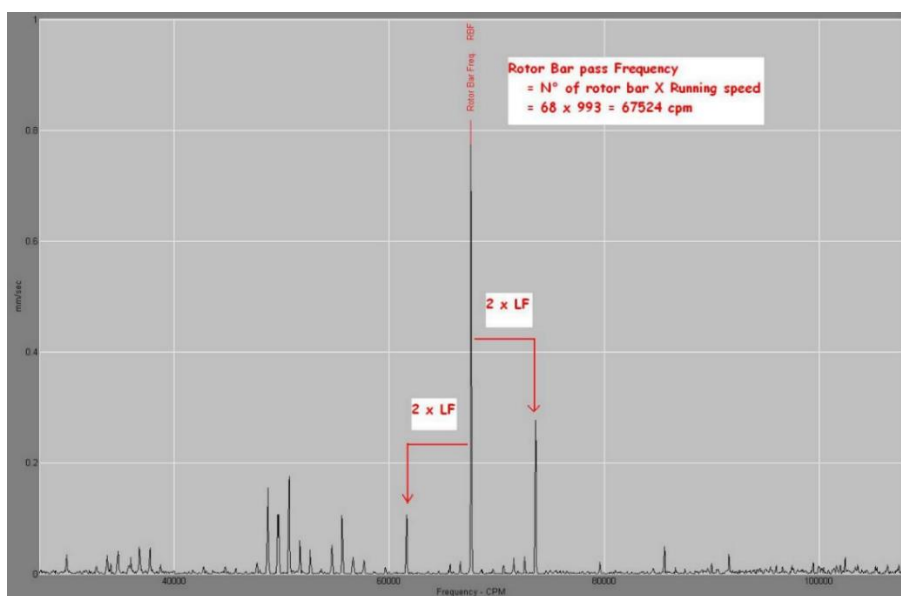
**Figure 4.2-7** Expected spectrum cracked rotor bar and for loose rotor bar.

Figure 4.2-7 shows two cases of rotor bar issues. In the first case the rotor bar is no more able to conduct current, this will generate impulse-like forces which generally amplify the harmonics of the rotational speed “1X”. Sidebands (as in the case of the eccentric rotor) will be proportional to the relative motion of the broken rotor bar with respect to the rotating magnetic field and the number of poles (PPF). In the second case a less severe damage generates modulation phenomena in the high frequency range. In the case of loose rotor bar, other conductive elements aim to compensate inducing a more intense currents, this phenomenon could be seen at the *Rotor Bar Passing Frequency* (RBF).

$$RBF = r_b f_r$$

being  $r_b$  the number of rotor bars and  $f_r$  the rotor speed.

Sidebands spaced by twice the line frequency from the RBF are due to the increased magnetic interaction between the rotating magnetic field and the currents flowing in the rotor conductor.



**Figure 4.2-8** Real measurements on an electric motor with a damaged rotor bar.

#### 4.2.4 Mounting Problems

Mounting problems are not directly caused by electric motor issues but from the coupling with system. The most common is the misalignment between the motor and the load.

Misalignment could be of two types, parallel or angular.

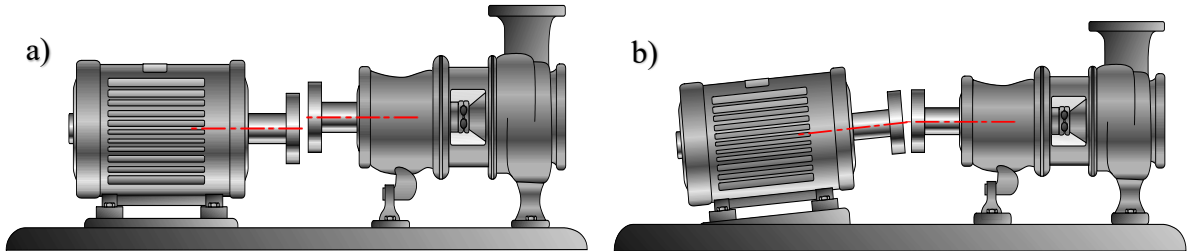


**Figure 4.2-9 a)** Parallel misalignment. **b)** Angular misalignment.

Parallel misalignment generates a static eccentricity in the motor, producing the same spectrum characterized by the “1X”, and its harmonics. The origin of the vibration could be investigated by uncoupling the load and comparing the measurements results. Figure 4.2-10 shows a real spectrum for a parallel misalignment issue; the “1X” and its second harmonic are clearly visible.

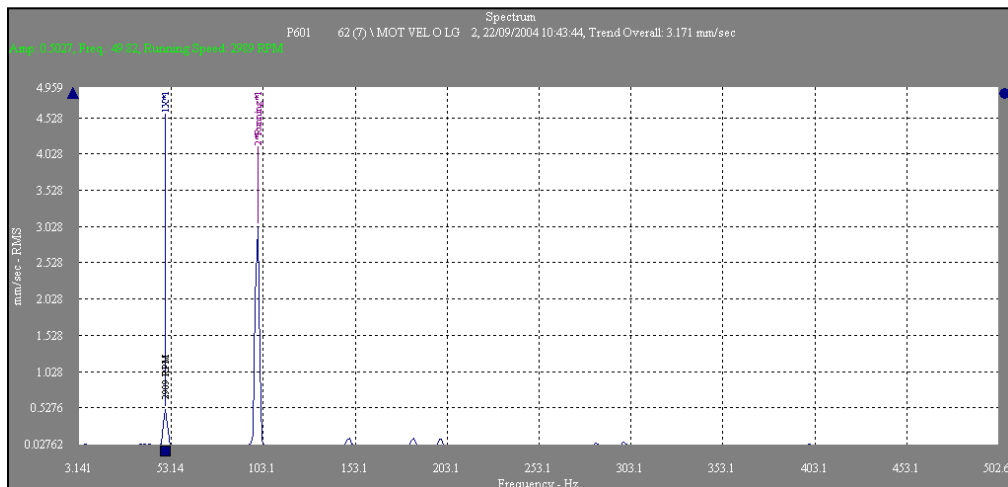


**Figure 4.2-9** Real spectrum of a motor mounted with Parallel misalignment.

Angular misalignment generates similar spectra, always inducing a deformation of the airgap. To distinguish from the two different types a second measure is required. While parallel misalignment generates unbalanced forces directed radially with respect to the rotation of the shaft, angular misalignment introduces an axial component. A second measure (performed in axial direction) could confirm the presence of angular misalignment.



## 5 Roller Bearings Vibration

---

Roller bearings enable relative motion between the stator and rotating part of the machine, transferring the applied load to the structure.

From a dynamics point of view, the bearing is both a passive machine element as well as an active exciter. The dynamic behaviour of the complete assembly in terms of stiffness, damping property and mass will be highly influenced by the bearing characteristic. Moreover, during operation the motion of the rolling elements set will introduce unavoidable vibrations. Even if bearing related vibrations have not been analysed in the test campaign, the goal of this chapter is to present the vibration of a rolling bearing and to compare them with the vibrations generated due to deviation from the ideal geometry.

### 5.1 Bearing Kinematics

Bearing vibration are strictly related to its velocity and geometry. In this paragraph, main kinematical relations will be presented in order to correlate the working speed to the frequency content of the generated excitation.

To keep the presentation as general as possible, kinematic relation will be written for an angular ball bearing (see Figure 5.1-1).

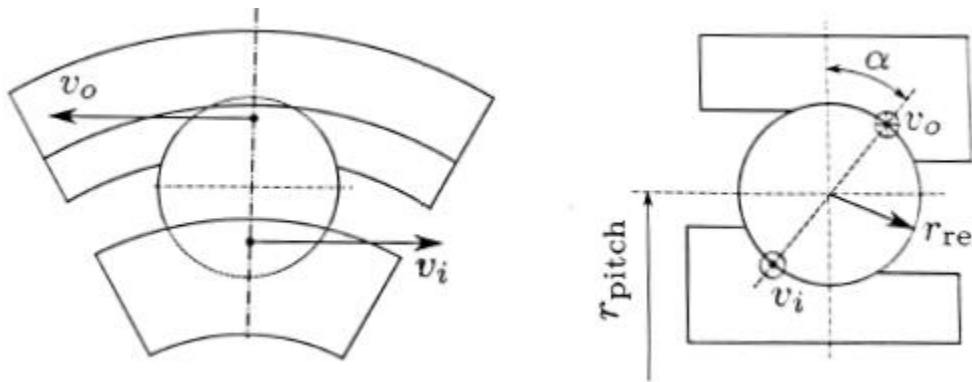


**Figure 5.1-1** Tangential velocity for the rolling element of an angular ball bearing with a clockwise rotating inner ring.

Under the assumption that the difference in the angle of the contact forces between the inner ring and the outer ring contact is small, the velocity at the contact point of the inner ring raceway can be expressed as:

$$v_i = 2\pi f_i (r_{pitch} - r_{re} \cos \alpha)$$

being  $f_i$  the inner ring rotation speed,  $r_{pitch}$  the pitch radius,  $r_{re}$  the rolling element radius and  $\alpha$  the contact angle.

Similarly, the velocity at the contact in the outer ring raceway can be written as:

$$v_o = 2\pi f_o (r_{pitch} + r_{re} \cos \alpha)$$

with  $f_o$  the angular velocity of the outer ring.

If there is no slip in the contact points the speed,  $v_c$ , at the centre of the rolling element can be derived:

$$v_c = \frac{v_i + v_o}{2}$$

which in angular frequency can be written as:

$$f_c = \frac{f_i}{2}(1 - \gamma) + \frac{f_o}{2}(1 + \gamma)$$

being  $\gamma = r_{re}/r_{pitch} \cos \alpha$ . It is usual to call  $f_c$  cage speed to avoid confusion with the rolling element frequency  $f_{re}$  which is the frequency of rotation of the rolling element around its own axis:

$$f_{re} = \frac{r_{pitch}}{r_{re}} (f_o - f_c)(1 - \gamma)$$

## 5.2 Perfect bearing vibration

A rotating bearing will generate vibrations due to the rotation of the rolling elements set. This is also true for a bearing with geometrically perfect raceways and optimal surface finish. By rotating the rolling elements set, the raceway is loaded by moving contact forces which generate vibration.

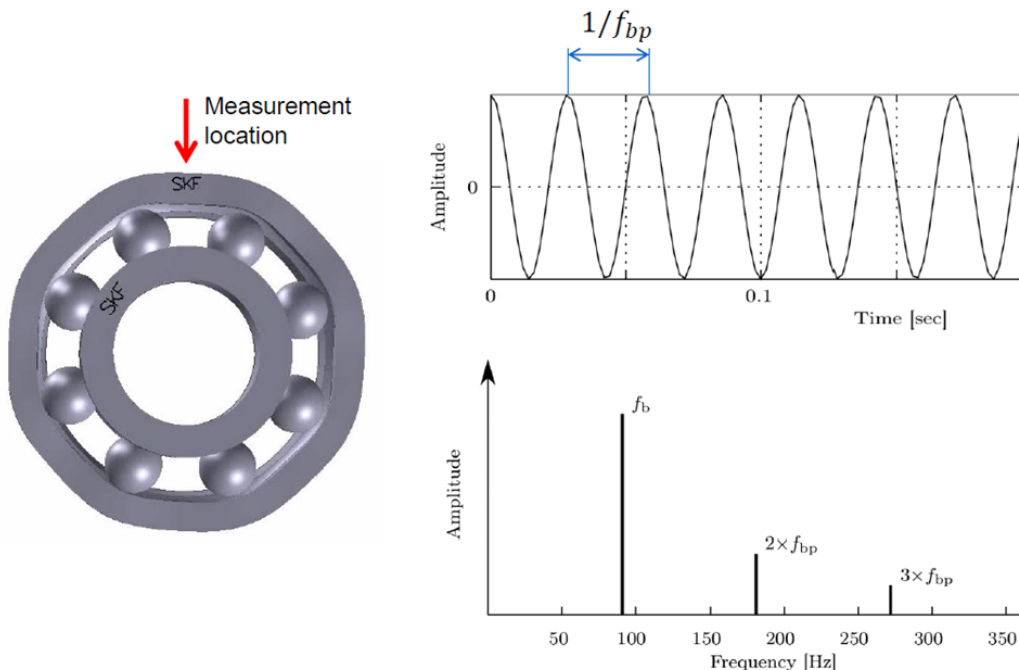
In the analysis presented in this section, it will be assumed that the contacts are equally loaded. This hypothesis is in contrast with actual bearing working conditions, in which the load is generally non-evenly distributed, but it is consistent with the real testing procedure used for the bearing defect analysis. In bearing defects test procedure, it is required to load bearings (also radial bearing) with an axial force: in this way the contacts points are equally loaded and the probability to detect components defect is increased.

Figure 5.2.1 shows a radial ball bearing axially loaded to obtain the condition of equally loaded contacts. The outer rigs will behave like an elastic element transmitting motion to the sensor that will perceive the passage of each rolling element as a pulse. The pulse train

repetition frequency will depend on the cage frequency  $f_c$  and on the number of rolling elements  $z$ .

The *ball-pass frequency*,  $f_{bp}$ , can be defined as:

$$f_{bp} = f_c z$$



**Figure 5.2-1** Perfect bearing vibration scheme.

Such vibrations are in general very low in amplitude and do not influence the general analysis of the system.

### 5.3 Local surface defects

Surface defects are local imperfections in a raceway that disturb the nominal contact pressure distribution during the motion of rolling elements. Typical examples of surface defects are indents and spalls due to surface fatigue. When a rolling element passes a surface defect, it encounters a change in contact load and contact stiffness.

Surface defect can be classified as *small* or *large* with respect to the contact area size (see Figure 5.3-1). *Small surface defects* influence the Hertzian contact area and the load distribution. This implies that the response to a small surface defect is similar to an impact.

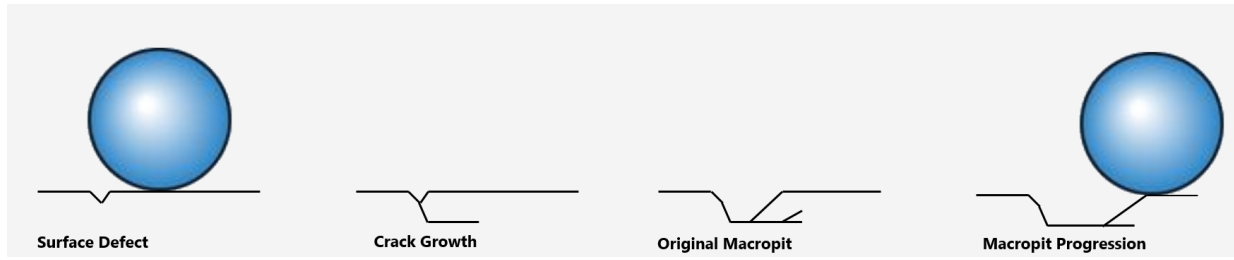


**Figure 5.3-1** Crack propagation and effect on the size of the defect.

For *large surface defect* the load on the rolling element decreases significantly and might even disappear during the passage. The response to such an excitation contains a "double pulse" with a possible varying frequency content due to difference in stiffness.

### 5.3.1 Surface defects Frequencies

By applying a regular monitoring practice, it is almost always possible to detect surface defect in the initiating phase allowing to avoid failure and to program maintenance stop. As expressed in previous paragraph, small surface defects generate impulse-like excitation whose repetition frequency and characteristic signal can be related to the location of the discontinuity (see Figure).

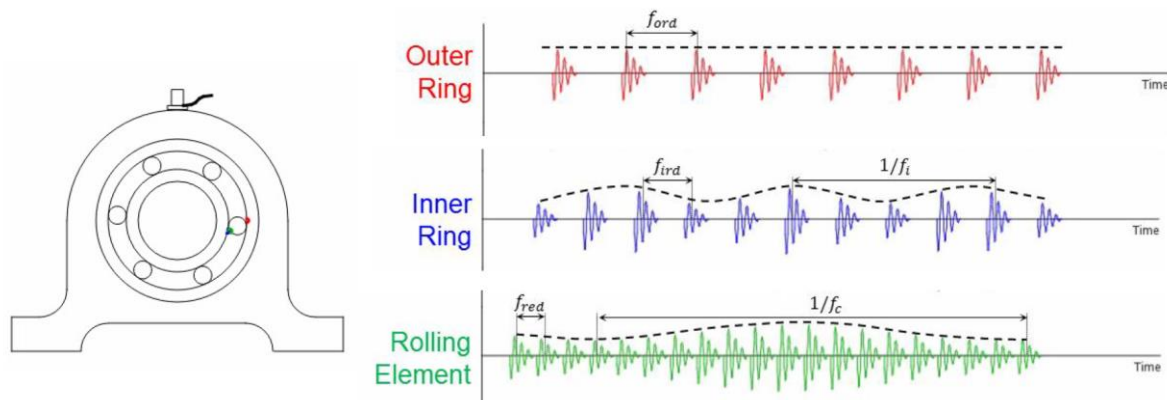


**Figure 5.3-2** Typical measurements for a bearing presenting defects on the outer ring (red signal), the inner ring (blue signal) and the rolling elements (green signal) for stationary outer ring,  $f_o = 0$ .

Due to fixed geometry each defect presents its own repetition frequency, called *bearing defect frequency*.

One of the main parameters to take into account when dealing with bearing surface defects is the defect position and its variability in time with respect to the sensor. The change in time of the position of the defects generates modulated signals: *inner ring* and *outer ring* modulation are reported in Figure 5.3-2.

Sequent equation can be derived:

- *Outer ring defect frequency*:

$$f_{ord} = z|f_c - f_o| \pm f_o$$

Is important to note that when  $f_o$  is not zero modulation phenomena can occur also for outer ring defect.

- *Inner ring defect frequency*:

$$f_{ird} = z|f_c - f_i| \pm f_i$$

- *Rolling element defect frequency*:

$$f_{red} = 2f_{re} \pm f_c$$

By definition, surface defects can be detected as impulsive phenomena which repeat themselves at a stated frequency dependent on the bearing geometry and kinematics. As presented in Chapter 3, the Fast Fourier Transform is not suitable for a rapid and intuitive analysis of this kind of signal. Envelope technique is used to analyze pulse train.

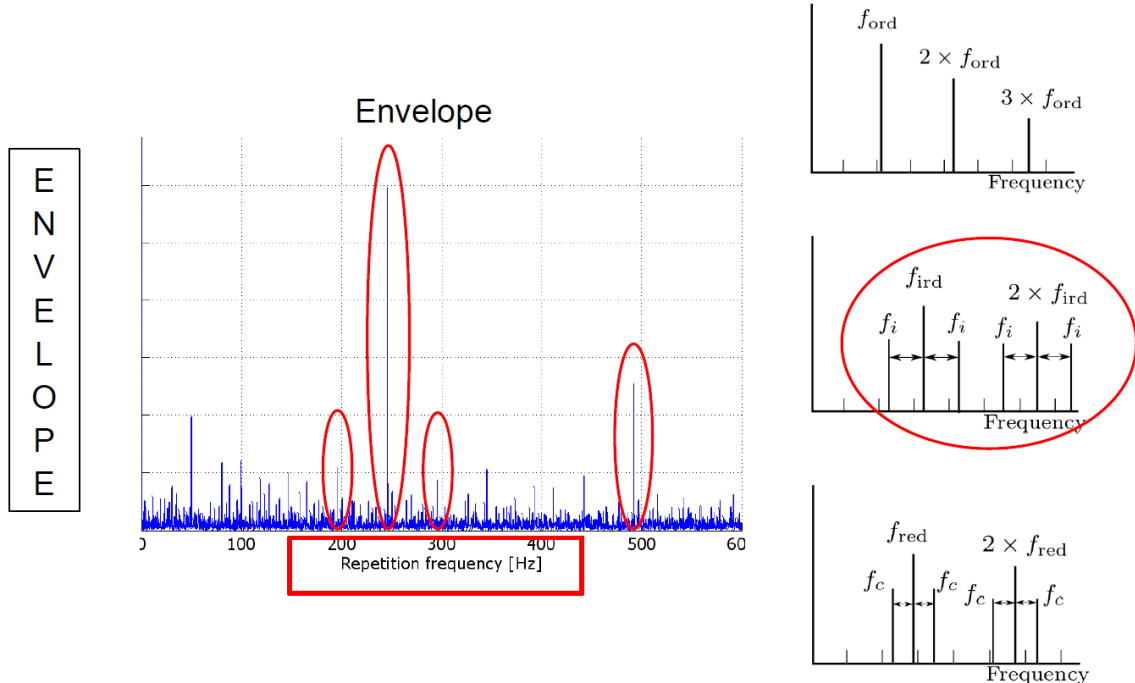


**Figure 5.3-3** Example of real measurement on an electric motor and Envelope techniques for bearing defect analysis.

Figure 5.3-4 shows a real measurement performed from an induction electric motor presenting a defect in the inner ring raceway. Repetition frequency and side bands are clearly visible in the envelope, allowing to define the pulses nature.



# 6 Acoustic

---

One of the main outcomes of this experimental thesis is to link the vibrational analysis of a typical three phase induction motor to its sound emission.

In this chapter a brief introduction to *Acoustic* will be presented analysing the main characteristic quantities, the perception of the sound and the instrumentation needed for measurements.

Although they share the same oscillating nature, *noise* and *structural vibration* are generally studied as separated phenomena. This is mainly due to the highly subjective nature of human sound perception.

We will refer as *sound* for wave propagating in a fluid (liquid or gasses) and to *vibration* for waves travelling in a solid medium.

## 6.1 Acoustic

Acoustics is the branch of physics that deals with the study of all mechanical waves in gases and liquids, analysing sound wave generation, propagation and *Psychoacoustics*.

### 6.1.1 Sound definition

Sound wave is defined as a perturbation, in the mean pressure level, travelling in a fluid medium.

A disturbance (source) induces particles to oscillate around their equilibrium position generating an alternance of high-low density zones propagating as *longitudinal wave* (see Figure 6.1-1).

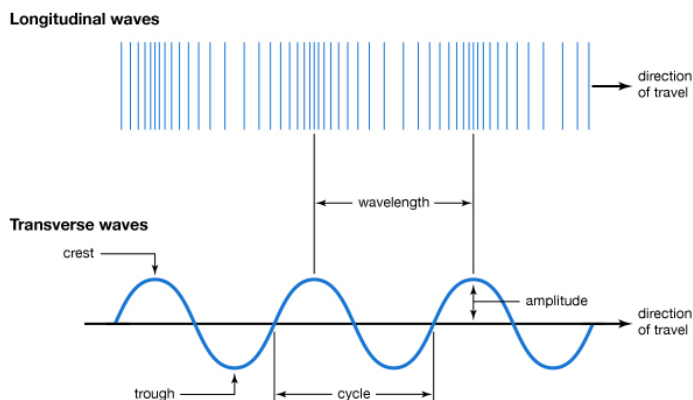


**Figure 6.1-1** Longitudinal and transverse wave difference.

Typical values for audible pressure perturbation range from  $10^{-6} \text{ [Pa]}$  to  $10^1 \text{ [Pa]}$  which are very low if compared to a mean pressure level, in standard condition, of  $10^5 \text{ [Pa]}$ .

According to the medium physical characteristic, the velocity of propagation, for a longitudinal wave is defined:

$$c_0 = \sqrt{KRT}$$

being  $K$  the bulk modulus,  $R$  the gas constant and  $T$  the absolute temperature. Typical value for dry air in standard condition is approximately  $343 \text{ [m/s]}$ .

Like any oscillatory phenomenon, sound can be studied in terms of (see Figure 6.1-2):

- Wavelength,  $\lambda$  (in [m]): which is the distance covered by the pressure wave in one complete cycle.
- Frequency,  $f$  (in [Hz]): which is the number of complete oscillations in a second.

These two main quantities are related by the propagation speed according to the rule:

$$\lambda = \frac{2\pi c_0}{\omega} = \frac{c_0}{f}$$

being  $\omega = 2\pi f$  the angular frequency (in [rad/s]).

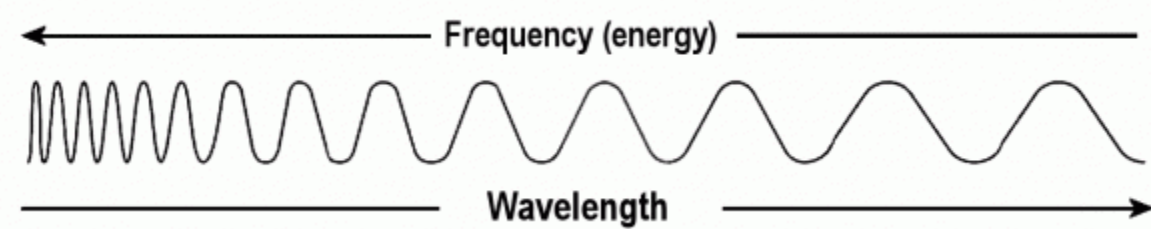


**Figure 6.1-2** Wavelength and frequency schematic relation.

*Human hearing range* is commonly given as 20 to 20.000 [Hz] (wavelengths from 17,2 to 0,017 [m], in standard condition).

Long waves are not easily interrupted by obstacles or absorption materials, on the other hand high-frequency signals carry a bigger amount of energy but, due to their lower wavelength, can be easily absorbed or reflected.

From the technical point of view this can be translated in the need of a clear understanding of the predominant frequencies in a signal, in order to choose the most efficient noise control system in relation to the analysed band.

### 6.1.2 Sound Pressure

Assuming to have a sound source emitting noise in all direction (see Figure 6.1-3), the air pressure  $P(\vec{x}, t)$  ([Pa]) will depend on position vector  $\vec{x}$  in space and time  $t$ . It consists of the

static part  $P_0(\vec{x})$  (which is the atmospheric pressure) and an oscillating part  $p(\vec{x}, t)$  excited by the travelling perturbation:

$$P(\vec{x}, t) = P_0(\vec{x}) + p(\vec{x}, t)$$

The fluctuating term  $p(\vec{x}, t)$  is referred to as *Sound Pressure*, nevertheless it is quite common to express it in term of root mean square values:

$$p_{RMS} = \begin{cases} \sqrt{\frac{1}{T} \int_0^T p(t)^2 dt}, & \text{for general wave} \\ \frac{p_{pk}}{\sqrt{2}}, & \text{for sinusoidal wave} \end{cases}$$

This is mainly because the  $p_{RMS}$  is proportional to the signal energy which is of high interest in acoustic measurements.

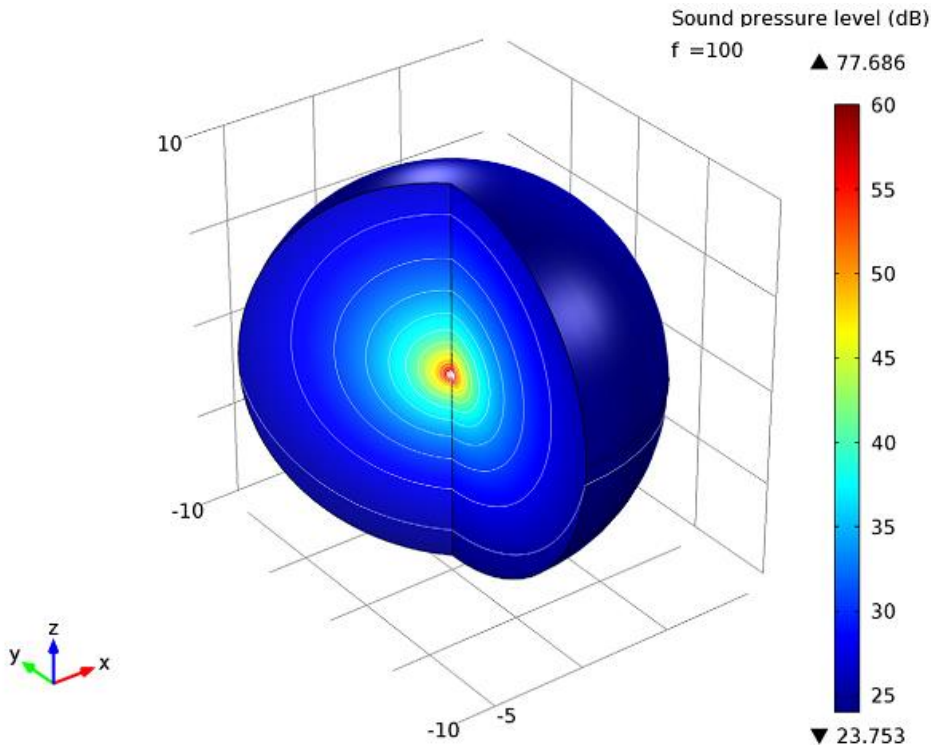


**Figure 6.1-3** Spherical distribution of the sound pressure level.

In acoustic, to describe the fluctuation of sound pressure as function of time and space vector, the *linearised homogeneous acoustic wave equation* is wildly used. Under the assumption of homogeneity and perfect elastic gas is possible to obtain:

$$\nabla^2 p(\vec{x}, t) = \frac{1}{c_0^2} \frac{\partial^2 p(\vec{x}, t)}{\partial t^2}$$

being  $\nabla^2$  is the Laplace operator.

Figure 6.1-3 shows that the energy released by the sound source is distributed on a spherical surface growing with the distance from the source itself. Under the hypothesis of absence of reflection phenomena, the sound pressure decreases to the inverse square law.

### 6.1.3 Acoustic Fields

Acoustic measurements are strictly related to environment. Acoustic wave interacts with obstacles and surrounding elements, which can absorb or reflect vibrations. This concept is of fundamental importance in sound pressure measurements. A receiver placed in an enclosure at a certain distance from the sources (see Figure 6.1-4) will not only record the direct perturbation but also its reflection and their interference.

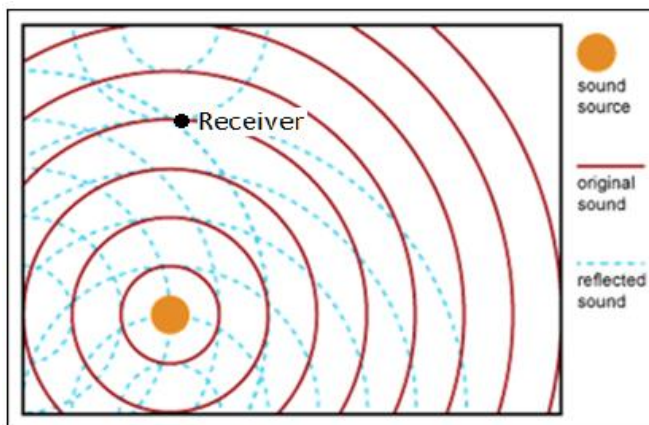


**Figure 6.1-4** Schematic propagation of sound wave from a spherical source in an enclosed space.

In order to take account for this phenomenon, different acoustic fields are defined, expressing the sound pressure as function of the receiver distance from the sound source (see Figure 6.1-5):

- Near field: that part of a sound field, usually within about two wavelengths of a noise source, where the sound pressure does not obey the inverse square law and the particle velocity is not in phase with the sound pressure.
- Free field: a sound field region with no adjacent reflecting surfaces. In practice a free-field can be said to exist if the sound pressure decreases according to the inverse square law. In this condition the sound pressure level will decrease of almost 6 [dB] by doubling the distance from the source.
- Reverberant Field: the region in an enclosure where the reflected sound dominates, as opposed to the region close to the noise source where the direct sound dominates.

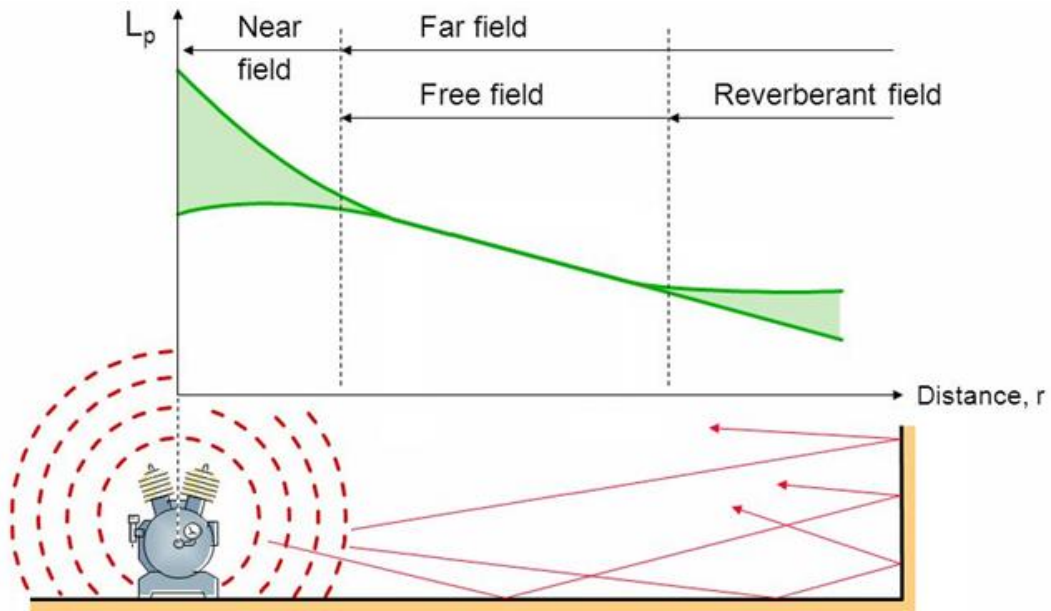


**Figure 6.1-5** Acoustic fields as function of distance from a non-point sound source.

For these reasons, sound pressure is not to be considered a characterising quantity of the sound sources, but it is strictly dependent from the receiver position and from the boundary condition.

#### 6.1.4 Sound Intensity and Sound Power

Sound power,  $\Pi$ , is a property of the sound sources, it is often used to quantify the radiated sound from an energetic point of view.

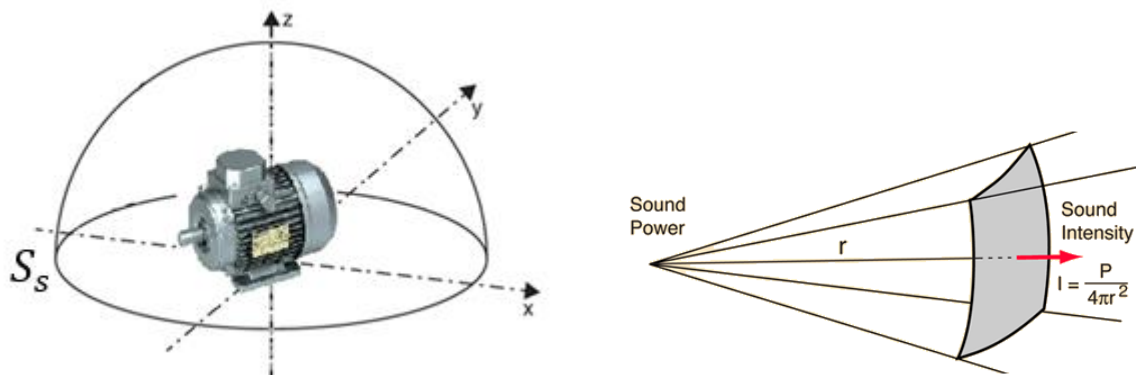


**Figure 6.1-6** Sound power radiation.

The time average of the power flowing in a unit area for a time interval  $[0, T]$  (Figure 6.1-6) is defined *Sound Intensity* vector,  $\vec{I}$ , (in  $[W/m^2]$ ):

$$\vec{I} = \frac{1}{T} \int_0^T p(t) \vec{u}(t) dt$$

being  $\vec{u}(t)$  the particles velocity vector.

By integrating the sound intensity on the  $S_s$  surface, the sound power can be defined as:

$$\Pi = \int_{S_s} \vec{I} \cdot \vec{n} ds$$

where  $\vec{n}$  is the unitary vector perpendicular to the surface  $S_s$ .

### 6.1.5 Sound Level and Decibel Scale

Experimental evidence (see Table 6.1-1) proves that human sensitivity follows a logarithmic scale. Therefore, in order to link measurements and perception, a logarithmic scale has been introduced.

Acoustic quantities (pressure, intensity and power) are, for this reason, often express in decibel scale [dB] as function of reference values:

- Sound Pressure level

$$L_P = 20 \log_{10} \frac{P}{P_0}$$

with  $P_0 = 20[\mu Pa]$  (hearing threshold).

- Sound Intensity level

$$L_I = 20 \log_{10} \frac{I}{I_0}$$

with  $I_0 = 10^{-12}[W/m^2]$ .

- Sound Power level

$$L_\Pi = 20 \log_{10} \frac{\Pi}{\Pi_0}$$

with  $\Pi_0 = 10^{-12}[W]$ .

Source of Sound/Noise	Sound Pressure (RMS) [ $\mu Pa$ ]	Sound pressure level [dB]
<b>Threshold of pain (at 1 [KHz])</b>	200,000,000	140
Air plane take-off	20,000,000	120
Pneumatic drill	2,000,000	100
Vacuum cleaner	200,000	80
Conversation speech	20,000	60
Living room	2,000	40
Whispering	200	20
<b>Threshold of hearing (at 1 [KHz])</b>	20	0

**Table 6.1-1** Sound pressure and sound pressure level at one meter distance from typical sound sources.

## 6.2 Psychoacoustics

The study of noise has to deal with the highly subjective nature of human's sound perception. Psychoacoustics is the branch of science studying the psychological and physiological responses associated with sound (including noise, speech and music).

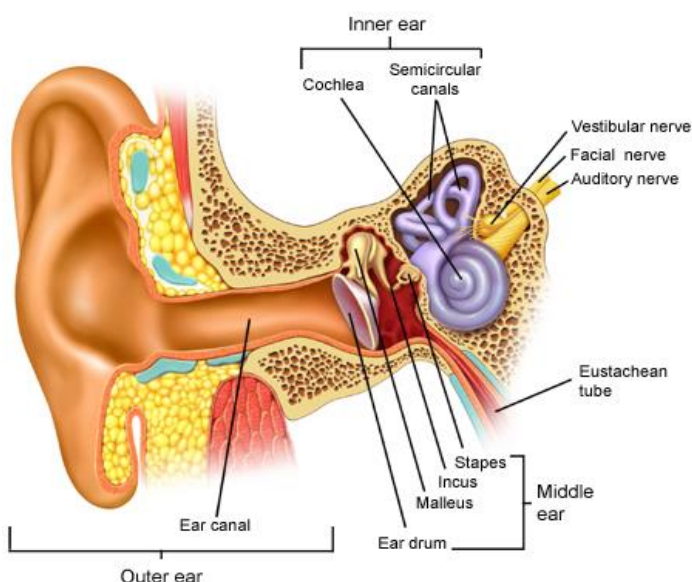


**Figure 6.2-1** Tympanic cavity anatomy.

Human sensing apparatus is made of three main macro-systems (see Figure 6.2-1):

- External Ear: it is the part devoted to the perturbation gathering. The parabola shape of external ear directs the radiation into the ear canal.
- Middle Ear: it is fundamentally made by the cinematic chain. External perturbations excite the eardrum which, through the malleus, incus and stapes, transfers the vibration to the internal ear.
- Internal Ear: it is the transducing apparatus. Vibrations are turned into electrical signals which can be analysed by the brain.

Like any other sensing system, human ear is effective in a limited, although wide, range of frequencies.

In order to correlate subjective auditory impression with physical parameters, non-physical quantities have been introduced from tests with human subjects. Such a study have been done to define an objective way to express auditory impression in a reproducible manner, allowing a scientific approach in the study of perceived noise.

### 6.2.1 Loudness

Loudness is a non-physical parameter used to define human ear sensitivity to different frequencies.

As said in previous paragraph, eardrum's membrane transfers vibration to internal ear, so its response to external excitation depends on its physical behaviours in terms of stiffness, damping and boundary conditions. As a physical vibrating system, eardrum will experience resonance and anti-resonance phenomena, in relation to the exciting frequency.

To quantify this phenomenon the Loudness scale has been introduced. Loudness is stated in the unit *phons* and it is scaled in such a way that at 1 [kHz] the phon scale is equal to the [dB] scale (see Figure 6.2-2 a).

Experimentally has been seen that human ear is most sensitive to frequencies between 1 [kHz] and 5 [kHz]. Following this observation isophones curves are derived from psychoacoustical experiments in which people had to judge when a pure tone had the same loudness as the reference tone at 1 [kHz].

The non-linear behaviour of human ear and the frequency sensitivity range are of main importance for noise problem in industrial application. Among all the vibration sources is important to identify not simply the higher emitter but the one which is highly perceived by the operator.

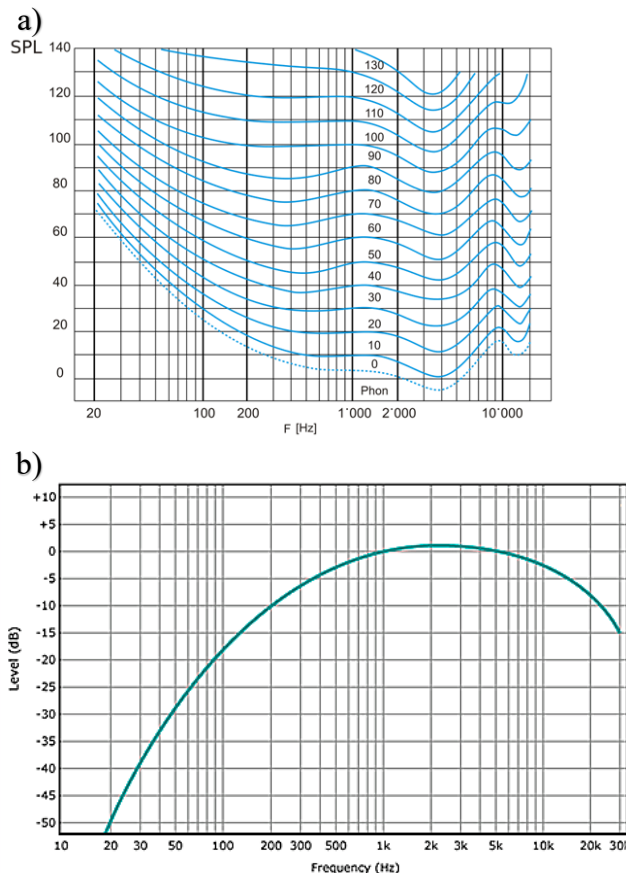


**Figure 6.2-2 a)** Equal loudness contour (isophones) for pure tones. **b)** A-weighting filter

In order to correct the measured sound level to the frequency dependency of human ear, filters have been introduced. One of the most used is the *A-weighting filter*. The 40 [phon] isophone (Figure 6.3-2 a) has been used as reference to construct the filter, by normalizing it to 0 [dB] at 1 [kHz] and by inverting it (see Figure 6.2-2 b).

### 6.3 Noise Sources and Sound Emission

In previous paragraphs sound has been analysed from a physical point of view presenting its characteristic and the quantity used for measurement without analysing its generation.

Dealing with induction motor, the excitation forces, which generate vibration, could be of different nature (as presented in Chapter 4 and in Chapter 5). Although they act as excitors, the vibration sources are seldom the components that effectively radiate sound. System components like the housing, casing and shields are in general responsible for the main part of the sound radiation.

The capability of structural vibration to generate sound will depend on its shape, the size and the vibration frequency.

### 6.3.1 Effective Sound Radiation

Effectiveness of sound radiation expresses the capability of a vibrating element to actually generate sound. To understand this concept the example of a baffled piston will be reported (see Figure 6.3-1).

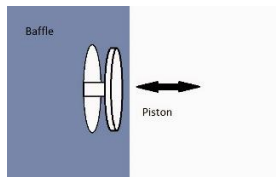


**Figure 6.3-1** Baffled piston scheme.

A baffled piston works like a loudspeaker and, at first, we assume that the piston vibrates at a very low frequency. In this condition the pressure changes generated by the moving surface are transduced in a change of speed of the fluid which follows the piston. This process is very ineffective for sound radiation because the perturbation generates a mass flowrate instead of a real pressure wave. To effectively radiate sound, the frequency of the piston has to increase enough to generate a traveling perturbation. Another important parameter is the piston surface. At the same frequency a large piston is more able to radiate sound than a small piston.

The frequency at which the process becomes effective is defined as *critical frequency*,  $f_{cr}$ , and depends on the size and shape of the piston. This concept can be extended to a wider context referring to a rectangular plate (which can be used to model a shield or a critical part of an application casing).

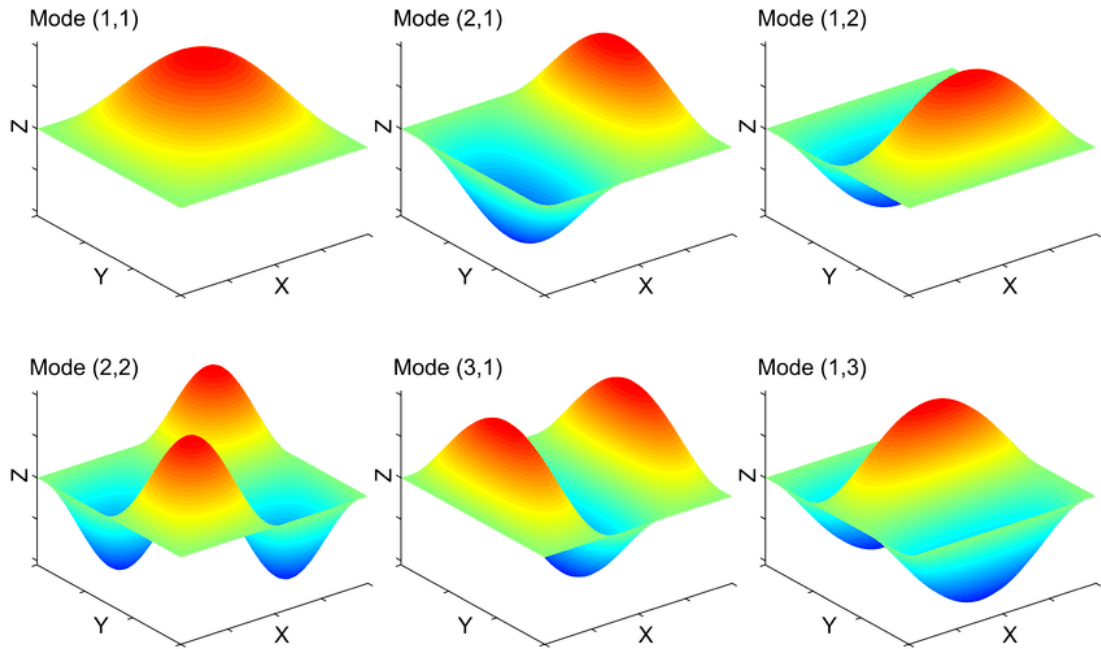


**Figure 6.3-2** Multiple eigenmodes of a simply supported rectangular plates.

If the size of the plates is considered fixed, for each mode (see Figure 6.3-2) an effective sound emission critical frequency can be found.

Without entering in the detail, an exciting phenomenon acting on the plates, will result in a vibration which will be a composition of its modes. If the frequency is high enough (according to the size of the emissive surface) each mode will contribute to the final emitted sound in relation to the excited frequency.

### 6.3.2 Transfer Path

The resulting sound emission of a structure, or in general of a system, is strictly correlated to the vibration source and to the emissive surface. As regards electrical motors, these two phenomena are normally related to different components. To perform a reliable emitted sound analysis it is important to take into account all the involved variables. This leads to the concept of *transfer path*.

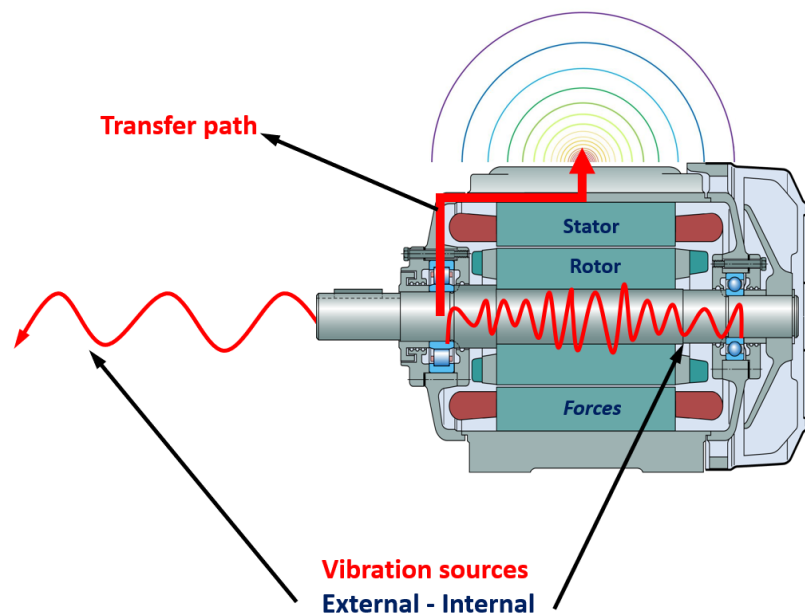


**Figure 6.3-3** Transfer path example for an electric motor.

Figure 6.3-3 shows an example of transfer path, the acoustic emission will be the composition of the internal and external vibration sources, but also of the casing characteristic. In real monitoring practice, measurements are moreover complicated by absorption and reflection phenomena and by background noise. All these concepts are to be considered when performing a sound measurement.

#### 6.4 Acoustic Measurements Instrumentation

Acoustic signals, like structural vibrations, can be acquired and analysed as explained in Chapter 3, the main difference being the sensing apparatus. Acoustic sensors are used to measure characteristic quantity like pressure oscillation, particles velocity and sound intensity. The most common sensor in sound field is the *Microphone*, which, based on the sound definition, is a pressure transducer designed to operate in a broad frequency spectrum (or at least in the range of audible wavelength). Microphones are composed by a moving diaphragm and a displacement transducer which converts the membrane motion into electrical signal. Microphones types differs from used technology, but the working principle is almost the same for all. The most used in measurements practice is the *Condenser Microphone* (see Figure 6.3-4).

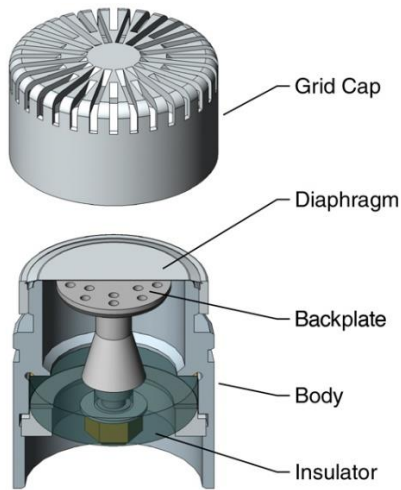


**Figure 6.4-1** Condenser microphone scheme.

The change in distance between the diaphragm and the backplate is transduced into a change in circuit capacitance, generating a variation into the output voltage. Like the vibration sensor presented in Chapter 4, microphones differ for sensitivity and bandwidth. The sensitivity is related to the tension in the diaphragm, while the bandwidth depends on its dimension. Generally, the bigger is the diaphragm size the lower is the minimum frequency that can be measured. Actual microphones are able to measure in a range from few Hertz up to the limit of audible frequencies.

#### 6.4.1 Sound Intensity and Particle Velocity Probe

To characterize the sound source in terms of emitted energy, sound intensity measure has to be performed. An *Intensity Probe* is an instrument used to measure sound intensity in one emission direction.

Intensity probe are made of two microphones placed at short distance one from the other.

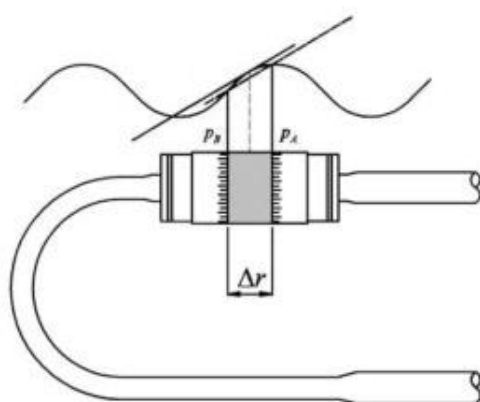


**Figure 6.4-2** Intensity probe Scheme.

Referring to Figure 6.4-2, from the pressure measurements  $p_A$  and  $p_B$ , it is possible to determine particles velocity along the  $r$  direction. Mean pressure and particle velocity can then be used to calculate sound intensity according to the law presented in Paragraph 6.1.4.

## 7 Application in scope

---

Within the *SKF's Electric Motor Application Noise Project*, several noise and vibration issues have been simulated in a controlled environment.

In this chapter the test campaign performed in *SKF Solution Factory Moncalieri (TO)*, will be presented.

According to the noise and vibration sources presented in Chapter 4, different electric motor damages have been insulated and simulated.

Test campaign has been implemented according to three main goals:

- Simulate real electric motor issues.
- Validate the theoretical model.
- Compare vibration and sound measurements.

Following the main outcomes of the project, tests session has been planned in order to highlight noise emission deriving from non-bearing related issues.

### 7.1 Test Bench Presentation

Test bench is composed of ten three phase electric motor of three different type (see Table 7.1-1). For each type, one motor has been reviewed and balanced to obtain a reference (Baseline) from both the vibration and the sound emission point of view, while the other have been specifically damaged to separately investigate different noise sources.

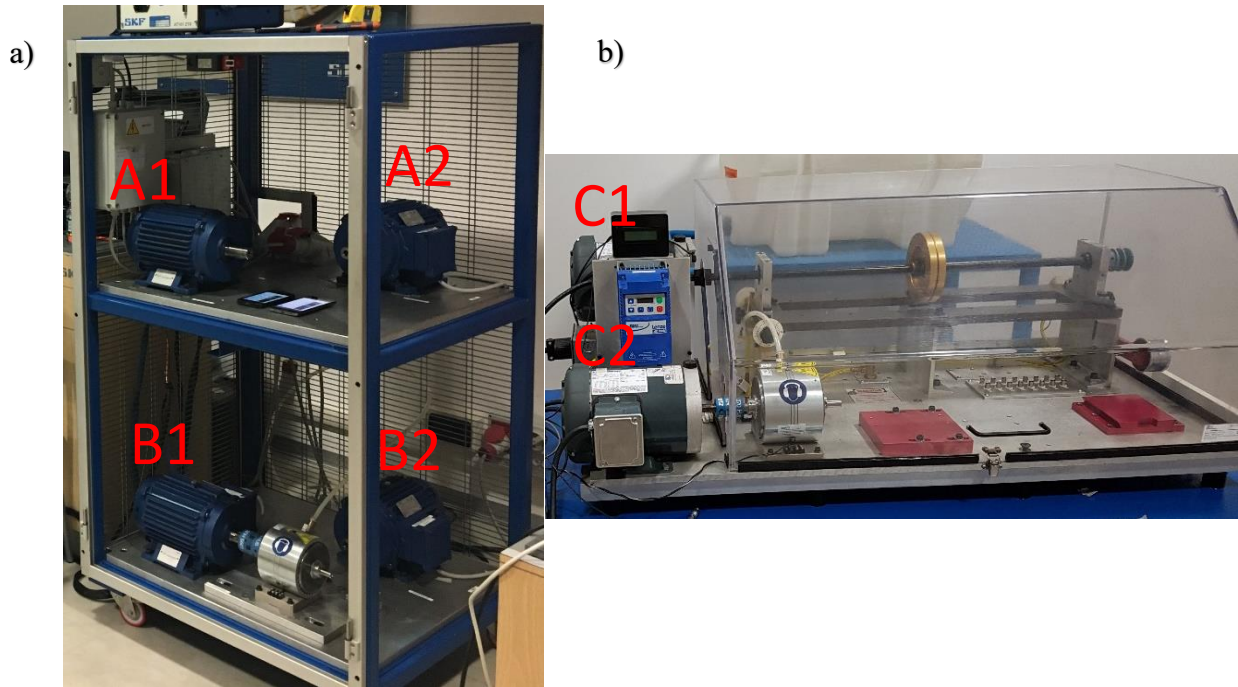
<b>Available electric motors</b>	<b><math>N_s</math></b>	<b><math>N_{rb}</math></b>	<b>Power [kW]</b>	<b>Quantity</b>	<b>ID</b>	<b><math>p</math></b>	<b><math>d_r</math> [mm]</b>	<b>Speed [rpm]</b>
Type 1 5 BES 100 LA 4	36	28	1.6	4	1;2;6;7	4	89.40	1430
Type 2 5 BES 100 L 2	24	18	1.6	2	8;5	2	79.30	2910
Type 3 D391	24	34	0.37	4	A,B,C,D	2	80.40	2850

Table 7.1-1 Analysed motor types and their characteristics.

Being  $N_s$  the number of stator slot,  $N_{rb}$  the number of rotor bars,  $d_r$  the diameter of the rotor and  $p$  the number of poles.

The test bench is composed of two station (see Figure 7.1-1), allowing to feed the induction electric motors in both direct drive and VFD mode, to apply a 20% load thanks to a magnetic

brake and to introduce different type of shaft misalignments. Other characteristics will be further discussed in the section devoted to specific damages.



**Figure 7.1-2** a) Station for motor type 1 and 2, and relative position. b) Station for motor type 3 and relative position.

### 7.1.1 Data Acquisition Instrumentation and Setup

Measurements instrumentation, as described in Chapter 4 and in Chapter 6, is composed by acoustic and vibration sensors and by Analog to digital converters.

All the measurements have been performed with two different acquisition systems in order to compare the obtained result.

The first acquisition system is composed by:

- Accelerometers: 3x *PCB TLD352C33 ICP*
  - Sensitivity: 10 mV / m/s<sup>2</sup> (100mV/g)
  - Freq range ( $\pm 5\%$ ): 0.5 – 10.000 [Hz]

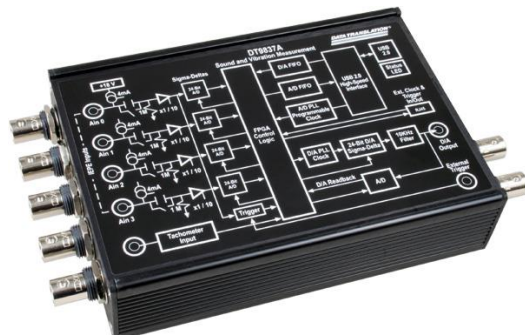


- Microphone: *PCB 378B02 ½ "* prepolarized free-field condenser microphone

- Sensitivity: 50mV/Pa



- Data acquisition: *Data Translation DT9837*
  - Sampling frequency: 40[KHz] (for vibration), 100 [KHz] (for sound emission)



- Tachometer: *Monarch Instruments Optical tachometer*

The second acquisition system is composed by:

- Accelerometers: 1x *SKF CMSS 2200*
  - Sensitivity: 100mV/g
  - Freq range ( $\pm 5\%$ ): 0,7 to 10 000 [Hz]



- Data acquisition: *SKF Microlog AX*
  - Used in “recorder mode”
  - Sampling frequency: 40 [KHz]



Both the measurements systems return compatible results; for the sake of brevity only the results obtained with the first acquisition system will be reported in sequent paragraphs. From now on, in the presentation all the cited instruments will be referred to the first sensing apparatus.

Vibration and sound measurements have been performed with an almost fixed setup:

- Three vibration sensors (accelerometers) have been placed (by the use of wax) on the *Drive End* side of the electric motor according to principal directions.

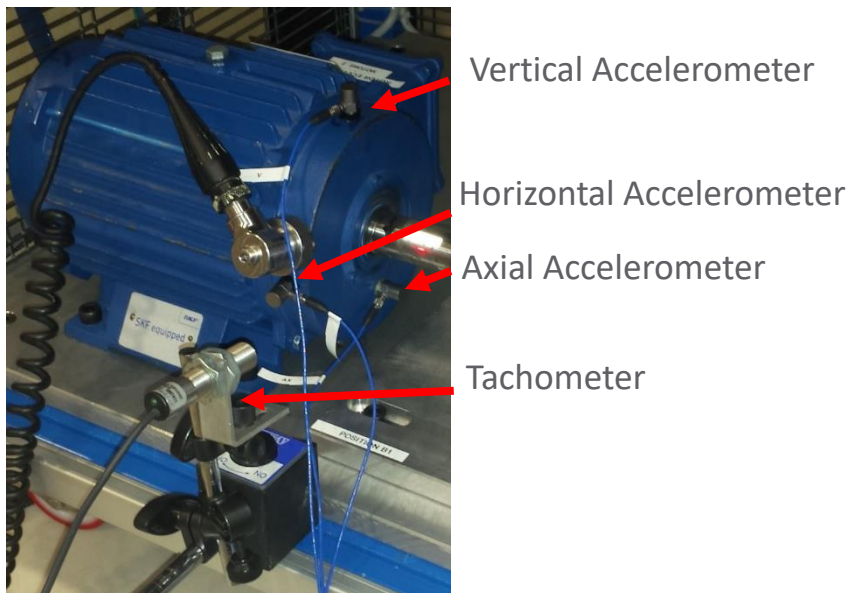


**Figure 7.1-2** Accelerometer and tachometer position.

- One microphone placed at one meter from the sound source and at one meter from the floor, pointed toward the emitter.

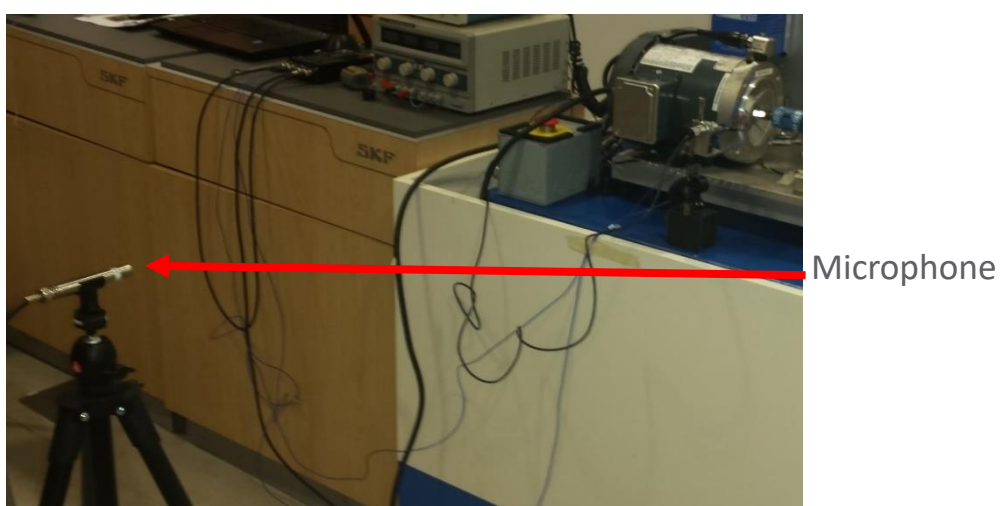


**Figure 7.1-3** Microphone position in the case of test station for motor type 3.

Almost all measurements have been performed with the maximum Sampling frequency for an acquisition time of 10 [s].

Variation from the proposed acquisition set up will be presented along with the measurement results.

## 7.2 Electromagnetic Tests Results

This paragraph will be devoted to the presentation of the measurements results of the test campaign performed in *SKF's Solution Factory, Moncalieri (TO)*.

Table 7.2 reports the list of performed tests according to the presentation order. To facilitate the comparison between the obtained results and the theoretical expectation, for each test the *Purpose* along with the reference theoretical paragraph has been reported.

<i>Electric Motor Type</i>	<i>EM Feeding</i>	<i>Purpose</i>	<i>Theoretical Reference (Paragraph)</i>
Type 1	Direct Drive	Baseline	4.2.1
Type 1	VFD_10[KHz]	Baseline VFD driven	4.2.2.3
Type 1	VFD_6[KHz]	Baseline VFD driven	4.2.2.3
Type 1	VFD_4[KHz]	Baseline VFD driven	4.2.2.3
Type 1	Direct Drive	Rotor Eccentricity	4.2.3.1
Type 1	Direct Drive	Rotor eccentricity 20% Load	4.2.3.1
Type 1	Direct Drive	Broken Rotor Bar	4.2.3.2
Type 1	Direct Drive	Broken Rotor Bar Load 20%	4.2.3.1
Type 2	Direct Drive	Baseline	4.2.1
Type 2	Direct Drive	Increased Air Gap	No Ref.
Type 3	Direct Drive	Baseline	4.2.1
Type 3	VFD_10 [KHz]	Baseline VFD driven	4.2.2.3
Type 3	VFD_6 [kHz]	Baseline VFD driven	4.2.2.3
Type 3	VFD_4 [kHz]	Baseline VFD driven	4.2.2.3
Type 3	VFD_10 [KHz]	Voltage imbalance	4.2.2.1
Type 3	VFD_10 [KHz]	Phase loss	4.2.2.2
Type 3	VFD_10 [KHz]	Static eccentricity	4.2.2.1

**Table 7.2** Performed tests list.

Each analysed motor will be presented (in terms of technical characteristic and specific damaging) along with measurements results.

### 7.2.1 Electric Motor 6, Baseline

Electric Motor 6 (EM 6) has been used as reference (baseline) for the motor type 1, it has been balanced and revised before the test campaign in order to make sure that there are not evident issues.

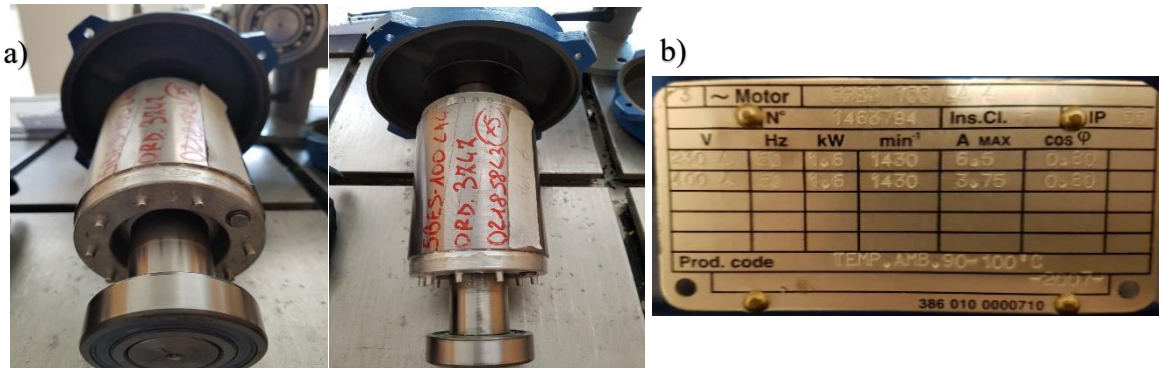


Figure 7.2-1 a) Rotor pictures. b) Nameplate.

Table 7.2-1 reports EM 6 characteristics, while Table 7.2-2 reports tests performed on this electric motor. Each performed test will be further presented in sequent paragraphs.

	<i>N<sub>s</sub></i>	<i>N<sub>rb</sub></i>	<i>ID</i>	<i>p</i>	<i>d<sub>r</sub>[mm]</i>	<i>Speed [rpm]</i>	<i>DE</i>	<i>NDE</i>
<b>EM Type 1</b>	36	28	6	4	89.4	1430	6206 2RS2 (SKF)	6206 2RS2 (SKF)

Table 7.2-1 EM 6 characteristics.

With the notation “DE” and “NDE” are indicated respectively the bearing mounted on the *drive end side* of the rotor and on the *non-drive end side*.

<i>Test Station</i>	<i>EM Feeding</i>	<i>Purpose</i>
1	Direct Drive	Baseline
1	VFD_10[KHz]	Baseline VFD driven
1	VFD_6[KHz]	Baseline VFD driven
1	VFD_4[KHz]	Baseline VFD driven

Table 7.2-2 Test performed on EM 6

#### 7.2.1.1 Baseline

Table 7.2-3 reports main significative quantity to be taken into account in the results interpretation. Being  $F_m$  the rotating magnetic field speed,  $F_r$  the rotor speed and,  $s$  the slip.

<b><i>EM Working Condition</i></b>	<b><i>Fm (Hz)</i></b>	<b><i>Fr [Hz]</i></b>	<b><i>s</i></b>
Idle	25	24.95	0.002

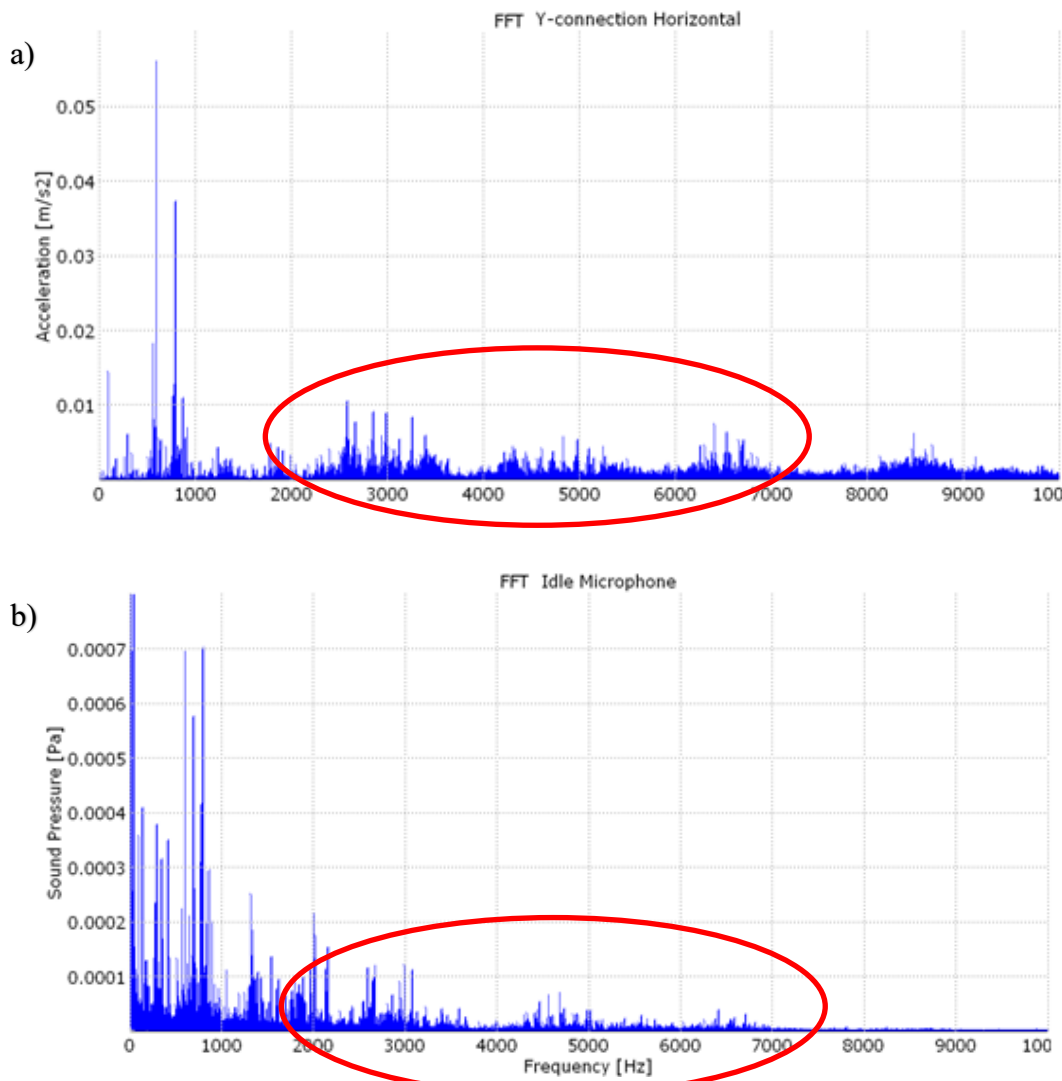
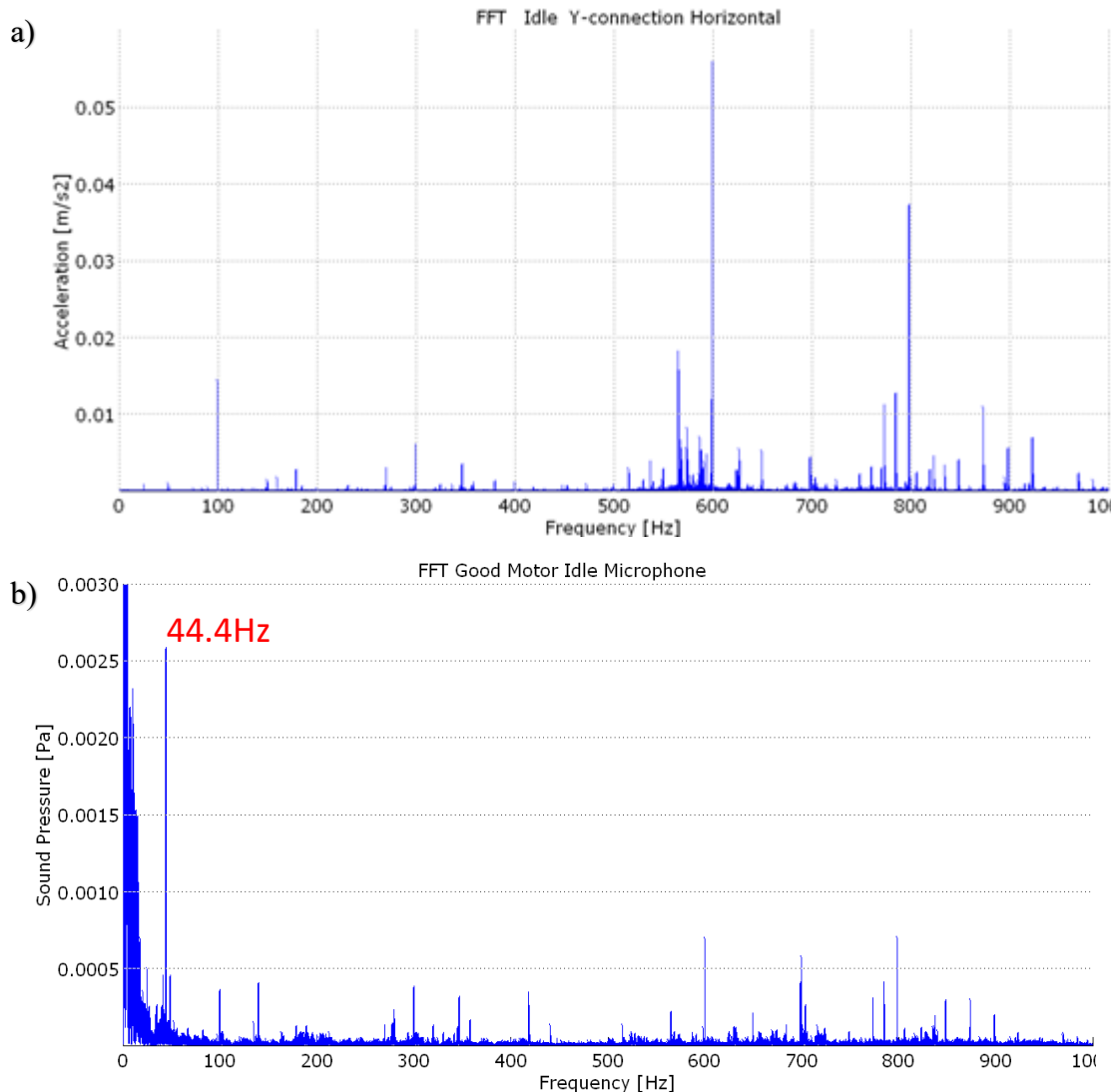
**Table 7.2-3** Main test parameters.**Figure 7.2-2 a)** Vibration measurement FFT. **b)** Acoustic measurement FFT.

Figure 7.2-2 shows that high frequency content (between 2 and 7 [kHz]) can be found in both spectra, so these frequencies are well radiated.



**Figure 7.2-3** a) Low frequencies vibration content. b) Low frequencies acoustic content.

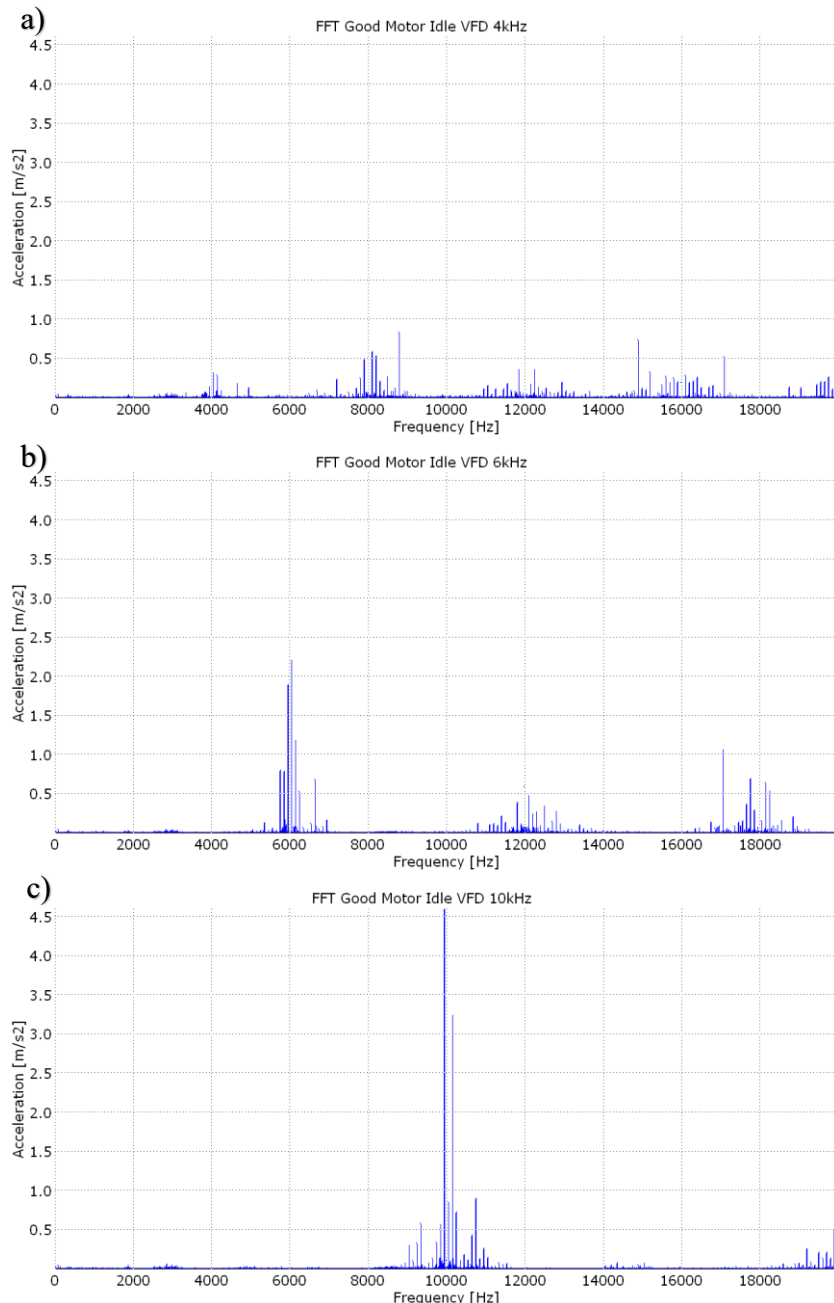
Analysing the low frequency content (Figure 7.2-3) it is possible to point out some differences. Peaks in the vibration spectra relative to 600, 700 and 800 [Hz] are less relevant in the sound spectra. This may be attributable to two reasons; this specific frequency could not be radiated efficiently by the system, or the sound is radiated directionally and not perceived by the microphone. Another important difference is a peak in the acoustic spectrum at 44.4 [Hz].

This vibration has not been identified from accelerometer in either direction, so it is probably due to background noise.

### 7.2.1.2 Baseline VFD Fed

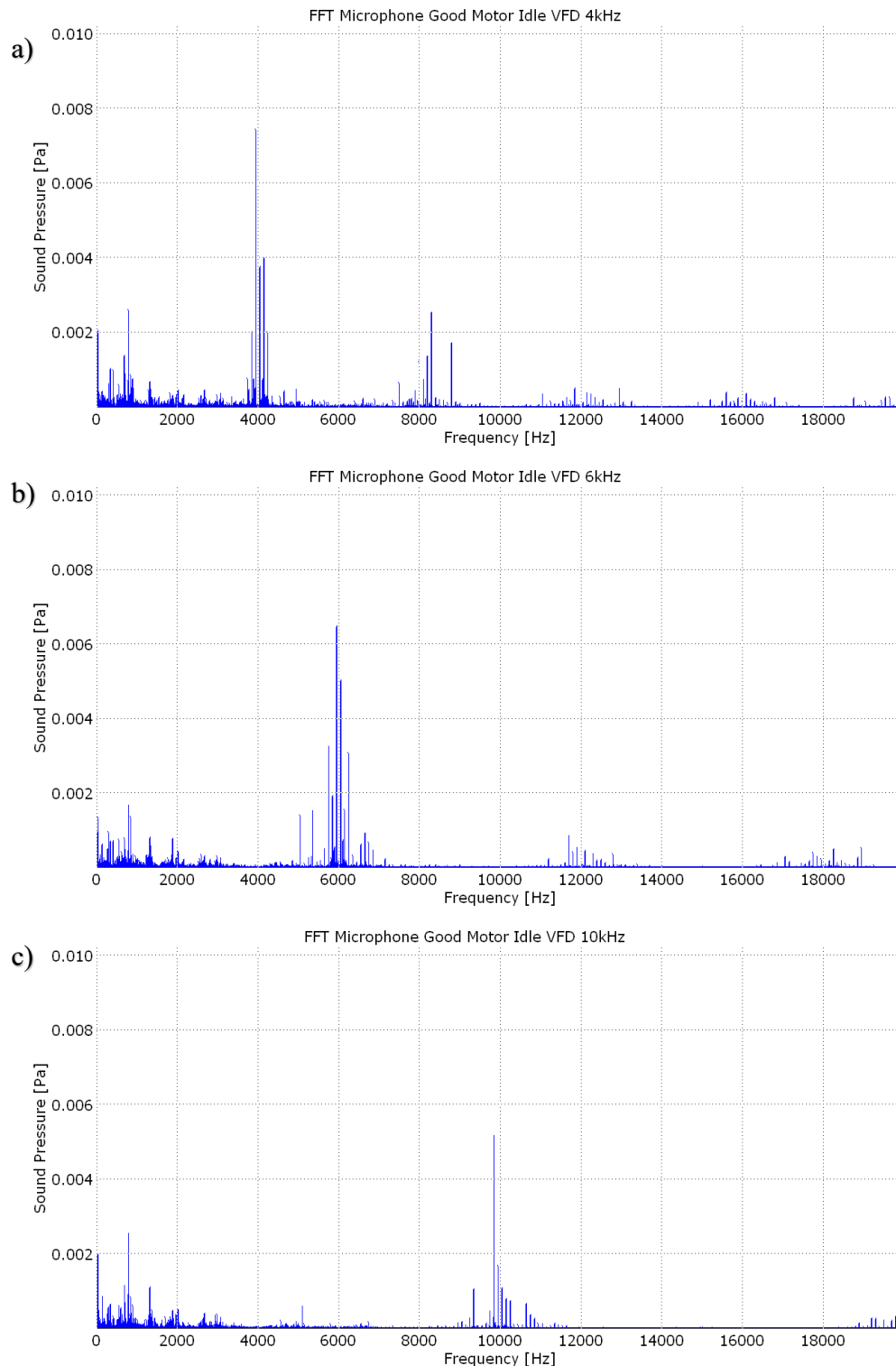
VFD devices allows to vary the electric motor input frequency and voltage in order to control the speed. Due to their working principles, VFDs introduce very annoying tonal sound in relation to the *carrier frequency*. For these tests the motor input frequency has been settled equal to the line frequency, while the carrier frequency has been varied.

Figure 7.2-4 shows the acquired vibration spectra for three different values of the carrier frequency: 4, 6 and 10 [KHz].



**Figure 7.2-4** Vibration spectra of EM 6 VFD fed, for different carrier frequency: a) 4 [KHz], b) 6 [KHz], c) 10[KHz].

Figure 7.2-4 shows that the amplitude of the vibration increases with the carrier frequency. It is important to note that the resonance frequency of the sensor is above 50[kHz] and the frequency response of the sensors is assumed to be within 5% up to 10[kHz].



**Figure 7.2-5** Sound spectra of EM 6 VFD fed, for different carrier frequency: a) 4 [KHz], b) 6 [KHz], c) 10[KHz].

Comparing the vibration and the acoustic results of Figure 7.2-5 it is possible to observe that the spectra are quite different. Sound spectra peaks amplitude is not influenced by the increasing in carrier frequency. Moreover, the effects of the carrier frequency harmonics, which is clear in the vibration spectra, is mitigated in the sound spectra. As a general rule, high frequency sound emission tends to be more directional, so the positioning of the microphones becomes crucial in high frequency signal acquisition.

Is important to note that even if increasing the carrier frequency results in a bigger amplitude of the generated vibrations, from a psychoacoustic point of view it will result in a lower perception of loudness (according to Equal Loudness contours presented in Chapter 6).

## 7.2.2 Electric Motor 2, Rotor Eccentricity

Electric Motor 2 (EM 2) has been used to simulate rotor eccentricity. EM 2 is of the same type of the baseline presented in Paragraph 7.2.1. The rotor has been partially grinded and the test has been performed both in idle condition and by applying a 20% of load in order to amplify the effect.

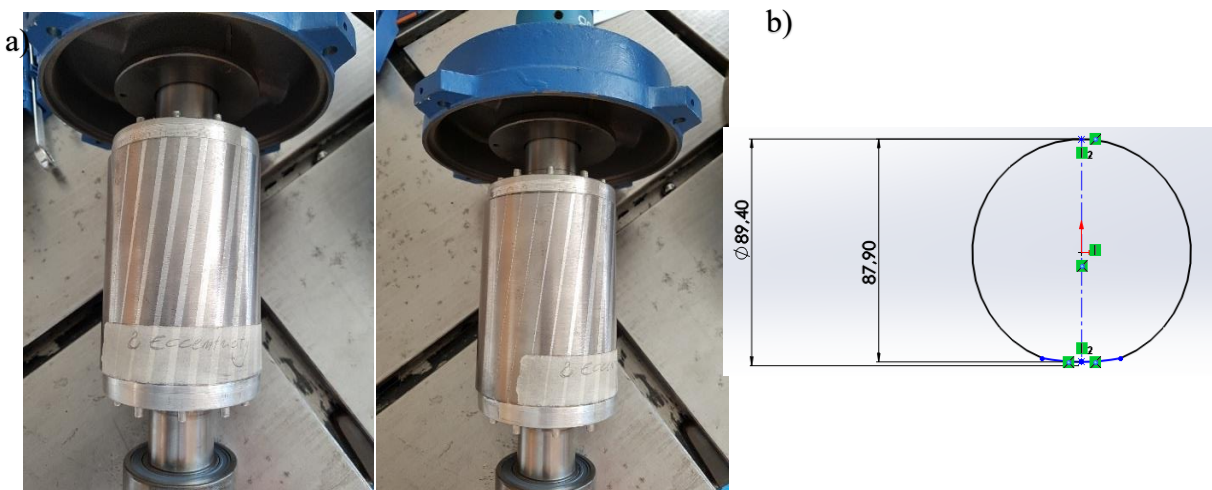


**Figure 7.2-6 a)** Rotor pictures. **b)** Grinding scheme.

The modification made generates a rotating unbalance of the magnetic field.

Table 7.2-4 reports EM 2 characteristics, while Table 7.2-5 reports tests performed on this electric motor. Each performed test will be further presented in sequent paragraphs.

	$N_s$	$N_{rb}$	ID	$p$	$d_r [mm]$	$d_{r*} [mm]$	Speed [rpm]
<b>EM Type 1</b>	36	28	2	4	89.4	87.9	1430

**Table 7.2-4** EM 2 characteristics.

With the notation “ $d_{r*}$ ” is indicated the diameter of the rotor measured in the point in which the air gap is maximum.

<b>Test bench</b>	<b>EM Feeding</b>	<b>Purpose</b>
1	Direct Drive	Rotor eccentricity (variable air gap)
1	Direct Drive	Rotor eccentricity
		Load 20% (brake cooling)

**Table 7.2-5** Test performed on EM 2

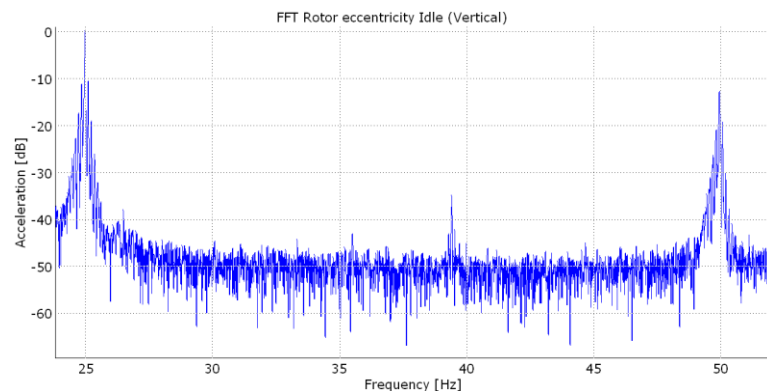
### 7.2.2.1 Rotor Eccentricity in Idle Condition

Table 7.2-6 reports main significative quantity to be taken into account in the results interpretation.

<b>EM Working Condition</b>	<b>Fm [Hz]</b>	<b>Fr [Hz]</b>	<b>s</b>	<b>PPF [Hz]</b>
Idle	25	24.97	0.0012	0.12

**Table 7.2-6** Main test parameter.

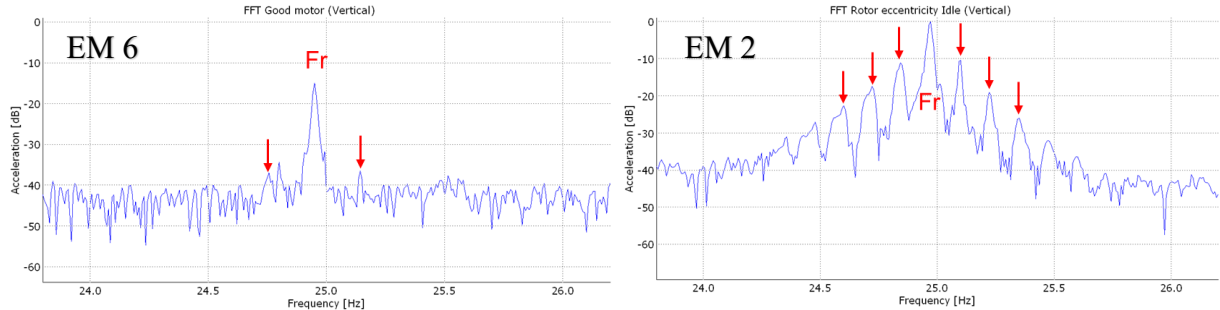
As presented in Chapter 4, a variable air gap will generate sidebands of the rotation frequency spaced by the pole pass frequency (PPF). In idle condition the slip frequency value is very low so to correctly identify side bands a high frequency resolution is required. For this reason, the acquisition time for the tests performed on EM 2 has been settled to 30 [s].



**Figure 7.2-7** EM 2 vibration spectrum.

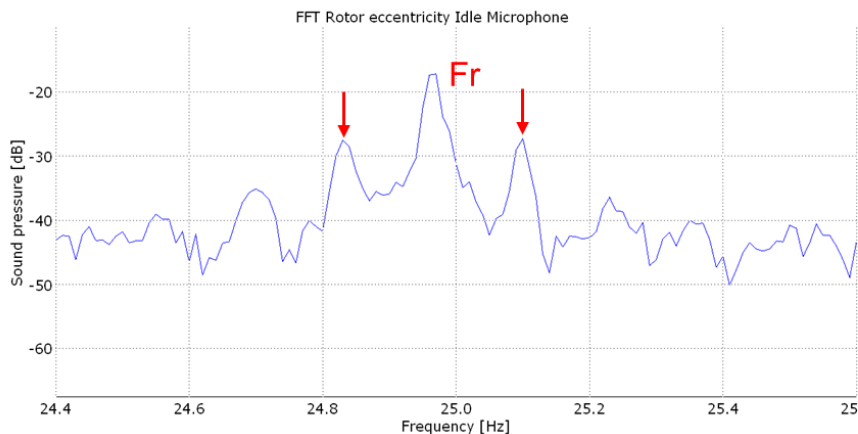
A general increase of peaks amplitude values has been observed (with respect to the baseline). Figure 7.2-7 reports the vibration spectrum of EM 2 for low frequencies band in decibel scale. The use of such a scale, in the presentation of sidebands and modulation phenomena, allows for a better visualization of the damage effects.

Figure 7.2-8 shows a comparison between the baseline (EM 6) and the electric motor under investigation. It is important to note that sidebands of the rotation frequency are present in both the spectra, the amplitude difference between the peak at the rotation frequency and the sidebands is often used to quantify the extent of the damage.



**Figure 7.2-8** Sidebands comparison between the baseline (EM 6) and the motor with the eccentric rotor (EM 2).

The same effect could be seen in the sound spectrum (see Figure 7.2-9).



**Figure 7.2-9** Sound spectrum of EM 2 in idle working condition.

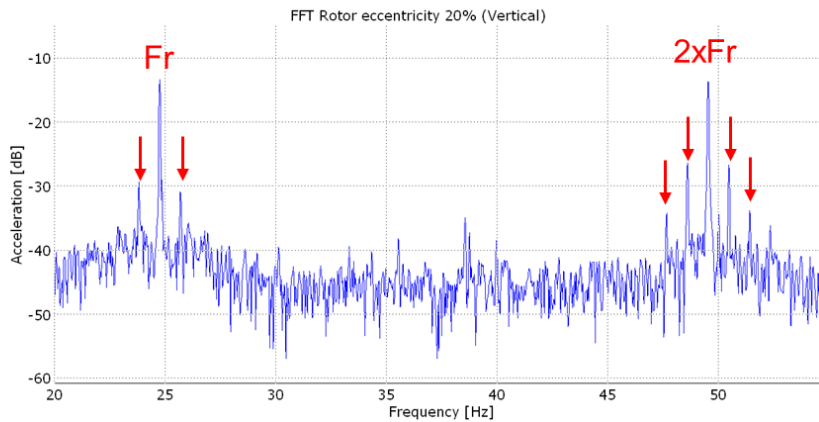
Such a modulation is clearly hearable by ear, generating a very characteristic sound emission.

### 7.2.2.2 Rotor Eccentricity 20% Loaded

All the effects analysed in previous paragraph are emphasised by adding a load (see Figure 7.2-10). In the second phase of the tests performed on EM 2, a 20% load has been added through a magnetic brake compressed-air cooled.

Table 7.2-7 reports main parameters for EM 2 with 20% load.

<b><i>EM Working Condition</i></b>	<b><i>Fm [Hz]</i></b>	<b><i>Fr [Hz]</i></b>	<b><i>s</i></b>	<b><i>PPF [Hz]</i></b>
20% Load	25	24.77	0.0094	0.94

**Table 7.2-7** Main test parameter.**Figure 7.2-10** Vibration spectrum of EM 2 with 20% load.

The cooling system needed for the magnetic brake introduce a high level of background noise. Therefore, for this measurement only vibration data have been acquired.

### 7.2.3 Electric Motor 1, Broken Rotor Bar

Electric Motor 1 (EM 1) has been used to simulate rotor bar issues. EM 1 is of the same type of the baseline presented in Paragraph 7.2.1. The rotor has been machined in such a way that 3 rotor bars were interrupted. The test has been performed both in idle condition and by applying a 20% of load in order to amplify the effect.



**Figure 7.2-11** EM 1, rotor bars machining.

Rotor bar interruption generates a rotating unbalance of the magnetic flux.

Table 7.2-8 reports EM 1 characteristics, while Table 7.2-9 reports tests performed on this electric motor. Each performed test will be further presented in sequent paragraphs.

	$N_s$	$N_{rb}$	ID	$p$	$d_r [mm]$	Speed [rpm]
<b>EM Type 1</b>	36	28	2	4	89.4	1430

**Table 7.2-8** EM 1 characteristics.

<i>Test bench</i>	<i>EM Feeding</i>	<i>Purpose</i>
1	Direct Drive	Broken Rotor Bar
1	Direct Drive	Broken Rotor Bar
		Load 20% (brake cooling)

**Table 7.2-9** Test performed on EM 1.

### 7.2.3.1 Broken Rotor Bars in Idle Condition

Table 7.2-10 reports main significative quantity to be considered in the results interpretation.

<i>EM Working Condition</i>	<i>Fm [Hz]</i>	<i>Fr [Hz]</i>	<i>s</i>	<i>PPF [Hz]</i>
Idle	25	24.93	0.003	0.3

**Table 7.2-10** Main test parameters.

As presented in Chapter 4, rotor bar interruption generates harmonics of the rotation speed and sidebands spaced by the pole pass frequency (PPF). In idle condition the slip frequency

value is very low so to correctly identify side bands a high frequency resolution is required. For this reason, the acquisition time of the tests performed on EM 1 has been settled to 30 [s].

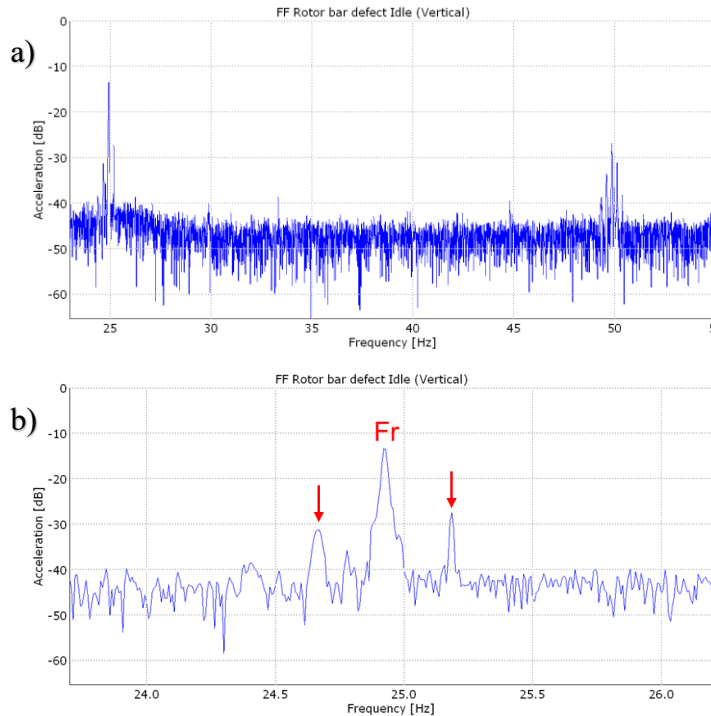


**Figure 7.2-12 a)** EM 1 vibration spectrum. **b)** Rotation frequency and sidebands magnification.

### 7.2.3.2 Broken Rotor Bars 20% Loaded

All the effects analysed in previous paragraph are emphasised by adding a load (see Figure 7.2-13). In the second phase of the tests performed on EM 1, a 20% load has been added through a magnetic brake compressed-air cooled.

Table 7.2-11 reports main parameters for EM 1 with 20% load.

<i>EM Working Condition</i>	<i>Fm [Hz]</i>	<i>Fr [Hz]</i>	<i>s</i>	<i>PPF [Hz]</i>
20% Load	25	24.77	0.0094	0,94

**Table 7.2-11** Main test parameter.

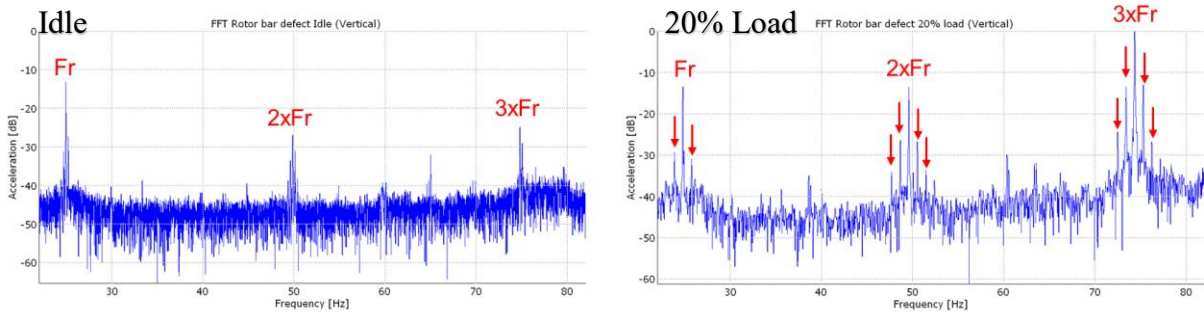


**Figure 7.2-13** Comparison of vibration spectrum for idle and loaded working condition.

The cooling system needed for the magnetic brake introduce a high level of background noise. So, for this measurement only vibration data have been acquired.

Is important to note that in literature is mentioned that damaged rotor bars generate peaks at the RBF frequency with sidebands spaced by twice the line frequency (see Chapter 4). This effect has not been observed (in any measuring direction) in the spectra of both the idle and the loaded tests. The main differences from the case of eccentric rotor (presented in Paragraph 7.2.2) can be founded in the prevailing presence of rotation speed harmonics (see Figure 7.2-14).

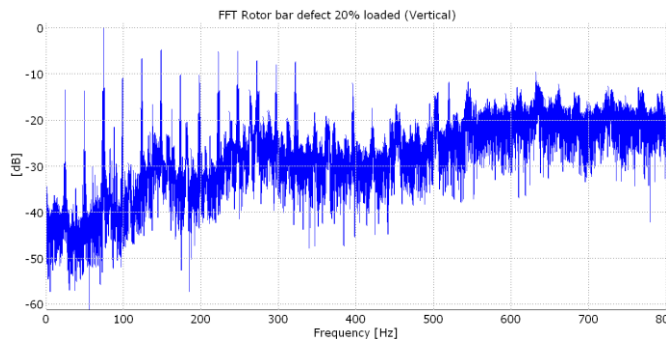


**Figure 7.2-14** Wide range vibration spectra for EM 1.

#### 7.2.4 Electric Motor 8, Baseline and Increased Air Gap

Electric Motor 8 (EM 8) has been used as reference (baseline) for the motor type 2, it has been balanced and revised before the test campaign in order to make sure that there are no evident issues.



**Figure 7.2-15** EM 8 nameplate.

Table 7.2-12 reports EM 8 characteristics, while Table 7.2-13 reports tests performed on this electric motor.

	$N_s$	$N_{rb}$	$ID$	$p$	$d_r[\text{mm}]$	Speed [rpm]	$DE$	$NDE$
<b>EM Type 2</b>	24	18	8	2	79.3	2910	6206 2RS2 (SKF)	6206 2RS2 (SKF)

**Table 7.2-12** EM 8 characteristics.

<i>Test bench</i>	<i>EM Feeding</i>	<i>Purpose</i>
1	Direct Drive	Baseline
1	Direct Drive	Increased Air Gap

**Table 7.2-13** Test performed on EM 8

Performed test results are aligned with experimental outcomes derived from *Type 1 Electric Motor*.

Tests has been performed into two steps, at first the baseline has been acquired, then the original rotor has been substituted by a grinded rotor with a lower diameter (76[mm]). For the sake of brevity only the main consideration will be reported. Table 7.2-14 reports the difference between main measured values.



**Figure 7.2-16** Grinded rotor picture for increased air gap test.

<b>EM 8 Baseline</b>	<b>Speed Fr amp. [m/s<sup>2</sup>]</b>	<b>2xFl amp. [m/s<sup>2</sup>]</b>	<b>RMS</b>
<b>Horizontal</b>	0.014	0.149	0.91
<b>Vertical</b>	0.020	0.063	1.06
<b>Axial</b>	0.015	0.007	2.57

<b>EM 8 with Increased Air Gap</b>	<b>Speed Fr amp. [m/s<sup>2</sup>]</b>	<b>2xFl amp. [m/s<sup>2</sup>]</b>	<b>RMS</b>
<b>Horizontal</b>	0.013	0.067	0.76
<b>Vertical</b>	0.019	0.018	0.77
<b>Axial</b>	0.022	0.008	1.59

**Table 7.2-14** Baseline and Increased air gap measurements.

Experimental results presented in Table 7.2-14 shows a general slight decrease in excitations amplitude that will result in a lower sound emission. This result is related to the dispersion of the magnetic field due to an increased airgap. In this working condition the currents flowing in the conductors are less intense and the motion of the rotor smoother. Although in this condition there is a decrease of the emitted sound, it implies a loss in torque and higher values of slip which may generate rotor bars issues.

### 7.2.5 Electric Motor A, Baseline

Electric Motor A (EM A) has been used as reference (baseline) for the motor type 3 (see Figure 7.2-17), it has been balanced and revised before the test campaign to make sure that there are no evident issues.

Unless otherwise stated, tests on electric motors type 3 have been performed in VFD driving mode settling a line frequency of 50 [Hz] and a carrier frequency of 10[KHz].



Figure 7.2-17 Electric Motor Type 3 Nameplate.

Table 7.2-15 reports EM A characteristics.

	<i>N<sub>s</sub></i>	<i>N<sub>rb</sub></i>	<i>ID</i>	<i>p</i>	<i>d<sub>r</sub>[mm]</i>	<i>Speed [rpm]</i>	<i>DE</i>	<i>NDE</i>
<b>EM Type 3</b>	24	34	A	2	80.4	2850	6203 DJ (NSK)	6203 DJ (NSK)

Table 7.2-15 EM A characteristics.

All the tests have been performed on the test station for motor type 3 (see Figure 7.1-1). In order to confirm results becoming from motor types 1 and 2, and to exclude any dependency on the test station, vibration and sound measurements for the baseline in direct drive and VFD mode have been acquired.

Table 7.2-16 reports tests performed on this electric motor.

<b>Test Station</b>	<b>EM Feeding</b>	<b>Purpose</b>
2	Direct Drive	Baseline
2	VFD_10 [KHz]	Baseline VFD driven
2	VFD_6 [kHz]	Baseline VFD driven
2	VFD_4 [kHz]	Baseline VFD driven

**Table 7.2-16** Test performed on EM A

Tests results are perfectly aligned with the ones coming from motor type 1 and 2. Only one significative difference can be highlight. Motor type 3 is equipped with a cooling fun with 11 blades, this characteristic will introduce an imbalance and an air-born sound emission which can be notice in both the sound and the vibration spectra.

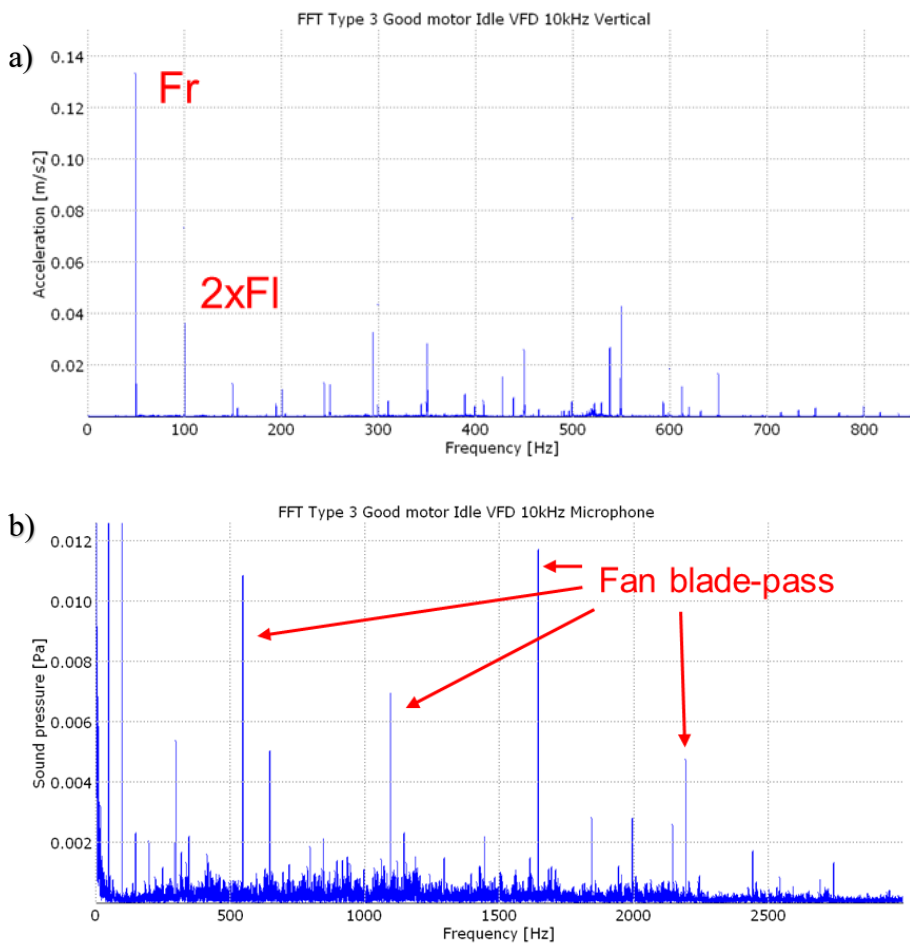
**Figure 7.2-18** EM A VFD driven with carrier frequency settled at 10 [KHz]: **a)** Vibration spectrum, **b)** Acoustic spectrum.

Figure 7.2-18 shows clear peaks at the *Fan Blade Pass Frequency (FPF = number of blades · Fr)* and its harmonics.

## 7.2.6 Electric Motor D, Electrical Issues

Electric Motor D (EM D) has been used to simulate electrical issues. EM D is of the same type of the baseline presented in previous paragraph. The motor itself do not show any damage while the electrical issues has been simulated using external components that will be presented in further paragraphs.

<i>Test bench</i>	<i>EM Feeding</i>	<i>Purpose</i>
2	VFD_10 [KHz]	Voltage Imbalance
2	VFD_10 [KHz]	Phase Loss

Table 7.2-17 Tests performed on EM D.

### 7.2.6.1 Voltage Imbalance

To introduce a voltage imbalance a rheostat connected only to one feeding phase has been used. The rheostat introduces a static (with respect to the sensing apparatus) disturbance which will result in an increase of the peak at twice the feeding frequency (line frequency).

<i>2xFl (100Hz) Amplitude</i>	<i>Baseline</i>	<i>Voltage imbalance Minimum</i>	<i>Voltage imbalance Maximum</i>
<b>Horizontal [m/s2]</b>	0.148	0.114	0.348
<b>Vertical [m/s2]</b>	0.074	0.089	0.095
<b>Microphone [Pa]</b>	0.021	0.008	0.011

Table 7.2-18 2xFl amplitude comparison for different values of voltage unbalance.

Table 7.2-18 shows amplitude outcomes for the peak at twice the line frequency. Vibration values increase with the unbalancing level, while from the acoustic point of view no significative changes can be highlighted.

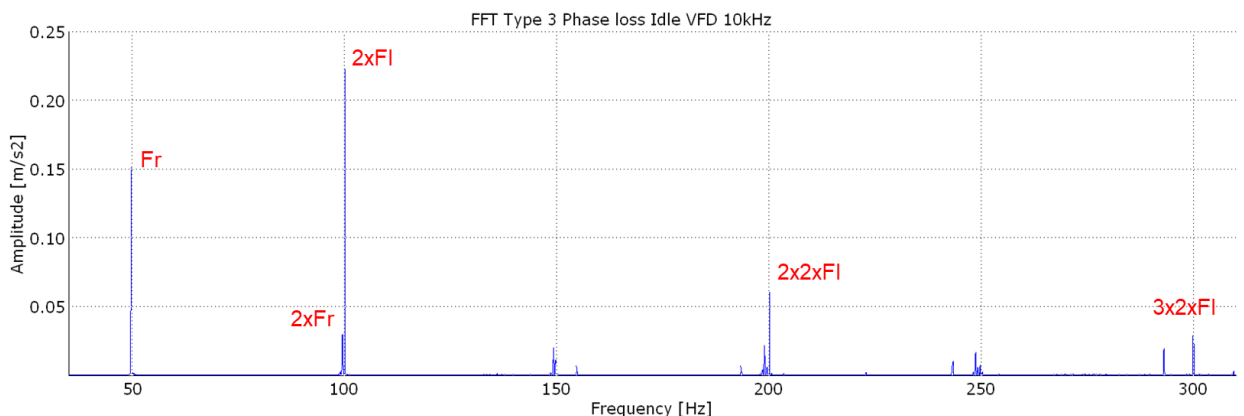
### 7.2.6.2 Phase loss

To simulate a connection issues one of the feeding line has been disconnected. The missing of a feeding phase generates a static imbalance of the magnetic field (with respect to the sensing apparatus) which will result in an increase of the peak at twice the feeding frequency and its harmonics (see Figure 7.2-19).

<b>2xFl (100Hz) Amplitude</b>	<b>Baseline</b>	<b>Phase Loss</b>
<b>Horizontal [m/s2]</b>	0.148	0.692
<b>Vertical [m/s2]</b>	0.074	0.223
<b>Microphone [Pa]</b>	0.021	0.026

**Table 7.2-19** 2xFl amplitude comparison in the case of missing feeding phase.

Table 7.2-19 shows that vibration level is in general increased if compared to the baseline, on the other hand not significative variations are detectable in the acoustic spectrum.

**Figure 7.2-19** Vibration Spectrum for EM D in phase loss configuration.

### 7.2.7 Electric Motor C, Static Eccentricity

Electric Motor C (EM C) has been used to simulate static eccentricity. EM C is of the same type of the baseline presented in Paragraph 7.2-5.

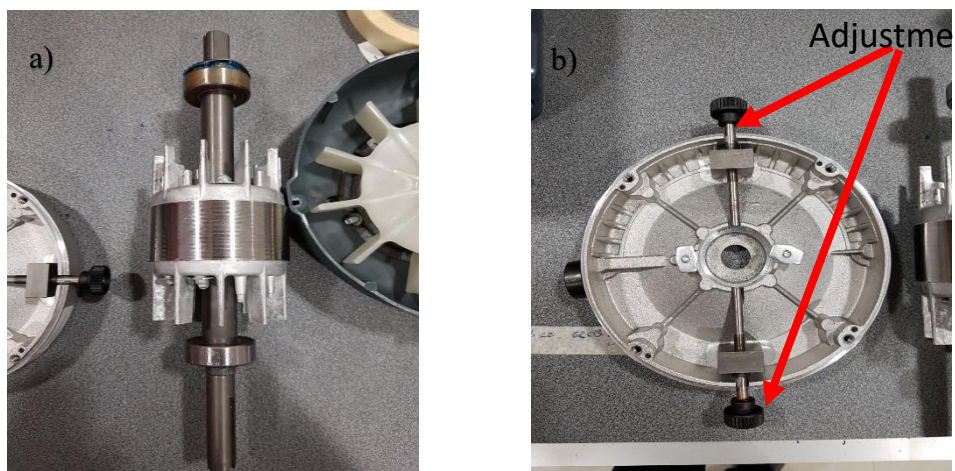
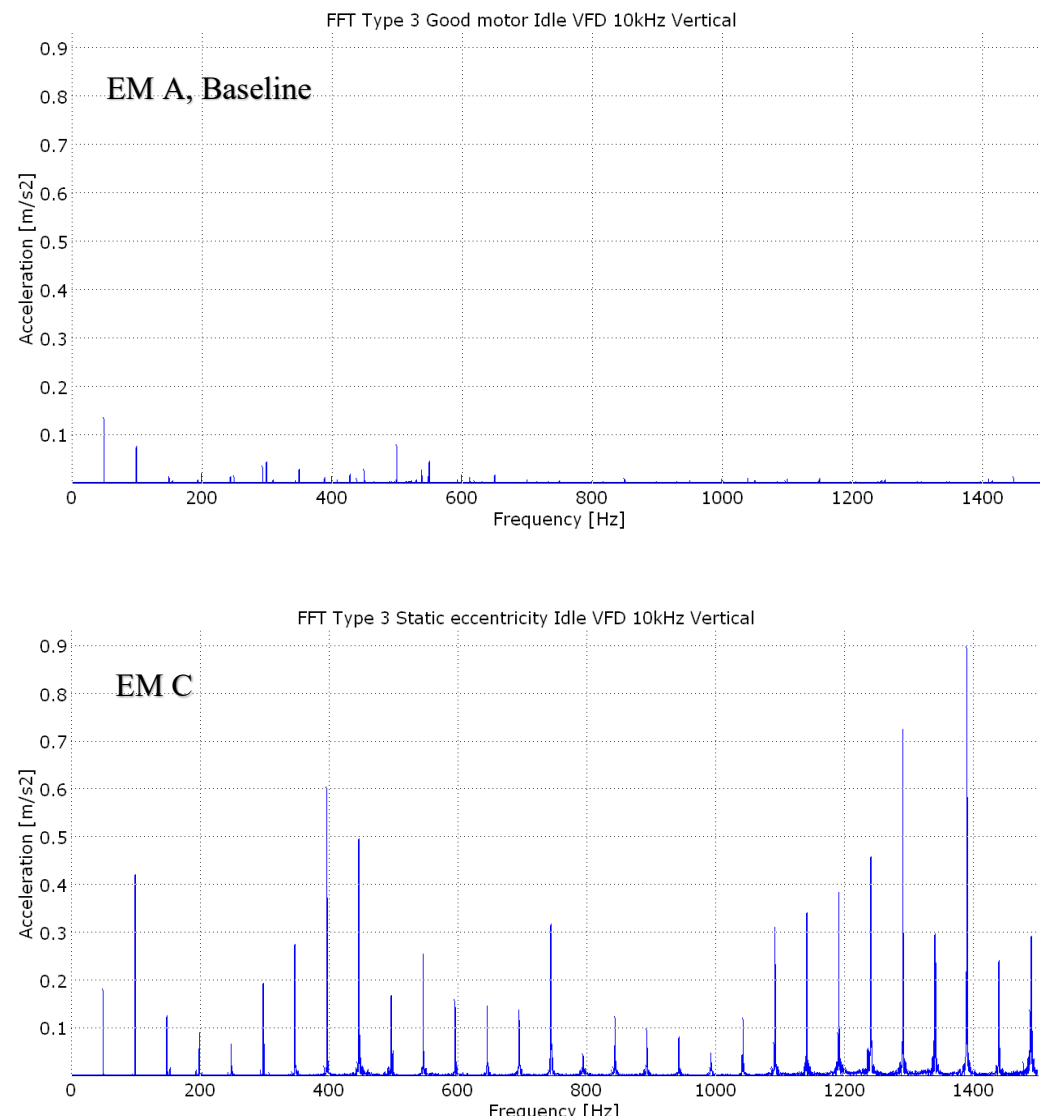
**Figure 7.2-20** a) EM C rotor. b) Bearings housing for EM C.

Figure 7.2-20 b shows how the bearing housing has been modified (on both side) to admit a shaft misalignment. Bearing housing has been realised with 1,5[mm] of radial clearance with respect to bearing nominal dimensions, by acting on the adjustments screws it is possible to generate shaft misalignments. For this test, the rotating shaft has been shifted in order to be not centred with the stator rotating magnetic field, generating a static unbalance (as presented in Paragraph 4.2.2) which will affect the peak at twice the line frequency and its harmonics (see Figure 7.2-21).

<i>Test bench</i>	<i>EM Feeding</i>	<i>Purpose</i>
2	VFD_10 [KHz]	Static Eccentricity

**Table 7.2-20** Tests performed on EM C.



**Figure 7.2-21** Comparison between the baseline for electric motor type 3 and the motor under investigation.

## 8 Conclusions

---

Within the *SKF's Application Noise Project*, this thesis fulfils the request for a clear identification of noise issues coming from non-bearing related sources in Induction Three Phase Electric Motors. Test campaign performed at the *SKF Solution Factory Moncalieri (TO)*, provides a crucial link between specific vibration sources and their sound emission. From the comparisons between vibration and sound spectra (with reference to performed tests) it is possible to establish that, in low background noise condition:

1. The frequency content of the noise and vibration spectra is comparable in the majority of analysed cases. Particularly representative example is test reported in Paragraph 7.2.2.1.

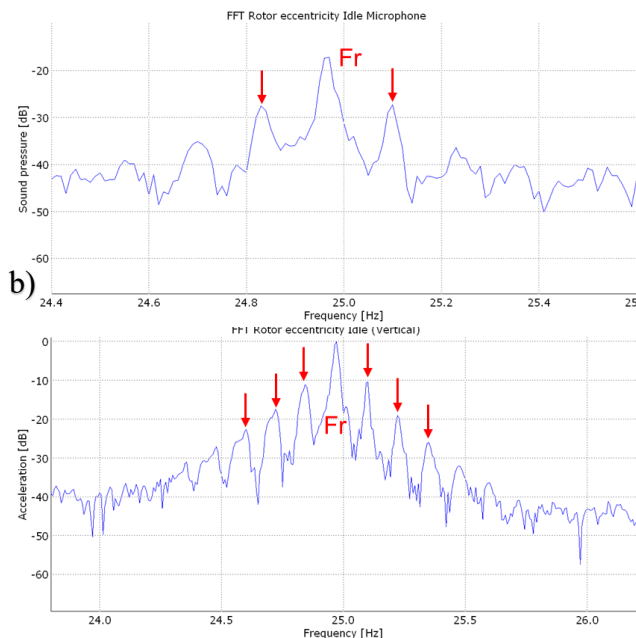


**Figure 8-1** EM 2 Eccentric rotor: a) Sound spectrum, b) Vibration spectrum.

2. Relative importance of the peaks amplitude is different from acoustic to vibration spectra. Demonstrating the impact of the transfer path and of the effectiveness of sound radiation on the emitted noise. Particularly representative example is test reported in Paragraph 7.2.1.1.

Experimental results prove that emitted sound is on the one hand related to the vibration sources and on the other hand highly influenced by system characteristics.

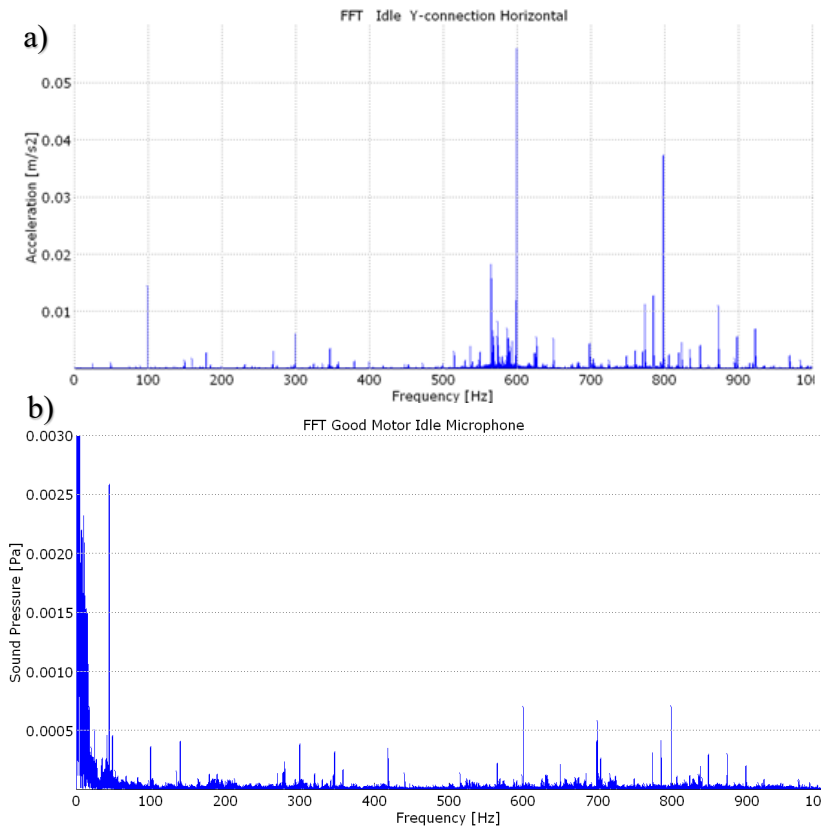


**Figure 8-2** EM 6 Eccentric rotor: **a)** Vibration spectrum, **b)** Sound spectrum.

According to reported results is possible to state that noise and vibration measurements are not competing techniques, but, as a matter of fact, they are complementary in the characterization of electric motors applications.

To avoid false problem identification, before applying any noise control technique, both measurements are required. Sound measurement is needed to point out the system best radiated wavelength, while vibrational analysis is used to correlate it to its source.

## 8.1 SKF's Application Noise Project Current Progress

Cooperation between different research teams working on the *SKF's Application Noise Project* culminated in the presentation of a structured approach to noise issue and troubleshooting. The *OACS method* (Observation, Analysis, Confirmation, Solution) has been designed for Application Engineers facing a customer noise complain.

OACS method is composed of 4 steps:

- Observation: in this phase all the application informations are collected in terms of components, characteristics and working condition. Acquired informations will be used in the analysis phase and at the same time enrich the database.
- Analysis: in this phase vibration and sound measurements are acquired and analysed to characterise the excitations and the associated vibration. All acquired measurements are stored in the database.
- Confirmation and Solution: in these last phases detected issues are checked and a solution is proposed.

According to the project's main outcomes, an internal training course has been launched, collecting great feedback. Moreover, a reference website has been instituted with a double intent; to guide Application Engineers in noise issues management and to facilitate the database filling.

a)

**E-motor N&V Guidelines**

A step-by-step procedure for effectively solving noise and vibration issues in industrial e-motor applications (OEM & end customers).

The general workflow of the guidelines is illustrated in the figure below. It follows the structured "OACS" procedure described in the SKF N&V handbook: "Noise and Vibration in Bearing Systems".

⚠ These pages are viewed best with Google Chrome and Mozilla Firefox.

Observation	Analysis	Confirmation	Solution
<b>@Office:</b> <ul style="list-style-type: none"> <li>- Application data</li> <li>- Agree on measurement plan</li> </ul> <b>@Customer:</b> <ul style="list-style-type: none"> <li>- Confirm complaint</li> <li>- Pre-screening</li> <li>- Measurements</li> </ul>	<b>@Office:</b> <ul style="list-style-type: none"> <li>- Data analysis</li> <li>- Diagnostics</li> </ul>	<ul style="list-style-type: none"> <li>- Diagnostics validation</li> <li>- Find root cause</li> </ul>	<ul style="list-style-type: none"> <li>- Propose solution</li> <li>- Validate solution</li> </ul>

**Tools**

- Database in the [Application Noise Cases SharePoint site](#).
- Detailed step-by-step E-motor N&V guidelines (this site).
- N&V Analysis Tool: to request a license, send an email to: [noise.and.vibration@skf.com](mailto:noise.and.vibration@skf.com).
- Measurement equipment

The guidelines and N&V Analysis Tool can be found in the [Application Noise Cases SharePoint site](#).

▼ DATABASE

▼ TRAINING AND REFERENCE DOCUMENTATION

Observation Phase ➤

b) MEASUREMENTS MICROLOG

ANALYSIS PHASE

CONFIRMATION PHASE

BEARING INVESTIGATION

MOTOR/ASSEMBLY CHECK

SOLUTION PHASE

MEASUREMENT EQUIPMENT

The general instructions like sensor mounting and documentation are described in the first tab. To limit the amount of measurements the acquisition is divided into three categories ("noisy side", "other side" and "additional". These refer to specific measurements that have to be taken in chronological order.

**⚠ Document which side (DE or NDE) is related to the "noisy side" and "other side".**

Answer the following question first:

Is there a "good" motor available (same motor but without the problem)?  Yes  No

GENERAL INSTRUCTIONS	ACQ. NOISY SIDE	OTHER SIDE	<b>ADDITIONAL</b>	GOOD MOTOR
----------------------	-----------------	------------	-------------------	------------

Depending on the particular system configuration, there are certain additional measurements that have to be performed. To filter out the measurements that are not applicable to a particular case, answer the questions below first.

Is it possible to **switch-off the power** to let the motor run down?  Yes  No

Is it possible to **change the load** or to **decouple** the motor? ("No" if not applicable)  Yes  No

Is it possible to **change the VFD carrier frequency** or switch to **direct drive**? ("No" if not applicable)  Yes  No

Is it possible to **slowly increase the motor speed** from stand still to operating speed?  Yes  No

Is it possible to change the **axial pre-load**, i.e. change spring(s)? ("No" if not applicable)  Yes  No

Figure 8.1-1 a) Noise and vibration website, Homepage b) Noise and vibration website, Measurements section.

Figure 8.1-1 shows the reference noise and vibration webpage and an example of drop down menu with selectable options.

## Bibliography

---

- [1] SKF, *Rolling Bearings and Seals in Electric Motors and Generators*. PUB 54/P7 13459 EN, 2013.
- [2] C. Cesti, *L'Analisi delle Vibrazioni nella Manutenzione Predittiva*. SKF Industrie S.p.a, 1996.
- [3] Charles A. Gross, *Electric Machines*. CRC Press, 2007.
- [4] SKF, *Bearings damages and failure analysis*. No. 14219 EN, SKF Group Publications, SKF Group, 2014.
- [5] SKF, *SKF General Catalogue*. SKF Group, 2012.
- [6] G. van Nijen, P. van Dalen, G. A. Dimitrov, V. van Ravesteijn, J. Stam, F. Tatar, *Noise and Vibration in bearing Systems*. Tech. Rep. NL15E005, SKF Engineering & Research Centre B.V., 2015.
- [7] A. Fasana, S. Marchesiello, *MECCANICA DELLE VIBRAZIONI*. Clut Editrice, 2006.
- [8] P. Asinari, E. Chiavazzo, *An introduction to multiscale modeling with applications*. Società editrice Esculapio, 2013.
- [9] M. Norton, D. Karczub, *Fundamentals of Noise and Vibration Analysis for Engineers*. Cambridge university Press, 2003.
- [10] ABB, *Low Voltage General Purpose Motors*. ABB EN 12, 2006
- [11] National Electrical Manufacturers Association, *NEMA MG 1*. NEMA ID 100228, 2016.
- [12] <https://www.vfds.com/blog/what-is-a-vfd>, available on 01/04/2019.
- [13] [https://www.youtube.com/watch?v=AQqyGNOP\\_3o&t=186s](https://www.youtube.com/watch?v=AQqyGNOP_3o&t=186s), available on 01/04/2019.
- [14] <https://wwwpcb.com/>, available on 01/04/2019
- [15] <https://www.skf.com/it/index.html>, available on 01/04/2019
- [16] <https://www.nema.org/pages/default.aspx>, available on 01/04/2019
- [17] <https://www.iec.ch/>, available on 01/04/2019